FABRICATION AND CHARACTERIZATION OF

CALCIUM ALUMINATE GLASS FIBERS

by

PAUL R. FOY

A dissertation submitted to the

Graduate School - New Brunswick

Rutgers, The State University of New Jersey

In partial fulfillment of the requirements

For the degree of

Doctor of Philosophy

Graduate Program in Materials Science and Engineering

Written under the direction of

Professor George Sigel

And approved by

_____

_____

_____

_____

New Brunswick, NJ

October, 2008

ABSTRACT OF THE DISSERTATION

Fabrication and Characterization of Calcium Aluminate Glass Fibers

By PAUL ROBERT FOY

Dissertation Director:

Professor George H. Sigel, Jr.

Calcium aluminate glasses (CAG) offer excellent chemical durability, high strength, broad spectral transparency, and a refractory nature. This makes them ideal candidates for fiber optic power delivery and sensor systems in the infrared spectrum. CAG also have the potential to form ultra-low loss optical materials.

The fabrication of glass optical fibers from CAG was investigated in this study. High quality bulk glasses were obtained from the best industrial sources available. These glasses included silica and baria doped CAG compositions. A preform fabrication method was developed to obtain drawing samples. An optical fiber draw furnace was specially modified to achieve fiber drawing. A novel drawing method was also developed.

Solid and hollow CAG waveguides, and CAG core/silica clad waveguides were obtained from drawing preforms. This represents the first successful fiber drawing of this glass system. Teflon coating for optical cladding and strength protection was also investigated.

Infrared Spectroscopy was used to assess the attenuation in the drawn fibers. 7 dB/m at 2.7 μm with the baria doped CAG solid waveguide was recorded. This represents the lowest loss documented for fibers fabricated from CAG.

Laser power propagation through solid and hollow waveguides was investigated. 24 Watts of CO_2 laser power was delivered into a hollow baria doped CAG waveguide. 10.13 J/mm^2 of 2.94 μm Erbium YAG laser power was delivered through solid baria doped CAG waveguide.

Fiber strength testing was performed on the CAG fibers through four point bend testing. The best strength obtained was 1290 MPa for baria doped CAG.

Glass stability was assessed using Differential Thermal Analysis. Fiber surface crystallization products were characterized using Energy Dispersive Analysis, Scanning Electron Microscopy, a specially modified Hot Stage X-Ray, and Guinier Camera X-Ray Analysis. The surface crystallization analysis revealed the formation of $Ca_3Al_2O_6$ in the silica doped CAG fibers and $Ca_3Al_2O_6$ and $Ba_4Al_2O_7$ in the baria doped CAG fibers.

Reactive atmosphere processing using propane and NF_3 was investigated for reducing the surface crystallization during drawing.

ACKNOWLEDGMENTS

I would like to take this opportunity to express my gratitude to the many people who supported me throughout my graduate studies and research.

First, I would like to express my deepest thanks to Dr. George Sigel, Jr. He gave me the opportunity to work in the Fiber Optic Materials Research Program at Rutgers, and supplied endless enthusiasm, encouragement, and excellent technical guidance. I would also like to thank Dr. Ronald McCauley and Dr. Richard Lehman for their technical and personal support and encouragement. Also thank you to Dr. Lisa Klein for her continued support throughout my graduate career.

Dr. John Ballato has been an inspiration and good friend during my graduate studies and research. Thank you John, along with Dr. Sigel, for believing in me when I did not believe in myself. I will be eternally grateful to you both for pushing me to a level I did not think possible.

I would like to thank Ed Perry, Rajiv Datta, Thomas Stockert, Jeff Bonja, Todd Able, and Lois Johnson for their excellent assistance in my research.

I would like to thank Dr. William Bauer and Dr. Malcolm McLaren for inspiring me to reach beyond my perceived limitations. I could not have done this without your support.

I would like to thank T. Wade Hawkins for his friendship and technical assistance, especially during the writing of this dissertation.

I would like to thank Betty McGarry for her friendship and support during all these years.

I would like to also thank Gabe Puc for his technical assistance during our time as supervisors at the Rutgers Fiber Optic Materials Research Program, and especially for his friendship and support then and now.

I would like to especially thank my Mom and Dad for their love and support. You both taught me how to work hard and helped me to believe in myself.

Lastly, and most importantly, I would like to thank my wife Denise, and my daughters Jessica, and Sarah, for their encouragement, patience, and love. I love you all very much, and dedicate this dissertation to you.

TABLE OF CONTENTS

LIST OF TABLES

LIST OF FIGURES

I. INTRODUCTION

Calcium aluminate glasses (CAG) have been researched for nearly 60 years.[1,2] The principal driving forces behind this research were the search for materials that would transmit infrared radiation to at least 6 μm, have a softening range greater than 500°C, possess thermal shock and strength properties similar to conventional silicate glasses, and the ability for forming large sizes and intricate shapes for commercial development at a relatively low cost.[3]

These properties have led to the use of CAG as IR windows for guided missile domes.[4] Their excellent chemical durability, high strength, broad spectral transparency, and refractory nature also make them ideal candidates for various fiber optic power delivery and sensor systems for the infrared region.

Perhaps the most exciting area of interest is the potential of these glasses to form ultra-low loss optical materials. Away from electronic or molecular resonances, the largest contribution to total minimum attenuation, assuming there are no compositional fluctuations, comes from Rayleigh scattering losses caused by static density fluctuations. This scattering can be minimized by filling as many "holes" as possible, in the three-dimensionally coordinated oxide network, with cations smaller than divalent oxygen. This would produce the fewest broken molecular bonds. CAG satisfy this condition very well, which explains their potential low loss behavior.[5]

Lines,[6] et al., report a projected minimum total attenuation of as low as 0.015 dB/km at 1.9 um for CAG. This would be significantly better than the 0.16 dB/km for

present day silica-based optical fibers at 1.55 um. However, the difficulties in processing CAG materials, especially in fiber drawing, have limited their uses.

Though halide and chalcogenide glasses have also been investigated for low loss behavior, at the present time such non-oxide waveguides would operate at longer wavelengths than the silica wavelength of 1.55 μm. They would be incompatible with devices developed for present-day silica technology. In addition, halide and chalcogenide fibers are typically of low strength and cannot be used at elevated temperatures, while calcium aluminate glasses can achieve strengths comparable to that of silicate fibers and are appropriate for high temperature applications.[7]

CAG are difficult to manufacture and necessitate a rapid quench during processing in order to prevent devitrification. The drawing of these glasses into fiber has been inhibited by this rapid crystallization behavior. In addition, the refractory nature of the composition pushes the lowest eutectic temperature of the glass-forming region to over 1500°C. This causes corrosion problems from contact with platinum or ceramic crucibles.[6]

CAG tend to be moisture sensitive during processing and use. The immersion of these glasses into water at 85 $^{\circ}$C for one hour causes a lowering of transmission in the 2-4 μm region by as much as 8 and 40%. For this reason, Sassoon Advanced Materials Limited, one of the largest manufacturers of CAG, utilizes advanced vacuum glass melting technology and high purity starting materials. In this way the water peak at 2.9 μm is minimized.[4]

The fabrication of calcium aluminate glass fiber from the bulk glass is the major obstacle in achieving usable fiber systems based on this glass system. The potential of

the calcium aluminate glass system for low loss fibers provided the motivation for this dissertation. The objectives of this work include:

1. Select the best commercially available calcium aluminate bulk glasses for fiber fabrication.

2. Fully thermally characterize the calcium aluminate glasses under study.

3. Fully characterize the products of crystallization during the thermal processing calcium aluminate glasses.

4. Develop a fiber drawing process for fabricating calcium aluminate glass fibers.

5. Draw hollow and solid calcium aluminate glass fibers.

6. Investigate ways of improving calcium aluminate glass fiber fabrication.

7. Evaluate the mechanical strength of the resulting fibers.

8. Determine the optical transparency of the resulting calcium aluminate glass fibers.

9. Determine the feasibility of using hollow calcium aluminate glass fibers for laser power propagation.

10. Assess the performance of the resulting fibers for industrial applications.

II. LITERATURE SURVEY

II.1 Pioneering Research

II.1.1 Early Evidence of Glass Formation

The first recorded evidence of glass formation in the calcium aluminate system was documented by Shepherd, et al.[8] They examined the binary system of lime with alumina. The purpose of their study was to identify the primary crystal phases in compositions ranging from 40 to 60 percent alumina. They sought to obtain a phase diagram for this binary system. They developed a rapid quenching technique, in which samples could be melted in a small platinum crucible, and then dropped directly out of the bottom of the furnace and into a dish of mercury with water on it. In this way, they were able to bring the melt samples rapidly to room temperature. Glass was obtained in samples ranging from 40 to 60 percent alumina with this rapid quenching technique.

Rankin and Wright followed this study up with an investigation into the ternary system of calcia, alumina, and silica.[9] They utilized the same quenching technique described by Shepherd. The major focus of their work was to identify the constitution of Portland cement clinker. 7,000 heat treatments and subsequent optical examinations were performed on this ternary system. The rapid quenching technique identified extensive areas of glass formation in this system.

Rankin et al.,[10] investigated the ternary system of calcia, alumina, and magnesia. Again, the focus of the research was to identify principal crystal phases in various compositions within this ternary system. Extensive areas of glass formation were verified in this system using the rapid quenching technique described above.

H.F. McMurdie, and H.J. Insley[11] performed a study on the quarternary system

CaO-MgO-2CaO-SiO_2-5CaO.3Al_2O_3. Their goal was to determine the behavior of

magnesia in portland cement to establish the composition ranges where it appears as a

primary phase of crystallization. Samples were melted at various temperatures in excess

of 1,300^{o}C. They utilized the same quenching technique described by Shepherd.[8] In this

system they were able to obtain glass formation in compositions containing about 5

percent magnesia and less then 10 percent silica.

II.1.2 Early Investigations on the Role of Alumina in Glasses

Dimbleby, et al.,[12] performed the earliest investigations into the influence of

alumina on the properties of glass. They examined the effect of alumina on the heating

temperature, the coefficient of thermal expansion, the density, and the refractory index of

glass at ordinary temperatures. In addition, they examined the rate of melting and ease of

working at elevated temperatures. Attention was paid to devitrification tendencies in this

study. Two series of glasses were tested, one with a composition of

6SiO_2,$x$$Na_2O$,$y$$Al_2O_3$, where $x + y = 2$, and the other series starting with 6SiO_2, 0.9CaO,

1.1Na_2O, with the alumina in this series replacing lime molecularly.

Their results showed that the presence of small amounts of alumina tends to make

fusion of the glass somewhat easier than without it. If, however, the composition has

alumina in excess of about 3 to 5 percent, the founding temperature rapidly increases.

Also, they found the replacement of silica by alumina, weight for weight, can be carried

out without any effect on the thermal expansion. Replacement of silica by alumina, up to

a level of 10 percent, results in a slight increase in the annealing temperature. Beyond a

substitution level of 10 percent, the annealing temperature increase is considerably greater. In addition, research on these two series of glasses showed that the substitution of silica by alumina brings about an increase in the density of the resulting glass.

Weyl[13] discussed the role of alumina in glasses in 1943 in his book on colored glasses. He commented that in vitreous silicates the Al^{3+} ion plays the role of the Si^{4+} ion. Al_2O_3 cannot be considered of glass former by itself because it does not to fill the requirements essential for glass formation. These requirements are:

1. Alumina cannot form three-dimensional network of AlO_4 tetrahedra. The ratio of oxygen to aluminum is $3:2 = 1.5$. This value is too low, 2.0 is the minimum ratio required.

2. It cannot form three-dimensional network of AlO_3 triangles, such as boric oxide does, for obtaining three-fold coordination. The Al^{3+} ion ranges between those ions which prefer six-fold or octahedral coordination and those which prefer tetrahedral coordination.

When considering crystalline silicates, the AlO_4 groups are often found to take the place of SiO_4 groups. Since the Al^{3+} has only three positive charges, which is one less than the SiO^{4+} it is replacing, the electrical balance has to be done by introducing a single positive charge ion into the structure for each Al^{3+} ion. Al^{3+} forms tetrahedra only in the presence of alkali or alkaline earths.

Weyl[13] stated that even before the structural reasons were known, the glass technologist had taken advantage of the strengthening affect of the aluminum ion. When alumina is introduced into a soda-lime-silica glass, its chemical resistivity and viscosity

are considerably increased. This strengthening of the glass structure prevents devitrification.

Weyl described that Al_2O_3 can play the role of a glass-forming oxide only in combination with CaO, being that the only example of a pure aluminate glass was the vitreous calcium aluminate.

J.M. Stevels[14] examined the current knowledge on the structure of glass in a presentation in 1946. He described the special case of the Al^{3+} ion. Al_2O_3 itself does not satisfy the conditions described by Zachariasen and cannot be obtained in the vitreous state. According to Zachariasen[15], the requirements that must be satisfied by a crystal oxide to form glasses are:

1. Each oxygen ion is linked to more than two cations.

2. The oxygen polyhedra share corners with each other, not edges or faces.

3. The number of oxygen atoms surrounding the positive ion must be small (three or four)

4. There must be a number of oxygen polyhedra, of which at least 3 corners must be shared with another polyhedron.

Since Al_2O_3 itself does not satisfy the conditions of Zachariasen, it cannot be obtained in the vitreous state. However, the additions of small amounts of Al_2O_3 considerably improved the vitreous properties of silicate glasses. Since Al^{3+} ion can easily replace the Si^{4+} ion in a SiO_4 tetrahedron, it can play the role of the glass-forming ion. The AlO_4 tetrahedron is somewhat larger than that of the SiO_4 tetrahedra. The network irregularities arising from the addition of a few percent of AlO_4 tetrahedron in SiO_4 tetrahedra lead to improved vitreous properties.

At the time, J.M. Stevels was skeptical that the recently reported calcium aluminate glasses were actually vitreous. It was a well-known fact that a number of systems, especially those containing Al_2O_3, have a vitreous appearance. Upon further investigation by x-ray analysis, they were recognized as being crystalline. K.H. Sun[16] also examined the current knowledge on the structure of glass in 1946. Sun describes the vitreous state as "that state in which the range of the component atoms, ions, or molecules possesses a permanence similar that in the crystalline state and a randomness similar to that characteristic of liquids". Sun also described that almost any substance can be made into glass if it is sufficiently quenching or rapidly cooled in the liquid state from a temperature slightly above its melting point or liquidus temperature. This is particularly true if the size of the glass is not specified.

Sun places oxide materials into three categories. These include glass-forming and non-glass forming oxides. The non-glass forming oxides can be further divided into two groups: the modifiers and the intermediate oxides. The modifiers can be mixed with the glass formers to modify the properties of the glass. In essence, they weaken the network of the glass. The modifiers cannot form of glass by themselves and cannot form one when added in too large a quantity to a glass former.

The intermediate oxide group is usually very difficult to form a glass. However, some of these oxides may form a glass when mixed with modifiers on one side. Also, they may be mixed with the glass former in greater amounts that the modifiers could on the other. The first may be called the glass-forming intermediates, and the second may be called the modifying intermediates. The glass-forming intermediates are usually good

modifying intermediates, but not vice-versa. Al_2O_3 is a typical example of glass-forming intermediates.

Safford and Silverman[17] investigated the relationship of alumina and silica in glass in 1947. They had been impressed by recent information concerning the possibility of aluminum assuming a four-fold coordination value and replacing silicon of the same coordination value in orthosilicate tetrahedra in glass. Normally, it was understood that alumina in Al_2O_3 has a six-fold coordination value and a valence of three. Silicon in the tetrahedron has a valence of 4.

When alumina is introduced in place of silicon, a calcium ion may replace a sodium ion in the interstices. This will satisfy the valences. It had long been identified that when alumina is used in glass, more lime may be introduced to replace soda and to increase the stability of the glass. Alumina usually imparts increase chemical durability, viscosity, hardness, thermal endurance, tensile end compressive strength, reduces devitrification tendencies, and has an effect on thermal expansion similar to that of silica in the glass.

It was well established that silicon, and frequently aluminum, atoms in certain silicates and feldspars are surrounded by four oxygen atoms. These oxygen atoms are arranged at the corners of a tetrahedron. Cations such as potassium, sodium, calcium, and barium are situated at the interstices of the negatively charged framework of the tetrahedra. In this framework, the silicon and oxygen atoms and the alumina and oxygen atoms were believed to be held together by partially polar, covalent bonds.

Safford and Silverman acknowledged that all attempts at preparing pure or Al_2O_3 in the glassy state had failed in agreement with the rules of Zachariasen.[15] They viewed

it as highly unlikely that glasses in binary systems such as Na_2O-Al_2O_3 and CaO-Al_2O_3 could be prepared easily for examination by current x-ray techniques. Their preliminary investigations of the system Na_2O-CaO-Al_2O_3 failed to produce any evidence of glass formation. As a result, they decided to concentrate on additions of Al_2O_3 to soda-lime-silica glasses in order to formulate a semiquantitative picture of the coordination state of the aluminum atom in such glasses.

The Lorentz-Lorentz equation was used to evaluate partial molecular refractions of the component oxides in the glasses in their study. The partial molecular refractivities of Al_2O_3 in the glasses studied closely paralleled those calculated for crystals in which the coordination number of alumina is four. On the contrary, they deviated considerably from the refractions of Al_2O_3 where the alumina atom is surrounded by six oxygen neighbors. The calculated interionic distances for Si-O and Al-O favorably agreed with the known measured values on substances in which aluminum and silicon atoms assume a four-fold coordination.

From these results, Safford and Silverman concluded that the aluminum atom replaces silicon in the random tetrahedral network and that the cations Na^+ and Ca^{+2} are situated in the interstices of this open structure. The similar roles played by aluminum and silicon atoms permitted the explanation of the property contributions of alumina in terms of the modern view of glass networks.

J. E. Stanworth[18] acknowledged the earlier research into the role of alumina in glass formation and sought to examine it in further detail. He noted that the bonds between the glass forming cation and its oxygen neighbors have a substantially covalent nature. The percentage of the covalency of these bonds is higher than those linking their

neighboring oxygens to the non-glass forming cations. Na^+, K^+, Ca^{+2}, and Ba^{+2} are examples of the non-glass forming cations. He felt the most important features of the glass forming cations, which determined their behaviors in technical glasses, as:

1. Their coordination with three or four oxygen atoms.

2. The substantially covalent nature of the bonds to their neighboring oxygen atoms.

Stanworth was interested in determining whether or not glasses could be made containing high percentages of alumina and none of the glass-forming oxides. Tests were performed by melting pure, analytical reagent quality, alumina and calcium carbonate. The required proportions were heated in a platinum crucible in a gas-fired furnace at about $1500^{\circ}C$. When the melts were clear, they were poured directly into a cast iron mold of 1 inch diameter. The poured glass was then pressed using a cast iron plunger to form a disk of 1 inch diameter and thickness of approximately 0.25 inches. 200 grams of sample was melted each time.

Several different compositions were tried, but no crystalline-free glasses were obtained. The weight percentage composition, CaO-48.5 and Al_2O_3-51.5, corresponding to the compound 12 $CaO.7Al_2O_3$, was tried but only a small amount of glassy phase was obtained among the predominantly devitrified phase. He was, however, able to obtain a small amount of clear glass by taking fragments of the devitrified 12 $CaO.7Al_2O_3$ composition and melting it on a loop of platinum wire in an oxygen/coal gas flame.

Stanworth acknowledged that this calcium aluminate composition was capable of forming glass, but that more favorable compositions must be found to form calcium aluminate glasses in usable quantities.

Stanworth decided to concentrate on experiments to determine the amount of silica that must be added to the calcium aluminate composition to produce a good glass in usable quantities. A sample of weight percent composition 6.6 percent SiO_2, 48.6 percent Al_2O_3, and 44.8 percent CaO, readily formed a glass with no detectable devitrification. He concluded that calcium aluminate melts have a certain tendency to glass formation, and small additions of silica greatly increases this tendency.

Stanworth explained these results in terms of Zachariasen's theories, and the structure of crystalline calcium aluminate, $12CaO,7Al_2O_3$, as determined by W. Bussem and W. Eitel[19]. Figure II.1 shows one eighth of a unit cell of this compound that they constructed. This showed that:

1. The aluminum atoms are four-coordinated with oxygen forming AlO_4 groups.

2. Some of the AlO_4 groups (the Al atoms marked "2") are connected to four other AlO_4 groups. Other AlO_4 groups (the Al atoms marked "1") contain one oxygen (marked "1") which is part of only one AlO_4 group. This oxygen is located 3.4 Angstroms from the aluminum atom of the next AlO_4 group. The Al-O distance within an AlO_4 group is 1.78 Angstroms.

3. The calcium atoms are situated in the holes of the structure of AlO_4 groups.

Stanworth felt that the difficulty in forming larger samples of glasses in this calcium aluminate composition was related to the gaps between the AlO_4 groups. He regarded the effectiveness of small amounts of silica as making up for this defect in the calcium aluminate structure.

aluminium atoms
oxygen atoms
calcium atoms
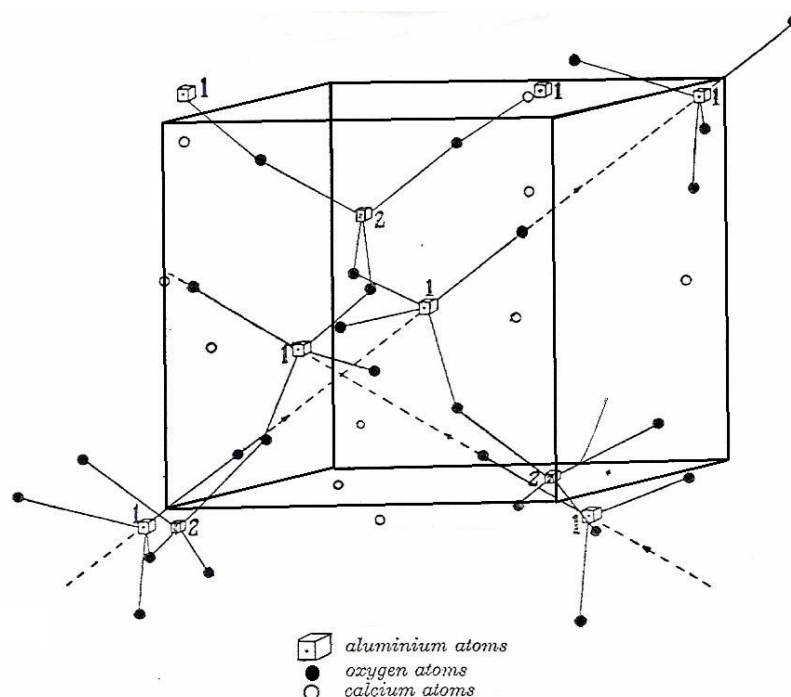
Note – In order to avoid confusion not all of the atoms are
included in the above diagram, and not all the atoms belong
to the one-eight unit cell. The diagram is drawn only for the
purpose of making clear the discussion in the text.

Figure II.1 – Positions of the various atoms in one-eighth of the unit cell of
$12CaO_7Al_2O_3$ (after Bussem, et al., reference # 19)

K.H. Sun[1] explored aluminate glasses in more detail in 1949. He synthesized

many calcium aluminate type glasses in hopes of producing a glass with optical

properties somewhere between that of crystalline CaO and Al_2O_3. Table II.1 shows the

refractory index, n, and the Abbe value, v, for crystals and glasses pertinent to this

discussion. These results indicate that the coordination state of aluminum in spinel and in

aluminate glasses are different. It is reasonable to assume then, that most of the

aluminum atoms in aluminate glasses take a four-fold coordination. If this were true, the

contribution of four-fold coordinated Al_2O_3 to the refractive index and Abbe value would

be about 1.5 and 42, respectively.

	n	ν	Remarks
Crystalline $AlO_{1.5}$ (or Al_2O_3, corundum)	$\omega 1.768^5$ $\varepsilon 1.760^5$	71^6 72^6	All Al in 6-fold co-ordination.
Crystalline MgO	1.73790^7	53.5^7	
Syn. $MgAl_2O_4$ Crystal	1.7258^8	63.5^8	At least ½ of Al in 6-fold coordination.
$AlO_{1.5}$—component in			
silicate glasses	1.53^9	56^9	Possibly more in 4- than in 6-fold coordination.
Crystalline CaO	1.837^5	46^{10}	
Ca-aluminate type of Glasses (Table II)	~ 1.70	~ 44	Mostly 4-fold co-ordination.

Table II.1 – Refractive index (n) and Abbe values (ν) for glasses and crystals in Sun's research (after Sun, reference # 1)

II.1.3 Liquidus Temperature Effect

H. Rawson[20] believed that the existence of systems where either component forms a glass was closely tied to the "liquidus temperature effect". This was especially true for binary systems such as that of $CaO-Al_2O_3$. He explained that the region of glass formation is often found in the region of composition where the liquidus temperature is low.

The "liquidus temperature effect" is caused by the second oxide lowering the liquidus temperature, thereby reducing the amount of thermal energy available at the liquidus temperature for breaking bonds. Figure II.2 shows the phase diagram for the $CaO-Al_2O_3$ system with the glass-forming region identified. The bond strength/liquidus temperature ratio will be higher for all binary compositions than for either of the pure components. Therefore, glass formation will be more likely at the eutectic composition.
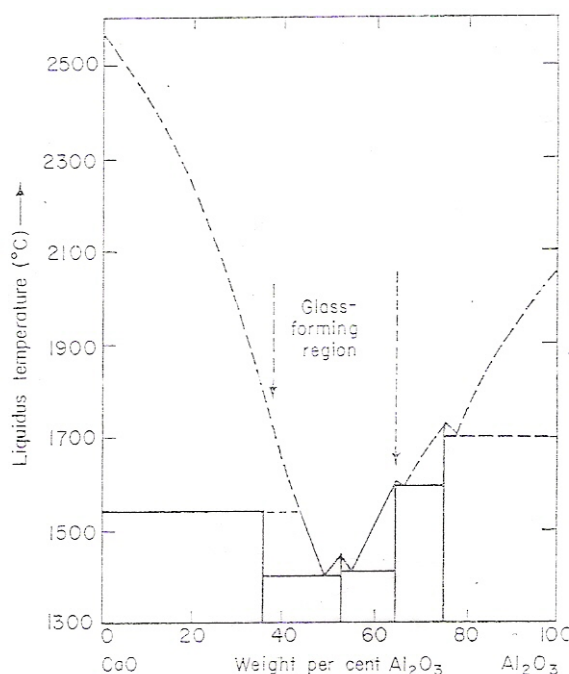
Figure II.2 – The glass-forming region in relation to the phase diagram for
the system Ca-Al$_2$O$_3$ (after Rawson, reference # 20)

II.2. Current Structural Investigations of Calcium Aluminate Glasses

V. A. Kolesova[21] performed infrared absorption spectroscopy on alkali
aluminosilicate glasses in order to determine the role of aluminum atoms in the glass
network. In infrared absorption spectra of aluminum containing crystalline silicates and
aluminates, he found that a band at 760 cm^{-1} corresponded to vibrations of the Al-O
covalent bond in the crystal lattice. If the Al atoms entered into the anionic framework of
the crystal lattice, a band would appear in this region of the spectrum. If this band was
absent in the spectra of aluminum silicates, the Al atoms act as cations. This same
spectroscopic criterion was used to determine whether the Al atoms are in the anionic or
cationic part of the structure in aluminosilicate glasses.

The following observations were made in the vibrational spectra of two component alkali silicate glasses as the alkali content increases:

1. The spectral band at 1000 cm^{-1} shifts towards lower frequencies. This band is attributed to vibrations of the Si-O-Si bonds. This shift indicates a decrease in the degree of polymerization of the SiO_4 tetrahedrons.

2. When the alkali oxide reaches 20 molar % in the glass, a band in the 920-980 cm^{-1} region of the spectra appears. This band increases in intensity as the alkali content increases. The band is attributed to vibrations of the Si-O bond in non-bridging oxygens. The number of non-bridging oxygens would increase as the amount of alkali-metal oxide increases in the glasses.

3. The band attributed to vibrations of Si-O-Si group, at 760 cm^{-1}, gradually decreases in intensity. This again indicates that the numbers of these linkages are decreasing.

The above information was used in the study of alkali aluminosilicate glasses. Figure II.3 shows the infrared absorption spectra of several three component alkali aluminosilicate glasses with increasing amounts of Al_2O_3.
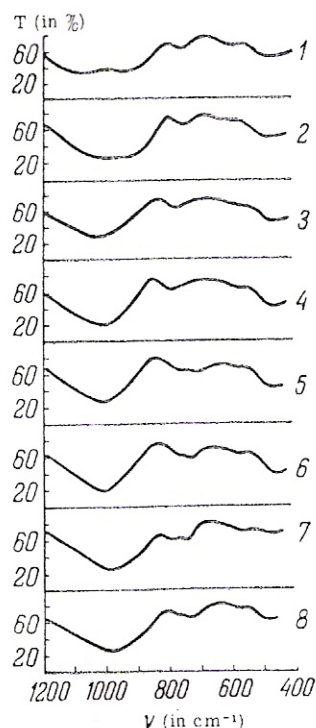
Figure II.3 – Infrared absorption spectra of three-component alkali aluminosilicate glasses (composition in molar %): 1) 31% Na_2O, 5% Al_2O_3, 64% SiO_2; 2) 30.3% Na_2O, 9.1% Al_2O_3, 60.6% SiO_2; 3) 16.6% Na_2O, 8.4% Al_2O_3, 75% SiO_2; 4) albite glass: 12.5% Na_2O, 12.5% Al_2O_3, 75% SiO_2; 5) 16.6% Na_2O, 12.5% Al_2O_3, 70.9% SiO_2; 6) jadeite glass: 16.6% Na_2O, 16.6% Al_2O_3, 66.4% SiO_2; 7) spodumene glass: 16.6 Li_2O, 16.6% Al_2O_3, 66.4% SiO_2; 8) nepheline glass: 25% Na_2O, 25% Al_2O_3, 50% SiO_2 (after Kolesova, reference # 21)

Kolesova first noted the region around 760 cm^{-1} in the alkali aluminosilicate glasses. The band for vibrations of the Al-O covalent bond should appear there. However, this spectrum is complicated by the fact that the spectrum of two component alkali silicate glasses (with no aluminum) has a band identified as one of the vibrations of Si-O-Si. The Si-O-Si band becomes weaker with progressive depolymerization of the glass network. In the spectrum of glass 1, which contains five molar % Al_2O_3, this band is flat and rather diffuse. Also, it is symmetric on the low frequency side. As the Al_2O_3 content of the glass increases, this band develops two maxima. The one at a low

frequency end gradually becomes stronger than the one at the higher frequency end. In the spectrum of nephaline glass, the highest concentration of Al_2O_3, the low frequency component of the band is much stronger. These results suggest that the higher frequency component of the band is derived from vibrations of Si-O bonds, and the low frequency component originates from vibrations of Al-O bonds.

As the Al_2O_3 content of the glass increases, there is an increase in the number of Si-O-Al bonds at the expense of Si-O-Si bonds. It is expected that the higher frequency component becomes weaker and the lower frequency component becomes stronger. This appearance and increase of a band corresponding to vibrations of the partially covalent Al-O bond in spectra of aluminosilicate glasses show that Al enters the anionic framework of these glasses, together with Si atoms, and takes part in the formation of the continuous structure of AlO_4 and SiO_4 tetrahedrons.

The band at about 1000 cm^{-1}, which is designated as vibrations of Si-O in the Si-O-Si system, shifts towards lower frequency with increasing Al_2O_3 content. This is consistent with the idea that Al atoms enter the glass network and replace the Si atoms. The valence vibration frequency of Al-O is lower than that of Si-O, and so it is expected that the system Si-O-Al is less rigid than the system Si-O-Si. Therefore, as the number of Si-O-Al bonds increase at the expense of Si-O-Si bonds, the maximum of the Si-O vibration band should shift towards lower frequencies. This is seen in practice.

In Figure 3, the band in the 950 cm^{-1} region is absent except for the spectrum of glass 1. This glass contains very little Al_2O_3. This indicates that the small number of Al atoms in the structure of glass 1 makes it close to that of two component alkali silicate glasses. In the structure, the Na atoms break Si-O-Si bonds, depolymerize the glass

network, and form Si-O bonds. The Na atoms are grouped near these single-bonded oxygen atoms and balance their charges.

In contrast, the spectrum of glass 2, which has about the same amount of Na_2O as glass 1 but twice as much Al_2O_3, shows one broad diffuse maximum in the 1000 to 950 cm^{-1} region instead of two bands usually found in alkali silicate glass spectra. As the Al_2O_3 content is increased to 25 molar %, the spectrum shows only one band, despite the increased content of alkali metal. This suggests that in these aluminosilicate glasses, the Na atoms no longer act to depolymerize the Si-O-Si network. The reason for this is that in the silicon-aluminum-oxygen network in these glasses, the SiO_4 and AlO_4 tetrahedrons are not equal. The AlO_4 tetrahedron carries an additional negative charge because the Al atom is trivalent and the coordination number of oxygen is four. The negative charge may be balanced by the charge of the alkali metal ion. It seems logical that the alkali metal ions will be situated near the AlO_4 tetrahedrons and not near the SiO_4 tetrahedrons. This would account for the absence of Si-O bonds in the network of alkali aluminosilicate glasses and a band in the 950 cm^{-1} region in the infrared absorption spectra of the glasses.

S. K. Chopra and C. A. Taneja investigated the coordination state of aluminum ions in $CaO-Al_2O_3-SiO_2$ glasses.[22] They were interested in determining the effect of varying the alumina content linearly, from 1 to 7 moles, on the density and refractive index of glasses with the composition 10 CaO, 8 SiO_2, n Al_2O_3.

Density, refractive index, and molecular refraction (K) are affected by a change in the coordination state of aluminum ions. For visible light, the molecular refractions are a measure of the deformation of electronic shells in the unit structure. Aluminum is a small cation of high charge. This makes it essentially non-deformable. Therefore, the

contribution of alumina to the molecular refraction (K_{Al2O3}) is based almost entirely on the refractions of the large, easily deformable oxygen ions. The density and refractive index of the glasses in this study decreased with an increase of alumina. The partial molar refraction of alumina increased with an increase in the content of alumina in these glasses.

The cation-anion distance is less for aluminum in a four-fold coordination state than for a six-fold coordination state. Therefore, the inter-ionic forces would be stronger. This would cause a greater deformation of the oxygen ions and a greater molecular refraction then when aluminum is in six-fold coordination.

A change in coordination of an ion is known to alter the molecular refraction contribution of the ion or the group surrounding it. Since the molecular refraction of the glass increased linearly with an increase of equal amounts of alumina, this signifies that the state of coordination of aluminum ions remains unchanged through the entire sample series. The slope of the linear curve, K/moles Al_2O_3, represents the partial molar refraction (K_{Al2O3}) of alumina. This slope was found to the 12.70. This agrees very well with the work of Safford and Silverman[17], in which they found Al^{3+} in four-fold coordination in glass had a molar refraction contribution of 12.55. They found Al^{3+} in six-fold coordination has a molar refraction contribution of 10.53.

M. Yamane and M. Okuyama investigated the coordination number of aluminum ions in alkali-free aluminosilicate glasses by means of Al Kα fluorescence x-ray spectra.[23] The density, thermal expansion coefficient, and the elastic moduli of the glasses were also measured. The physical properties of these glasses change depending

on whether the coordination number of the Al^{3+} is four or six, and with the variation of glass composition.

The glasses under study were compositions within the range XCaO·(100-X-Y)Al$_2$O$_3$·YSiO$_2$ (wt. %, 50$\geq X \geq$20 , 70$\geq Y \geq$20), and 20 MgO·(80-Y`)Al$_2$O$_3$·$Y$SiO$_2$ (wt. %, 65$\geq Y$`$\geq$45). The reference materials used for the Al Kα fluorescence spectra were Na-feldspar, in which Al^{3+} is in four-fold coordination and dickite, kaolinite, and α−Al2O3, in which Al^{3+} is in six-fold coordination.

M. Yamane and M. Okuyama were able to show that the chemical shifts for the glasses were independent of the CaO content but dependent on the Al/(Al + Si) ratio. In glasses with an Al/(Al + Si) ratio larger than 0.5, the chemical shifts of the Al Kα lines are similar to those of Na-feldspar, indicated that Al^{3+} ions are four-fold coordinated. In glasses with an Al/(Al + Si) ratio less than 0.5, the chemical shifts depended on the silica content of the glasses. The average coordination number of Al^{3+} ions in these glasses increases with silica content. This indicated that as the silica content in the glasses increased, Al atoms are pushed out of the role of network-forming ions in tetrahedra to being six-fold coordinated.

Morikawa, et al.,[24] investigated the short range structure of 12CaO·7Al$_2$O$_3$ glasses using x-ray techniques. The radial distribution function method with the intensity comparison method was utilized. Glasses were formed using a splat cooling method.[25] They sought to determine the nature of the glass forming ability of Al$_2$O$_3$-CaO glasses, and to investigate the structural differences between crystalline and glassy 12CaO·7Al$_2$O$_3$.

Knowledge of how the fundamental AlO_4 tetrahedra are linked is important for the structural analysis of glasses. However, it is difficult to deduce the way the AlO_4 tetrahedra are linked exclusively from the x-ray radial distribution curve. To assist in this analysis, Morikawa, et al., constructed structural models for $12CaO \cdot 7Al_2O_3$ based on crystal structures with similar compositions to the glass. The estimated coordination numbers of Ca and Al atoms are 5.6 and 4.2, respectively. Therefore, the assumption was made that the coordination numbers of network former and modifiers in structural models were four and about six, respectively.

For a structural model constructed from a three dimensional framework of AlO_4 tetrahedra, the crystal structure of $12CaO \cdot 7Al_2O_3$, was used. The average coordination numbers for Al and Ca in this crystal structure are four and six, respectively. For a structural model consisting of sheets of AlO_4 tetrahedra, the crystal structure of $5CaO.3Al_2O_3$ was used. This structural model is shown in Figure II.4. The average coordination numbers for Al and Ca in this crystal structure are also four and six, respectively. For a structural model consisting of chains of AlO_4 tetrahedra, the crystal structure of $(Mg, Fe, Ca)O \cdot SiO_2$ (pigeonite) was used. In this structure, the average coordination number of Si and (Mg, Fe, Ca) atoms are 4 and 6.5, respectively.
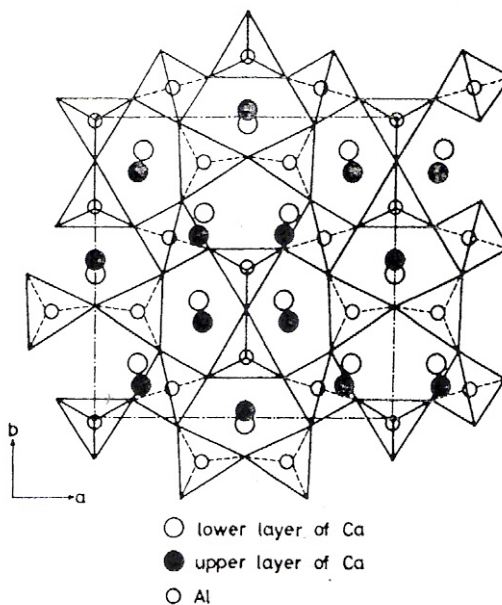
Figure II.4 – Part of the structure of 5CaO.3Al$_2$O$_3$ projected on
(001) (after Morikawa, et al., reference # 24)

Their results for the x-ray scattering intensities of the 12CaO·7Al$_2$O$_3$ glass were

consistent with the 5CaO.3Al$_2$O$_3$ model. They showed that the glass structure was closer

to that of the metastable phase rather than that of the stable phase of 12CaO·7Al$_2$O$_3$.

P. McMillan and B. Piriou[26] investigated the structure of calcium aluminate

glasses and crystals using Raman spectroscopy. The main focus of their research was to

examine the behavior of aluminum in a silica free glass environment. Acknowledging

that the calcium aluminate system did not form glasses easily except in a rather narrow

compositional range, they used a solar furnace melting technique[27] together with splat

quenching to prepare glasses over a wider composition range.

Raman bands for individual phases were assigned by comparing the spectra of a

number of compositions. The following compounds were observed in this study;

tricalcium aluminate (C$_3$A), calcium aluminate (C$_{12}$A$_7$), monocalcium aluminate (CA),

calcium dialuminate (CA$_2$), calcium hexaluminate (CA$_6$), and corundum (α-Al$_2$O$_3$). The

Raman spectra of the calcium aluminate glasses were partially assigned to molecular

groups by comparing the major spectra features of corresponding glasses and crystals.

Considering the molecular structures in the crystals allowed a better understanding of the

possible structures present in the glasses when direct comparisons were not possible. The

crystals in glasses in the CaO-Al_2O_3 system were described in terms of two sections: the

sub-system CaO-$CaAl_2O_4$ and the sub-system $CaAl_2O_4$-Al_2O_3.

P. McMillan and B. Piriou concluded that the Raman spectrum of vitreous

$CaAl_2O_4$ was consistent with a fully polymerized aluminate tetrahedral network. The

additions of CaO resulted in the appearance of the depolymerized aluminate tetrahedral

units triple-bonded AlO and double bonded AlO_2. They found that this was analogous to

binary silicate systems. Around the CA_2 composition, the structure is less well defined.

The brief appearance of aluminum in higher average coordination results from the

instability of the extended structures of depolymerized aluminate tetrahedra. As the

alumina content is increased past $CaAl_2O_4$, highly condensed aluminate tetrahedra begin

to appear in the glass structure. When the alumina content is increased further, these

aluminate tetrahedra are gradually replaced by distorted polyhedra of higher average

coordination.

Engelhardt, et al.[28], employed the high resolution solid state ^{29}Si and ^{27}Al magic

angle spinning nuclear magnetic resonance (MAS-NMR) spectroscopy to study the

structure of calcium aluminosilicate glasses. It is generally accepted that for silicate

glasses, the basic structural unit is the SiO_4 tetrahedron in which vitreous silica is linked

to four such tetrahedra by sharing oxygen atoms. If a metal oxide (MeO) is introduced, a

binary glass of the type MeO-SiO_2 is formed. Non-bridging oxygens, in which the

oxygen atoms are bonded to only one silicon atom, are produced. The net negative charge is balanced by the close proximity of the metal cation.

A ternary glass system of the type $MeO-SiO_2-Al_2O_3$ is even more complicated. In this situation, the glass network may be modified by the replacement of SiO_4 tetrahedra by AlO_4^-. The net negative charge may be compensated by the metal cations or by the formation of more non-bridging oxygens which are charge balanced by octahedrally coordinated Al^{3+} cations. In addition, alumina can be present in the glass as the neutral species $Al^{3+}(AlO_2^-)_3$ or as triclusters of three tetrahedral AlO_4 sharing a common oxygen.

^{29}Si nuclear magnetic resonance was capable of discriminating between the five different SiO_4 tetrahedra; those bonded with 0 through 4 other such tetrahedra. The designation for the structural unit, Q^m_n, was used in which m = 0-4, the total number of bridging oxygen atoms, and n equals the number of Al atoms connected by oxygen bridges with the SiO_4 tetrahedra in the glasses. ^{27}Al nuclear magnetic resonance provided additional information on the coordination number of aluminum atoms in the glass structure because of the well separated peaks for tetrahedrally and octahedrally coordinated aluminum observed in the spectra.

The results of their study on a series of $CaO-SiO_2-Al_2O_3$ glasses using ^{29}Si and ^{27}Al MAS-NMR spectroscopy were as follows:

1. The glass network is made up of one to three co-existing main types of different structural Q^m_n units. The overall chemical composition of the glasses determined the type and quantitative distribution of these units.

2. The Q^m_n units differed only by one bond (SiO double bonded to Al) and the tetrahedrally coordinated aluminum is preferentially bound to the most polymerized Q^m_n units in the glass.

3. The glasses with $CaO = Al_2O_3 \leq 0.5\ SiO_2$ form a fully polymerized, three-dimensional, cross-linked network. If the CaO is increased above the Al_2O_3 content, this leads to the depolymerization of the glass network.

4. The compositional range, $CaO \geq Al_2O_3 \leq 0.5\ SiO_2$, shows that the alumina is tetrahedrally coordinated and completely incorporated into the aluminosilicate network of the glasses. The compositions with $CaO < Al_2O_3$ or $Al_2O_3 > 0.5\ SiO_2$ (and $2CaO \leq SiO_2$) show that the aluminum is present as a neutral, extra network, species. These groups of $Al^{3+}(AlO_2^-)_3$ or triclusters of three tetrahedral AlO_4 sharing a common oxygen, do not act as network modifiers. If there is much more CaO than Al_2O_3 and SiO_2, calcium aluminate will be formed in these glasses.

Engelhardt, et al.[28], acknowledged that the results of their study are not fully consistent with those obtained from the Raman spectroscopy analysis of others.

J.E. Shelby investigated the formation and properties of glasses in the ternary system $CaO-Al_2O_3-SiO_2$.[29] His interest was due to the systems excellent chemical durability, high refractory nature, the high infrared transmission of glasses with no or little silica, and the potential for the production of high temperature glass ceramics[30] from these base glasses.

Figure II.5 identifies the glass-forming regions that Shelby identified in the calcium aluminosilicate system. A very wide range of glass compositions was identified in the system.
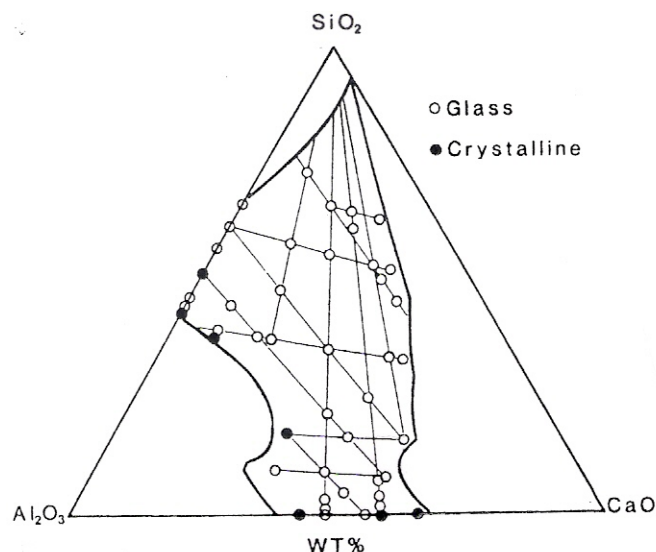
Figure II.5 – Glass-forming region in the calcium aluminosilicate system. A liquidus temperature of $1600^{o}C$ is indicated by heavy solid lines; lighter straight lines indicate compositional series studied (after Shelby, reference # 29)

Shelby performed measurements on the thermal expansion coefficient, the glass transition temperature, the dilatometric softening temperature and the refractive index on these glasses. His results suggested that the structural role of calcium and/or aluminum varies with composition. In compositions of 5 to 60 mole % silica, Shelby explained that a significant change in the structural role of calcium and/or aluminum occurs. The glass transformation and dilatometric softening temperatures increased gradually with decreasing silica content. If it were assumed that calcium merely acts as a modifier in this composition range, these two temperatures would continue to decrease with increasing calcium content. A glass structure with high calcium content and low silica and alumina content should have tetrahedra with no linkages between them. The results actually showed that the glasses became more coherent with increasing calcium content. This implies that the calcium is part of the network, rather than simply a modifying role in the glass structure.

Another interesting phenomenon occurs in compositions with 5 mole % silica.

The results of silica content versus glass transformation temperature indicate that there is

a sudden change in glass structure in this area. Figure II.6 shows these results. The glass

transformation temperature suddenly decreases as the silica content is decreased. In

addition, the difference between the glass transformation and the dilatometric softening

temperatures, $(T_d - T_g)$, increases sharply at about 5 mole % silica. Noting that this type

of behavior in other glass forming systems often indicates phase separation, Shelby

speculated that glasses containing < 5 mole % silica lie in the region of immiscibility.
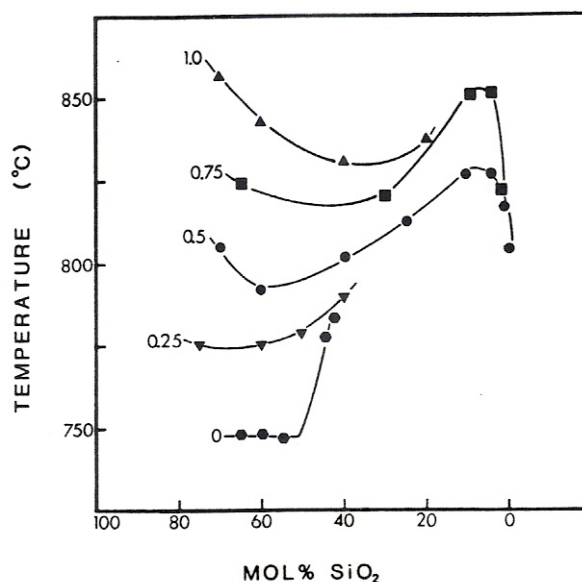
Figure II.6 – Effect of silica content on glass transformation temperature of glasses having a constant Al_2O_3 to CaO ratio, as indicated for each series on the figure (after Shelby, reference # 29)

L. A. Balewick and J. E. Shelby[31] discussed the role of alumina in glass structure

while researching the mixed intermediate effect in calcium aluminosilicate glasses.

Intermediates are defined as those oxides that can directly substitute for a glass former in

the glass network structure, but cannot form a glass by themselves. They term alumina as a classic intermediate oxide. The addition of large amounts of alumina to alkali silicate glasses will increase the viscosity and the glass transformation temperature, and decrease the thermal expansion coefficient of the glass. The changes in these properties suggest that alumina ions enter into the structure in four-fold coordination. They substitute directly for silicon in network, and eliminate non-bridging oxygens.

This direct substitution of aluminum for silicon in the vitreous network substantiates the classification of alumina as an intermediate oxide. This is especially true in that alumina does not form a glass by itself, from a melt, using routine cooling rates. Another factor in considering the classification of alumina as an intermediate has follows: the SiO_4 tetrahedron has a net 4- charge. This charge is balanced through formation of bridging oxygens. These bridging oxygens are linked at all four corners of each tetrahedron with an adjacent tetrahedron. On the other hand, AlO_4 tetrahedra have a net 5- charge. This charge cannot be compensated for by the formation of four bridging oxygens. This tetrahedral unit must be associated with another positive charge. An adjacent alkali ion, in this case a calcium ion, must supply this charge. The use of this calcium ion will, however, present another problem. The net 2+ charge of the calcium ion will force a clustering effect, in at least a pair of RO_4 tetrahedra, and thus will only supply a net 1- charge each.

Balewick and Shelby's research focused on whether the replacement of a monovalent modifier by a divalent modifier has any effect on the lack of interaction between intermediate ions. In other words, does the forced clustering of intermediate tetrahedra results in the appearance of a mixed intermediate effect? In order to obtain

this information, they measured the density, the refractory index, and the infrared spectra of ternary and four component calcium aluminosilicate glasses.

Balewick and Shelby were able to show that alumina occupies isostructural sites in the calcium aluminate glass network. The clustering of the intermediate ion - oxygen tetrahedra does not induce a mixed intermediate oxide effect. By this it is meant that the proximity of the intermediate ions does not force interactions which resulted in non-additive behavior.

Nishida, et al.,[32] examined calcium aluminate glasses in order to determine the relationship between the local structure and physical properties such as the glass transition temperature (Tg) and the high optical transparency in the IR region. ^{57}Fe-Mossbauer spectroscopy[33] was used to determine the glass structure, and DTA measurements were made to obtain the values for Tg. The calcium aluminate glasses were prepared with 5 or 10 mole % Fe_2O_3 for the Mossbauer study.

Nishida, et al., were able to show the following results:

1. Introduction of CaO into the Al_2O_3 matrix results in the formation of non-bridging oxygens in the AlO_4 tetrahedra.

2. The local distortion of the glass network becomes more noticeable within an increasing ionic potential (Z/r) of the alkaline earth metal ions (Ca^{2+}) present at the interstitial sites which are neighboring the oxygen atoms.

3. The Tg of the oxide glasses is proportional to the distortion of the network-forming oxygen polyhedra.

4. The high optical infrared transparency of the aluminate glasses is closely tied to the noticeable local distortion and large number of non-bridging oxygen atoms in the AlO_4 tetrahedra.

The glass formation and thermal properties of low silica containing calcium aluminosilicate glasses was investigated by Higby, et al.[34] They concentrated on CaO-Al_2O_3-SiO_2 glasses containing less than 25 mole % silica. The structure of glasses in this ternary system were studied by investigating the trends in properties such as the refractive index, the glass transition temperature, and the viscosity, as the amounts of the three components were varied.

The additions of silica broadened the range of the CaO/Al_2O_3 compositional ratios that would result in glasses. This indicated that the addition of silica stabilizes the glasses from devitrification. If the silica content was held constant, an increase in the CaO/Al_2O_3 ratio would correlate with a decrease in the glass transformation temperature (Tg). In contrast to this, as silica was added to a silica free glass composition, there are maxima in Tg at a fairly low (< 15 mole %) silica content. Upon further increasing the silica content, Tg decreases steadily.

The refractive index was also affected by the composition. As the silica content was increased, the refractive index decreased. As the CaO/Al_2O_3 ratio was increased, the refractive index increases.

Higby, et al., explained that the Ca^{2+} ions provide charge compensation to the $(AlO_4)^-$ tetrahedra up to a point of charge neutrality ($CaO/Al_2O_3 = 1$). As the calcium content is increased, the Ca^{2+} ions act as network modifiers, inducing the formation of non-bridging oxygens (NBO). If the CaO/Al_2O_3 ratio is increased, the non-bridging

oxygen concentration will increase. One Ca^{2+} ion will charge compensate for two $(AlO_4)^-$ tetrahedra. Therefore, a glass with a CaO/Al_2O_3 ratio of 1.0 and no silica would be a fully connected, charge compensated structure. A composition of this type crystallized immediately when melted by the conventional techniques used in their study.

The Tg data that were obtained in this study were consistent with the appearance of non-bridging oxygens with increasing CaO content in the silica free calcium aluminate glasses. As the CaO/Al_2O_3 ratio increased from 1.34 to 1.8, Tg decreased by 12 degrees Kelvin. This is logical in that it is expected that the presence of non-bridging oxygens will decrease the connectivity of the network of the glass and therefore decreased Tg.

The increase in a refractive index in silica free calcium aluminate glasses is due to the increase in the non-bridging oxygen content. Generally speaking, as the concentration of non-bridging oxygens in the glass structure increases, the polarizability of the oxygen ions increase. This causes an increase in the refractive index. As the CaO/Al_2O_3 ratio increased from 1.34 to 1.8, the refractive index changed by 0.015. As the silica content increases, this relationship of higher refractive index with higher CaO/Al_2O_3 ratio remains.

If the CaO/Al_2O_3 ratio is held constant and the silica content of the glasses is increased, the silica replaces CaO and Al_2O_3 in constant proportion. The refractive index on the glass decreases with an increase in silica content. In this situation, there is a decrease in the polarizability of oxygen ions as silica is added.

The Tg of the calcium aluminate glasses increased significantly with the addition of small amounts of silica, and then decreased as more silica was added. This suggests that a changing role of silica occurs as the silica content is increased for a given

CaO/Al_2O_3 ratio. These results are consistent with those of Engelhardt, et al.[28] At silica contents of 7.7 and 9 mole %, the silica network was fully depolymerized. This means that the silica tetrahedra were not bridged to one another and did not appear to be joined to the aluminate network. At higher silica content, i.e. 26.7 and 27 mole %, Engelhardt's research indicated that the silica was becoming part of the network because SiO_4 species with bridging oxygens were detected. The silica tetrahedra were bridged to aluminate tetrahedra if there were any bridging, and the number of non-bridging oxygens per silica tetrahedra depended on the CaO/Al_2O_3 ratio.

Higby, et al., suggested a possible model for the changing role of silica in the aluminate network. If a given calcium ion either compensates for the net negative charge on a AlO_4^- tetrahedra or induces a non-bridging oxygen between them, it is possible that a Ca^{2+} ion acting to produce a non-bridging oxygen would be in close proximity to another, charge compensating Ca^{2+} ion. SiO_4 tetrahedra do not require charge compensation. A calcium ion that is near a Si-NBO group will be more isolated from other positively charged calcium ions then if it would be associated with an Al-NBO group. The calcium ions would therefore become associated with silica tetrahedra instead of alumina tetrahedra. The aluminate network would then reconnect, causing an increase in Tg. This process of grabbing non-bridging oxygens and reconnecting the aluminate network occurs only as long as silica tetrahedra can exist without becoming a significant component of the glass network, and as long as there are non-bridging oxygens to grab. As the silica content increases further, the silica tetrahedra become a part of the basic glass network. This causes a bridging of the silica tetrahedra with alumina tetrahedra.

Higby, et al.,[35,36] also investigated the effects of silica additions on the stability and infrared transmission edge of calcium aluminate glasses. Two compositional series were investigated. The first contained a constant CaO/Al_2O_3 ratio with varying silica content, and the second contained constant silica content and a varying CaO/Al_2O_3 ratio.

Figure II.7 shows the results of additions of silica on the stabilization of the glasses. The crystallization temperature minus the glass transition temperature ($T_x - T_g$) was used as a measure of glass stability. Figure 7 shows that ($T_x - T_g$) increased as the silica content increased. This clearly shows the stabilizing effect of silica additions in calcium aluminate glasses.
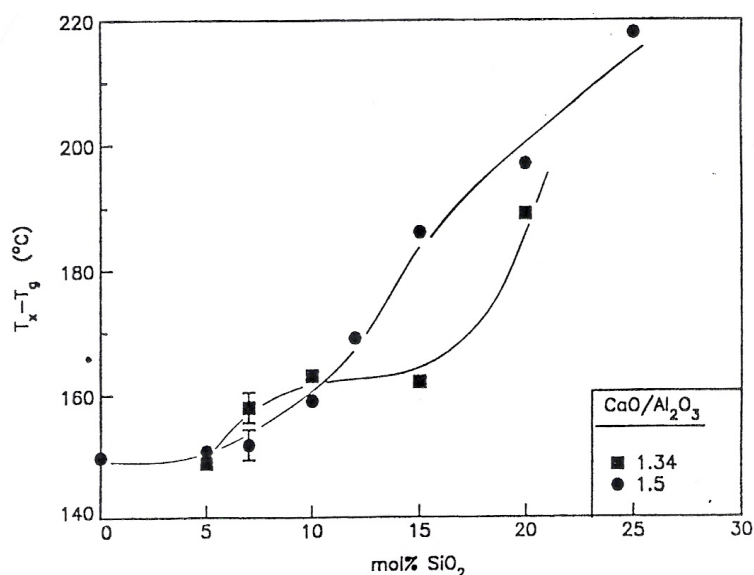
Figure II.7 – Effect of SiO_2 content on T_x-T_g for CaO/Al_2O_3 =
1.3 and 1.8 (after Higby, et al., reference # 35)

The glass stabilization information is useful for determining important parameters for using these glasses in fiber optic applications. For example, in order to produce an optical fiber, a glass blank (preform) must be heated in a furnace and drawn into fiber.

The drawing process must occur at a temperature above Tg so that the viscosity is low enough to fiberize the glass. The temperature cannot be so high that the glass is crystallized and therefore useless as a light guide.

The infrared cut-off wavelength for thin sections of silica is at about 4.5 μm.[2] As the percentage of silica in the calcium aluminate glass increases, the Si-O band will increase in intensity and become in more significant part of the infrared spectrum. Therefore, as the silica content in the glasses increased, the infrared cut-off value will move to shorter wavelengths. This effect is clearly seen in Figure II.8.
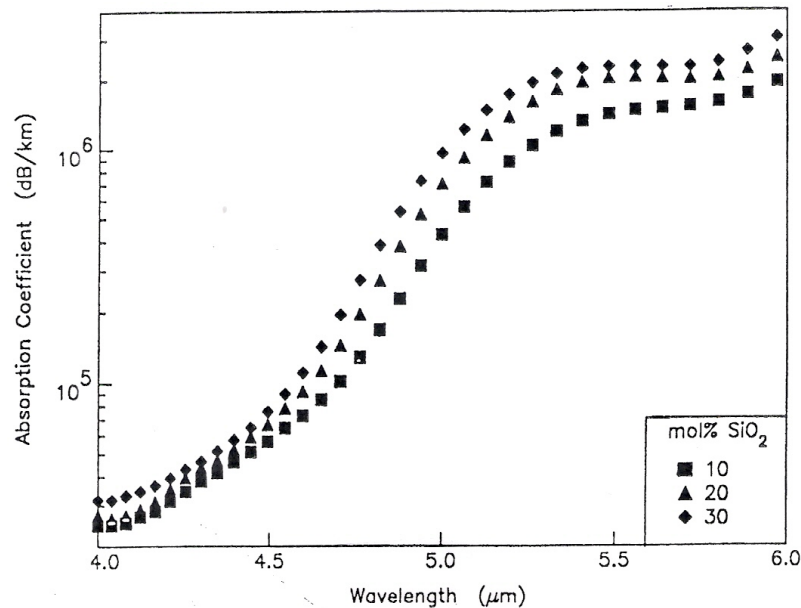
Figure II.8 - Effect of SiO_2 content on the multiphonon edge for
$CaO/Al_2O_3 = 2.0$ (after Higby, et al., reference # 35)

C. Huang and E.C. Behrman[37] performed a systematic investigation on the structure of calcium aluminosilicate glasses as a function of their composition. Extensive Fourier Transform Infrared Spectroscopy (FTIR) was used in this investigation. The composition ranges studied were; Al_2O_3: 0 to 39 mole %, SiO_2: 10 to 75 mole %, and CaO: 13 to 65 mole %.

In their FTIR analysis, they attribute a band seen near 475 cm^{-1} as the vibration of the bridging oxygen. The shift noted in this band toward lower frequencies, with the addition of alumina, is explained as an increase in the number of Si-O-Al bonds. These Si-O-Al bonds have a smaller force constant. The band noted near 700 cm^{-1} is attributed to the AlO$_4$ tetrahedra. The band noted near 800 cm^{-1} is attributed to the Si-O bending and Al-O stretching with the aluminum ions in four-fold coordination.

Calcium ions and aluminum ions affecting the Si-O bonds cause the bands in the 850 cm^{-1} to 1300 cm^{-1} region. The low energy side of this region is most likely due to Si(OAl/Ca)$_3$ and Si(OAl/Ca)$_4$. The band noted near 960 cm^{-1} is attributed to the stretching vibration of the Si-O bond in the Si(OAl/Ca)$_2$ group. The Si(OAl/Ca)$_2$ group is a silicon-oxygen tetrahedra that has two corners shared with aluminum-oxygen or calcium-oxygen polyhedra. The sub region of 1050 cm^{-1} to 1100 cm^{-1} is attributed to the vibration of the Si(OAl/Ca) group. The vibration of this Si(OAl/Ca) group is the stretching vibration of the silicon-oxygen bond of the SiO$_4$ tetrahedra with one corner shared with an aluminum or calcium polyhedron.

Figure II.9 shows the FTIR spectra on glasses with a constant CaO content of 20 mole % and a changing Al$_2$O$_3$ content. The band near 800 cm^{-1}, which is due to the motion of bridging oxygens of the Si-O-Si group, disappears as the silica content decreases. In glasses with a Al$_2$O$_3$/CaO ratio of 0.5, there is always excess lime. As a result, aluminum ions should not be octahedrally coordinated. The excess lime causes an increase in non-bridging oxygens as the amount of silica is decreased. The Si-O stretching vibration mode shifts to frequencies below 1100 cm^{-1} and the band around 800 cm^{-1} appears again. This is a result of the large number of AlO$_4$ tetrahedra. This band

around 800 cm^{-1} is a result of the stretching vibration of Al-O in AlO$_4$ tetrahedra. The 800 cm^{-1} band is the strongest at a silica content of 10 mole %. This is due to their being more alumina tetrahedra than silica tetrahedra at that composition. Another indication of the formation of AlO$_4$ tetrahedra is the increase in the band near 700 cm^{-1}.
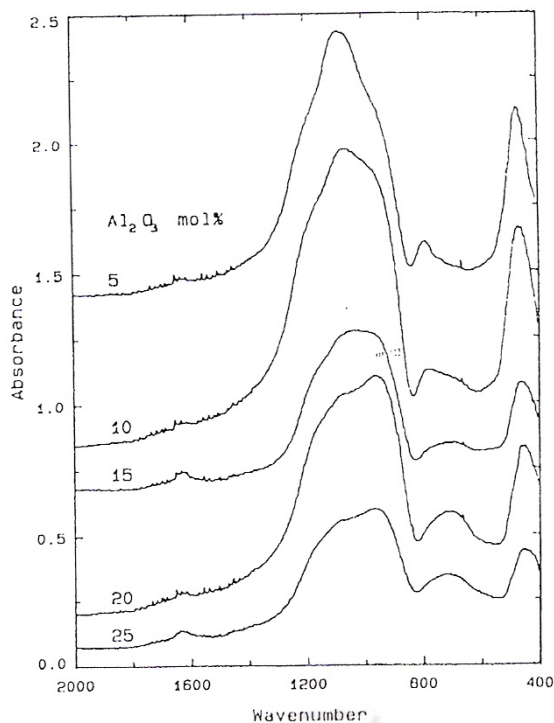
Figure II.9 – FTIR spectra of glasses of constant CaO content
of 20 mol% (after Huang, et al., reference # 37)

C. Huang and E.C. Behrman[37] concluded that the aluminum ions are four-fold coordinated in all the glasses based studied. Charge balancing is attained by the oxygen vacancies and/or triply bonded oxygens associated with the AlO$_4$ tetrahedra. Their results agreed well with those of McMillan[26] and Kolesova[21].

A high-temperature ^{27}Al NMR and Raman spectroscopy study was performed by B.T. Poe, et al., on calcium aluminate liquids[38]. NMR spectra were obtained at 2500 K

by using CO_2 laser heating and sample levitation inside the NMR magnet. High temperature Raman spectra of $CaAl_2O_4$ and $Ca_{12}Al_{14}O_{33}$ glasses and liquids were obtained up to a temperature of 1928 K.

The high-temperature ^{27}Al NMR study indicated that the average aluminum coordination value increases as a function of increasing Al_2O_3 content in calcium aluminate liquids. Both five and six-coordinated aluminum species became more apparent with increasing alumina levels.

The "in situ" high-temperature Raman spectroscopy indicated that the calcium aluminate liquids are composed of molecular aluminate species that are similar to those in the glasses. High-temperature Raman spectra did not show any changes due to network configurational changes above Tg. The only changes in the Raman spectra occurring with temperature were vibrational in nature. These occurred well below the glass transition temperature.

I. Daniel, et al.[39], looked at structural changes in calcium aluminate ($CaAl_2O_4$) glass at high pressure and temperature using Raman spectroscopy. The Raman spectrum was observed as a function of pressure at room temperature up to about 15 GPa. The Raman spectrum was observed as a function of temperature at ambient pressure up to 1650°K.

The "in situ" high pressure experiments indicated that there is a pressure induced increase in the aluminum coordination state. This began at pressures between 8 to 10 GPa. At the same time, there was a coordination increase around the bridging oxygens, through the formation of $^{(3)}O$ species. When the pressure was gradually removed, the glass sample did not completely return to its normal state and retained some of the high

pressure features. I. Daniel, et al.[39], attributed this to changes in the inter-tetrahedral Al-O-Al linkages, as was reflected in the spectra. The results suggested that some highly coordinated species remained in the decompressed state.

The "in situ" high temperature experiments also showed some interesting structural changes. As the glass temperature was increased through the glass transition temperature ($\sim T_g = 1178^oK$), the Raman spectra showed the growth of bands at 600 and 1100 cm^{-1}. I. Daniel, et al.[34], attribute this to the removal of O^{2-} ions from the fully polymerized aluminate network. They feel this resulted in the $^{(3)}O$ species. These $^{(3)}O$ species, or "triclusters" are coordinated by three tetrahedral aluminate groups.

Cormier, et al.[40], investigated the structure of three calcium aluminosilicate glasses with low silica content. The compositions investigated in their study included calcium aluminosilicate samples with the ration of $CaO/Al_2O_3 = 1.6$, and the SiO_2 mole % equal to 0, 10 and 20. Their investigation utilized x-ray and neutron diffraction to determine the coordination states of Si, Al and Ca, in the compositions. By combining these two characterization techniques, an improved understanding of the aluminosilicate network, and the local environment around each constituent element, was obtained.

The data collected by Cormier, et al.[40], suggest that Si and Al are located in tetrahedral sites, and Ca in octahedral sites, for all compositions. Silicon appears to become part of the aluminate network at low mole percentages. This fact is inconsistent with the findings of Higby, et at.[34], who suggested that Si is linked mainly to non-bridging oxygen in low Si mole percentages. Cormier, et al.[40], data also show that there is no evidence of structural modifications through the addition of silica. Also, silicon additions do not seem to play a major part in the changes in Tg. Since there is no

apparent change in coordination around the constituent elements, Cormier, et al.[40],

suggest that medium range molecular rearrangements could account for the change in Tg

with increasing silicon content. Two suggested causes are changes in the arrangement of

Ca neighbors around aluminum, or changes in the network polymerization.

Hannon and Parker[41] also investigated the structure of calcium aluminate glasses

with neutron diffraction. Their method utilized high real-space resolution pulsed neutron

diffraction. Two compositions were studied, $CaO-Al_2O_3$ glasses with 30 and 38 %

Al_2O_3. The glasses were formed using the splat-quenched technique. Their data

indicated that aluminum is tetrahedrally coordinated in both these glasses. The bond

length between aluminum and oxygen was calculated to be 1.76 angstroms. There did

not appear to be any aluminum atoms in higher coordination with oxygen. Calcium was

shown to have well defined bond lengths with oxygen of 2.34 angstroms. There was

some evidence of higher coordination states for calcium with oxygen, with six

coordination being the most probable. However, this exact coordination state was

difficult to resolve because of the overlap with the oxygen-oxygen coordination in these

glasses.

An interesting study was recently done by Benmore, et al.[42], using pulsed neutron

and high energy x-ray diffraction to study calcium aluminate glasses. The glasses were

formed using container-less cooling of liquid droplets that were heated in a laser beam

and suspended in an aerodynamic resonator. The compositions under study were

$CaO:Al_2O_3$ glasses at the 64:36 mol% eutectic and 50:50 mol%, respectively. By

combining the neutron and high energy x-ray diffraction techniques, a detailed picture of

the glass structure was achieved. Benmore, et al.[42], feel that these techniques are highly

complementary due to the neutrons being more sensitive to the positions of the lighter oxygen atoms, and the x-ray scattering being more sensitive to the positions of the heavier Ca and Al component interactions. Container-less aerodynamic levitation was used in order to resolve some of the disparities in previous research on bond lengths and coordination number of Ca and Al. They feel these disparities could result from sensitivity to glass synthesis conditions.

The results of Benmore, et al's.[42], research indicated that the 50:50 mol% glass was composed mainly of AlO_4 tetrahedra, and the 64:36 mol% eutectic glass was predominately a mixture of both AlO_4 and AlO_5 polyhedra. The Al-O bond length was shown to be 1.76 angstroms in the 50:50 mol% glass, and 4.8 angstroms in the 64:36 mol% eutectic glass.

The study of calcium coordination showed interesting results. The average calcium coordination decreased from 5.6 oxygens in the 50:50 mol% glass, to 3.9 oxygens in the 64:36 mol% eutectic glass. However, there was only a 0.02 angstrom shift in the Ca-O bond length between the two compositions. They felt the Ca coordination is either very low or highly distorted in the 64:36 mol% eutectic glass.

The result that the coordination of Al increased with decreasing Al content in the glass was surprising. They explained this in terms of the Ca ion donating oxygen to the aluminum. If this fact is true, then Ca and Al can both be viewed as acting as network formers in these glasses.

Neuville, et al.[43], sought to obtain more information on the local Al and Ca environment in glasses in a recent study using x-ray absorption at the Al and Ca K-edges.

X-ray absorption near-edge spectroscopy (XANES) was the technique that was used. This technique has shown to be particularly sensitive to glass structure.

Glasses under study were compositions along the joins CaO/Al_2O_3 equal to 1, 1.57, and 3. The glasses were formed by melting in a platinum crucible, then dipping the bottom of the crucible in distilled water. The compositions under study are shown in Figure II.10. Spectra of calcium aluminate crystals were used as references.
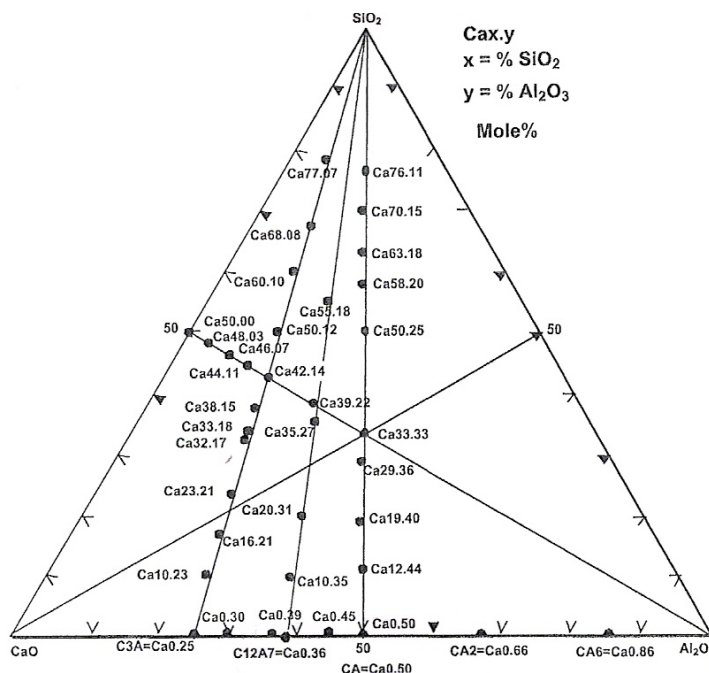
Figure II.10 – SiO_2-Al_2O_3-CaO ternary system (in mol %) with the glass compositions and calcium aluminate crystals used in Neuville, et al., study. (After Neuville, et al., reference # 43)

The compositions studied encompass the range from Ca playing a roll only as charge compensation near $(AlO_4)^-$ tetrahedral to calcium silicate glasses where Ca has the role of a modifier associated with non-bridging oxygens. Neuville, et al.[43], referenced the spectra against that of anorthite crystal. Their results showed that there was little change in the Ca environment between whether it was in a modifying or a charge

compensation site. They proposed that a similar environment around Ca is present, where 6 to 7 oxygen neighbors are in a distorted state.

Neuville, et al.[43], propose that the bridging oxygens of the $(AlO_4)^-$ tetrahedra is modified by composition. Al is present with 2, 3, and 4 bridging oxygens in calcium aluminate glasses, and enters preferentially into 4 bridging oxygen sites with an increase of Al_2O_3 or SiO_2. This causes a change in the connectivity and topology of the glass network and can explain the anomaly in Tg at low silica contents as observed by Higby, et al.[34].

II.3. Nucleation and Crystallization in Calcium Aluminate Glasses

Li and Mitchell[44] performed an extensive investigation on the nucleation and crystallization behavior in calcium aluminate glasses. Their feeling was that there was a lack of understanding in this area. High strength, low loss fibers from calcium aluminates could only be obtained if the crystallization kinetics in the surface and bulk glass matrix were fully understood and controlled. Properly prepared samples could produce nanostructured materials with improved mechanical properties. Extensive crystallization in poorly nucleated samples will cause a decrease in their mechanical properties.

Nucleation and crystallization behavior of both surface and bulk crystallization was studied using differential thermal analysis (DTA), x-ray diffraction (XRD), scanning electron microscopy (SEM), and optical microscopy.

The eutectic composition of 46.5 wt. % CaO, 53.5 wt% Al_2O_3, was the focus of their research. The glass samples were formed by pouring the glass melt and quenching

between two steel plates. The resulting glass was then ball milled and screened to eight different particle sizes. This enabled the collection of DTA data as a function of particle size.

The DTA data showed at least one exothermic peak in the temperature range of 940°C to 1040°C for all samples. The exothermic peak location is due to the onset of crystallization. The location of the exothermic peak was related to the heating rate and particle size. As the heating rate and particle size increased, the exothermic peak shifted to higher temperatures. The XRD results on the resulting crystallization determined that there was two crystalline phases, $Ca_{12}Al_{14}O_{33}$ ($Ca_{12}A_7$) as the major phase, and $CaAl_2O_3$ (CA) as the minor phase. The average particle size was determined to be 35 nm.

The DTA data suggested that the glass particle samples crystallized primarily through surface crystallization. As the particle size increased, the crystallization peak height decreased. The surface to volume ratio increases with decreasing particle size. Therefore, smaller particles will have more surface area than larger particles of the same sample mass, and likewise a larger amount of surface nuclei with decreasing particle size.

Li and Mitchell[39] determined the activation energies by two methods, the Kissinger and the Augis-Bennett method. Activation energies were calculated as 739 +/- 4 kJ/mol by the Kissinger method, and 694 +/- 4 kJ/mol by the Augis-Bennett method. Through the use of SEM and optical microscopy, two crystal structures were noted, dendritic, and spherulitic. In situ XRD and SEM determined that the two distinct peaks noted in the DTA data of monolithic, non-powder glass samples were one for surface crystallization, and one for bulk crystallization.

II.4. Development of Fibrous Glasses with High Elastic Moduli

        G.R. Machlan[45] investigated calcium aluminates for the development of high

modulus glasses. Higher modulus glasses were required for the fiber reinforcing of

plastic materials for strong, low weight composites for the military. The physical

property requirements for the glass to be considered for producing high modulus glass

fibers were:

1. The glass melt had to be viscous is enough above the liquidus temperature so that

fibers could be formed continuously from the melt.

2. The glass had to have a liquidus temperature that was low enough so that it could be

melted and worked in platinum bushings.

3. The chemical durability of the resulting fiber had to be comparable with commercially

available fibrous glass.

4. The resulting glass fiber had to have strength that was comparable to commercially

available fibrous glass.

        The calcium aluminate glass system was chosen because it was believed that the

high modulus of calcium oxide and aluminum oxide would transfer into the glassy

system. In the initial phases of the investigation, he determined the extent of glass

formation in the calcium aluminate system, the modulus of elasticity of these glasses, and

whether properties compatible with fiber formation could be obtained. Machlan reported

that the calcium aluminate glasses generally had high liquidus temperatures, extremely

fluid melts, and rapid rates of devitrification during cooling. These characteristics made

it difficult for nearly all of the glasses to be fiberized by the continuous filament process.

It was only through the addition of small quantities of other oxides, which lowered the

liquidus temperature and increased the viscosity of the melts, that fiberization was possible.

Machlan was able to produce calcium aluminate glasses with bulk elastic moduli between 14 x 10^6 psi and 17 x 10^6 psi. The best fibrous glass produced had a modulus of 13.25 x 10^6 psi. Subsequent heat treatment of these fibers restored the modulus to nearly 15 x 10^6 psi. Glass-plastic composites were produced with properties equivalent to or greater than glass-plastic composites produced from standard textile glass in a similar manner. The best fiber glass was produced from a composition of 27.5 % CaO, 5.2 % MgO, 1.7 % BaO, 5.9 %, Na_2O, 3.0 % K_2O, 46.5 % Al_2O_3, and 9.1 % B_2O_3.

W. Capps and D. Blackburn[46] also investigated glass fibers having high Young's moduli of elasticity. The purpose of their work was to develop glass fiber for reinforced structural material. Greater strength-to-weight ratios and greater rigidity over a wide temperature range was among those improvements being sought. At that time, commercially available glass fibers had about the same Young's modulus of elasticity as aluminum at ordinary temperatures. However, these fibers had significantly higher modulus of elasticity at 750°F. Because of these characteristics, it was believed that glass fibers could be used to reinforce lightweight metals much in the same way as they are used to reinforce plastic materials.

During the course of their research, they identified calcium aluminate glasses as having moduli that were much higher than those of ordinary commercial types of glasses. The Young's modulus of these glasses was identified as being as high as 15 million psi and more.

The National Bureau of Standards had first developed calcium aluminate glasses in an effort to make glasses having good infrared transmission in the wavelength region where silica has a marked absorption. It was interesting during this initial research, but incidental at the time, that these glasses had such high Young's moduli. The composition of this glass was 43 weight percent CaO, 10 weight percent BaO, and 47 weight percent Al_2O_3 with a modulus of 15.8 million psi.

S.D. Brown and G.Y. Onoda[47,48,49] continued to work of Machlan for developing glasses of high elastic modulus. High elastic modulus glasses were required to increase the rigidity of plastic bodies that are reinforced with glass fibers. These composites are attractive for applications where weight is an important consideration because of their high strength to weight ratio as compared with structural metals.

Brown and Onoda conducted an extensive investigation of glass formation among alumina based oxide compositions. Alumina-based systems appeared particularly attractive because of the very high modulus possessed by crystalline alumina (55 million psi) compared with that of silica (10 million psi). They reported that the presence of CaO and a small amount of silica were necessary for good glass formation in this system. Glasses of high modulus are obtained when the interstices of the glass network are filled with ions of high field strength. The interlocking forces caused by the cations in the interstices have a greater effect on a modulus than the forces between the network forming ions themselves. High modulus glasses are characterized by a lower content of network formers (i.e. Si, Al, B) and a higher content of network modifying ions (i.e. Mg, Ca, Ti).[50]

In the ternary system Al_2O_3-SiO_2-CaO, Brown and Onoda investigated more than 300 compositions. They found good glasses at the following compositions, in mole percent:

1. 30 Al_2O_3, 4 SiO_2, 66 CaO

2. 30 Al_2O_3, 10 SiO_2, 60 CaO

When higher quantities of Al_2O_3 were added, the sample melts devitrified.

Brown and Onoda revealed that a necessary, although insufficient, condition for glass formation is that the ratio of oxygen ions to network forming cations (Al^{3+} and Si^{4+}) the between 2.35 and 2.6. If it is assumed that all of the Al^{3+} are tetrahedrally coordinated, the average number of bridging oxygens per tetrahedron is between 2.8 and 3.3.

Using the above two glass compositions as a base, they investigated the substitution of certain oxides to improve the properties of the glasses. The best glass they produced contained a composition of:

$$30\ Al_2O_3,\ 4\ SiO_2,\ 60\ CaO,\ 6\ MgO$$
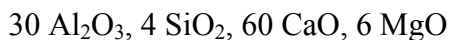
This glass was selected as having the best combination of high modulus (16 million psi), high specific modulus (5.5 million psi), and stability of these properties to small compositional variations.

Brown and Onoda tried several different bushing designs in order to produce glass fibers without much success. Nozzle diameters of 2540, 1270, and 635 μm were tried. In each case, beads of glass formed at the tip of the bushing. These beads either froze and devitrified, or if higher temperatures were used, the bushing flooded. In the best case, only short lengths of fiber were produced.

Glass fiberization was studied by an up-draw process in order to determine the causes of fiberization failure. Fibers were drawn from the top surface of glass melts when the glass had cooled sufficiently to attain the necessary viscosity for fiberization. Several thousand feet of continuous fiber was produced by this method. The success of this method indicated that the control of temperature at the bushing tip for obtaining the correct drawing viscosity is the important parameter.

The fiberization studies of Brown and Onoda were continued by Schroeder, et al.[51,52] A novel fiber pulling apparatus was constructed and fiber of a few thousand feet were manufactured. This fiber pulling apparatus is shown systematically in Figure II.11. The glass sample was contained in a rotating ring shaped crucible that passed under a radiative heating element. The glass sample was, then, alternately melted and frozen as the crucible rotated. In between the molten and frozen zones, fiber could be drawn. This technique was found necessary because all previous fiber drawing experiments, using a variety of stationery bushings, failed. The cause of these failures was because of rapid crystallization of the glass at the orifices. The kinetics of crystallization indicated that the under-cooled portion of the glass be entirely consumed into the fiber or quickly removed from the drawing point and reheat above the liquidus before re-cooling to the fiber pulling temperature.
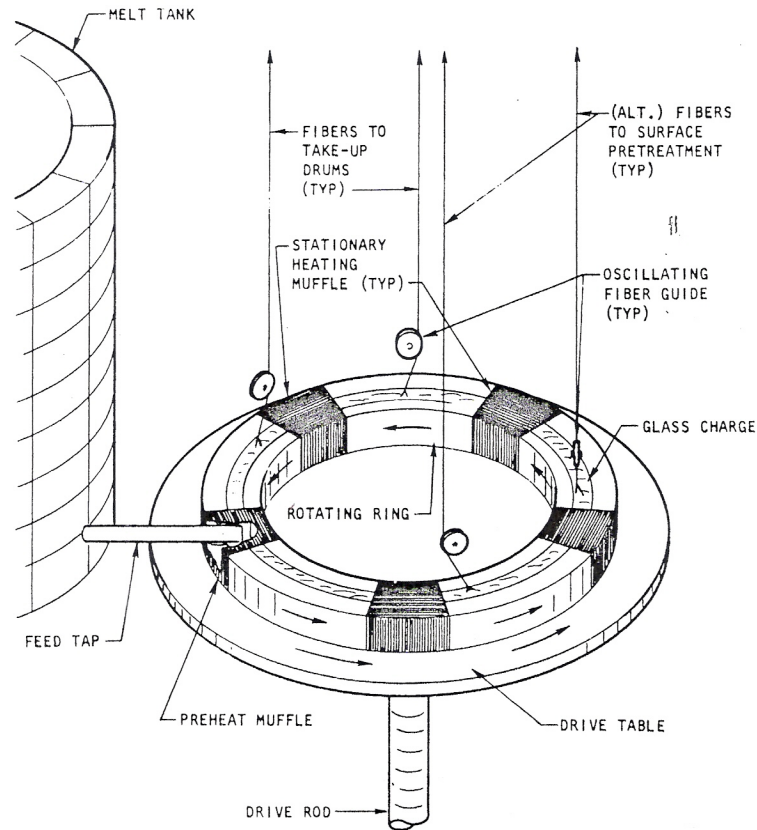
Figure II.11 – Schematic concept of production-scale continuous fiber
drawing apparatus (after Schroeder, et al., reference #'s 51 and 52)

Schroeder, et al., also investigated a means of increasing the static fatigue
resistance of calcium aluminate fibers by the use of protective coatings, made composites
of these fibers in a resin matrix, and investigated the potential of improving existing
properties by controlled conversion of fine grained glass ceramic material. Their results
were as follows:

1. They were able to increase the static fatigue resistance by the use of an effective
    combination of protective coating, coupling aging, and/or highly wetting resin
    formulation.

2. The first calcium aluminate fibers/epoxy resin composites were made. The highest modulus and strength values achieved were 9.9 Mpsi and 182 ksi with a standard epoxy resin and commercial coupling agent.

3. Controlled conversion of the calcium aluminate glass to a homogenous, fine grain crystalline microstructure was achieved.

II.5. Inviscid Melt Spinning

An interesting new technique for obtaining glass fibers was developed by Cunningham, et al.[53] They explained that for a typical molten material of low viscosity, a jet of this material is unstable with respect to surface tension and will break up into small droplets. This breakup into small droplets will occur long before the material has time to freeze. In order to obtain filaments from inviscid melts, it is necessary to either stabilize the jet or increase the freezing rate by several orders of magnitude. Their work focused on the first of these two options.

Inviscid spinning of filaments is accomplished by causing a chemical reaction to form a thin layer on the surface of the jet immediately after it exits an orifice. This stabilizing film prevents the droplet formation of the jet. Normal heat transfer processes can then cause freezing of the material into filament.
Cunningham, et al., discovered that this film stabilizing technique could produce ceramic oxide filaments. They noted that the stabilizing film must be formed by a vapor deposition process. The vapor deposition process that proved successful was the pyrolytic technique.

The pyrolytic technique involved extruding the molten ceramic oxides into the hydrocarbon atmospheres. The thermal energy of the liquid jet material would pyrolyze the hydrocarbon to produce a stabilizing film of pyrolytic carbon. This technique can be used up to the temperature at which the ceramic oxide is reduced by the carbon film. If the temperature is high enough so that the ceramic oxide is reduced by the carbon film, gaseous carbon monoxide is formed. Carbon monoxide will interfere with the formation of carbon stabilizing films.

The inviscid melt spinning technique was successfully used to produce filaments in the CaO-Al$_2$O$_3$, CaO-Al$_2$O$_3$-SiO$_2$, and CaO-Al$_2$O$_3$-MgO system. Spinning temperatures of 1500 to 1950 $^\circ$C were used to produce filament from these compositions. The filaments that were produced at the time were not fully characterized. Wallenberger, et al., [54,55,56] obtained the fibers produced by Cunningham and evaluated them in great detail. They also provided, in greater detail, the description of the inviscid melt spinning process and equipment. A schematic diagram of this equipment can be seen in Figure II.12. They describe the process as taking a predetermined mixture of alumina and calcia powders, placing it in a tungsten crucible, and back flushing argon. The sample is gradually heated to a melt under a mild vacuum and argon is reintroduced above and below the crucible. When the temperature reached 100 $^\circ$C above the melting point, propane was introduced below the crucible and the argon pressure over the melt is increased. The molten jet would then be extruded through an orifice in the bottom of the crucible. If a stable jet was consolidated, a straight fiber would be obtained; if a deflection plate was inserted, a coiled fiber would be obtained; and if the jet stability was lost, a fiber with frozen Rayleigh waves as well as shot would be produced. The 17

amorphous calcium aluminate fiber compositions that were originally investigated are

listed in Table II.2.
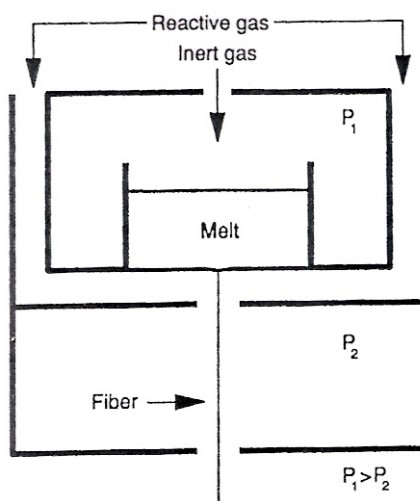
Figure II.12 – Schematic drawing of the inviscid melt spinning process. For calcium aluminate fibers the reactive gas was propane, the inert gas was argon. (after Wallenberger, reference #54)

Fiber No.	Measured (nominal) wt%				Spin temp. (°C)
	Al_2O_3	CaO	MgO	SiO_2	
S-Glass	(25)		(10)	(25)	
1	51.5	41.0	7.5		1500
2	(54)	(46)			1500
3	54.0	39.0	3.0	4.0	1700
4	54.1	38.9	3.0	4.0	1700
5	54.6	39.0	2.5	3.9	1500
6	54.8	38.9	2.5	3.8	1500
7	56.5	43.5			1500
8	59.0	40.8	0.2		1500
9	59.1	40.9			1700
10	60.8	39.1	0.1		1700
11	(65)	(35)			1700
12	66.5	33.5			1700
13	66.8	33.2			1700
14	66.8	33.2			1800
15	(67)	(33)			1700
16	67.6	32.4			1700
17	80.2	19.8			1800

Table II.2 – Amorphous Calcium Aluminate Fibers: Composition and
Spin Temperature (after Wallenberger, reference #54)

Wallenberger, et al.,[57,58] described all the fiber samples as having a carbon sheath. For some of the samples, this sheath was so thin that the fiber appeared to be optically transparent. For other samples, the sheath was so thick that the fiber was black and opaque. The thick sheath often had two components; a crust layer that could be removed by mechanical means, and a thin, chemically modified layer that had a thickness of less then 200 nm.

Wallenberger, et al.,[59,60] evaluated the tensile strength of these 17 fiber samples from Cunningham. All fibers showed brittle fracture, which usually initiated at surface flaws. Using an Instron, they recorded tensile strength of 21 to 151 kpsi, with fiber diameters of 141 to 450 μms. The gauge lengths were 0.25 inches and 2.0 inches. The high temperature strength of these samples was also evaluated.[61,62] Seven amorphous fiber samples were measured at 750 degrees C., 1,000 degrees C., and 1,250 degrees C. These samples are listed in Table II.3. Measured tensile strength ranged from 65 to 151 kpsi at room temperature, 32 to 129 kpsi at 750 $^{\circ}$C, and 0.2 to 18 kpsi at 1000 $^{\circ}$C. The 80.2 percent alumina sample showed a tensile strength of 4 kpsi at 1250 $^{\circ}$C. These calcium aluminate fibers seemed to lose their strength quickly because of changes that occurred at the crystallization temperatures (969-1021 $^{\circ}$C).

Al$_2$O$_3$ Content %	Fiber Diameter μm	Measured Tensile Strength Kpsi (# of specimens tested)			
		R.T. [1]	750°C	1000°C	1250°C
54.0	200	65(3)	43(3)	.3(3)	—
59.0	225	107(3)	32(3)	2(3)	—
60.8	220	78(3)	50(3)	.2(3)	—
66.8	105	105(3)	72(3)	.4(3)	—
66.8	218	109(5)	95(3)	5(2)	—
67.6	111	111(3)	45(3)	3(3)	—
80.2	150	151(3)	129(3)	18(3)	4(1)
S-Glass		600	185	0	

Table II.3 – Tensile strength of as spun, amorphous fibers
(after Wallenberger, reference #'s 61 and 62)

An S-glass fiber sample was used as a control against the seven calcium aluminate fiber samples. The S-glass control had tensile strength of 600 kpsi at room temperature, 185 kpsi at 750 °C, and 0 kpsi at 1000 °C. These high temperature strength results suggest that their crystallization temperatures might ultimately limit the tensile properties of these calcium aluminate fibers. In addition, the calcium aluminate fibers might tolerate temperatures 100 to 200 °C higher than S-glass fibers in fiber reinforced composites.

The infrared transmission properties of these calcium aluminate fibers were also evaluated by Wallenberger, et al.[59,61] The fibers were embedded in a resin and cut to 0.43 mm in length. These fiber cross sections were metallographically polished and the spectral transmission was measured in the axial direction. Visible, near-infrared, and infrared spectrum out to 7.0 μms was obtained on these cross-sections. The IR spectrum was similar to those of the bulk glasses used in military and commercial applications.[62] The transmission curves can be seen in Figure II.13.
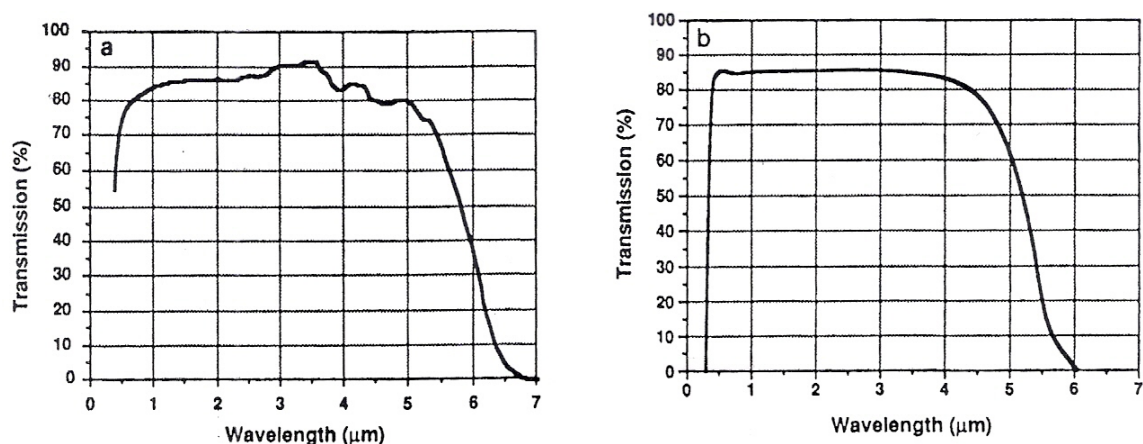
Figure II.13 – Anhydrous calcium aluminates. (a) Glassy fiber with 56.5% alumina; (b) bulk glass with 40.8% alumina (after Wallenberger, reference #62)

Wallenberger, et al.[63], investigated manually drawing fiber from glass blanks supplied by Sassoon Advanced Materials Limited.[64] Two samples were investigated. One was silica containing, and one did not contain any silica. The non-silica containing sample was an alumina-calcia-magnesia-baria glass (46.1-36.1-4.0-13.8). The sample containing silica was an alumina-calcia-magnesia-silica composition (46.1-36.1-4.0-13.8). Fibers were made by up, down, and horizontal drawing. The up drawing process involved taking a piece of the calcium aluminate blank and melting it in a platinum crucible. The surface of the cooling melt was contacted with an ordinary glass rod and fiber was pulled up from the melt. The down and horizontal drawing was accomplished by melting the center section of a calcium aluminate preform with an oxy-acetylene torch. During a down drawing process, one end of the glass sample was suspended, and fiber was drawn down. During the horizontal drawing process, both ends were pulled away from each other during heating process to produce the fiber.

Wallenberger, et al.,[65] reported that "strong" fibers, up to two meters in length, were made from the melts of both compositions. The fibers were produced by up draw

and horizontal drawing. The low silica fiber samples had average reported strengths of 0.2 mpsi and a maximum strength of 0.4 mpsi for a 10 μm fiber diameter. The non-silica sample showed the same fiber strengths as the low silica sample but for a 20 μm fiber diameter. No mention was made in this reference of the diameter tolerances held during these fiber pulling processes.

Wallenberger, et al.,[65] investigated the surfaces of fibers after exposing them to be to 82 degrees C. and 95 percent relative humidity in a steam box for 24 hours. Carbon coated fibers manufactured by inviscid melt spinning and uncoated fibers made by manual drawing were evaluated. The carbon coated fiber with 67 percent alumina remained nearly unchanged after the hot wet treatment. The non-silica containing sample showed a massive over-growth of calcium rich crystals after this hot-wet treatment. These calcium rich crystals were identified as $CaCO_3$ by x-ray diffraction. Electron microprobe x-ray showed that the crystallization proceeded inward from the fiber surface. Overall, the hydrolytic stability of uncoated calcium aluminate fibers between 46 percent alumina and 67 percent alumina was poor. The carbon sheath or coating obtained by inviscid melt spinning provides no improvement at alumina levels lower than 54 percent. However, at higher alumina levels (68 percent) there is a drastic improvement in hydrolytic stability.

The carbon coating obtained by the inviscid melt spinning technique, was investigated in greater detail by Wallenberger, et al.[65] As previously stated, the decomposition of propane forms a black carbon sheath or film on the surface of the fibers. This carbon sheath can be thermally or mechanically removed. Scanning electron microscopy of polished cross sections showed that the sheath was up to 600 nm thick.

The carbon rich skin was found to be a permanent, integral part of the fiber. The depth of this carbon rich skin was not able to be resolved using the scanning electron microscope. In order to obtain a depth profile on the carbon rich permanent skin, sputtered neutral mass spectrometry (SNMS) was employed. This technique showed that the carbon rich skin was approximately 20 to 50 nm thick. This technique also showed that the carbon sheath on the fiber surface could be up to about 800 nm thick.

Wallenberger, et al.,[66,67,68] evaluate calcium aluminate glass fibers in terms of their product outlook and product value. They possess a higher modulus than S-glass, and as such, can be used to form composites that yield major weight and energy savings in cars, aircraft, and aerospace components. Stiffer composite parts could also be useful in the emerging bridge and construction markets. They possess superior alkali resistance that is an important advantage in cement composites.

The infrared transmission properties of calcium aluminate glass fiber opens up the potential for their use as infrared sensing fiber. In that they are much less expensive to produce, they appear capable of replacing commercial single crystal sapphire fibers. Wallenberger estimated that the costs of fully developed calcium aluminate fibers would not exceed $6.6 dollars/kg as opposed to commercial sapphire fibers at $4400 dollars/kg However, single crystal sapphire fibers do offer superior high temperature capability ($\sim$1400 ^{0}C) in relation to that of calcium aluminate fiber ($\sim$950^{0}C).

Y. Sung and J. Sung[69] investigated the crystallization behavior of CA glass fibers produced by inviscid melt spinning. Differential thermal analysis, (DTA) was used to study as-spun and fully nucleated CA glass fibers. Different heating rates were used during the DTA scans. The results were analyzed to estimate the activation energy and

the modes of crystallization. In addition, x-ray diffraction was used to determine the products of crystallization.

DTA analysis was performed from 600 to 1200 $^{\circ}$C with heating rates of 10, 15, 20, 30, 40, and 60°C/min. All scans were performed in an air atmosphere. The activation energy for crystallization was determined from these results by applying Kissinger analysis, and Ozawa analysis was used to obtain the crystallization mode.[69] Fully nucleated fiber samples were obtained by taking as-spun fibers and heat treating them. Heat treatment was done at the glass transition temperature (Tg) for 1, 2, 4, and 6 hours to obtain total nucleation. DTA was employed after heat treatment to determine the time for complete nucleation.

The Kissinger DTA analysis method yielded the activation energy by examining the peak temperatures and peak heights on the DTA curves. As the heating rates increased, the peak temperatures and peak heights increased. This variation in crystallization peaks is used to estimate the activation energy for crystallization and crystallization mode. According to the Kissinger analysis on the as-spun CA fibers, the activation energy for crystallization was 569 kJ/mol. Fully nucleated fibers had an activation energy of 546 kJ/mol. This lower activation energy for the fully nucleated samples is attributed to the increased number of nuclei versus the as-spun fiber samples. The determination of the crystallization mode is used to differentiate between surface and bulk crystallization. Ozawa analysis showed that the as-spun CA fibers had predominately a bulk crystallization mode, with a small portion of surface crystallization. Ozawa analysis on fully nucleated samples showed the same predominant bulk crystallization to surface crystallization, but with a slightly higher surface crystallization

component. X-ray diffraction analysis on the crystallized CA fibers showed the existence of two major crystalline phases, $Ca_{12}Al_{14}O_{33}$ and $CaAl_2O_4$.

B.S. Mitchell[70] used micro-Raman analysis to study CA glass fibers produced by inviscid melt spinning. The micro-Raman technique provides compositional and chemical bonding information as in traditional vibrational spectroscopies, such as Fourier Transform Infrared Spectroscopy or Raman techniques. Micro-Raman has the advantage of a smaller analysis spot size of 2 μm, providing information on compositional changes within a small area. Mitchell collected two sets of micro-Raman spectra, along various points on the fiber surface along the length, and in 2 μm increments along the cross-section starting at the surface and moving inward.

Results of the micro-Raman analysis revealed that pyrolytic graphite is present in a band of 15 μm in the fiber surface. This was consistent with the results along various points on the fiber surface along the length. Analysis of the fiber area inside of this 15 μm band in the fiber bulk was consistent with amorphous calcium aluminate ($CaAl_2O_4$).

II.6. Alternate Compositions

J.A. Durham and S.H. Risbud[71] investigated low silica calcium aluminate oxynitride glasses. Glasses were synthesized by quenching $CaO-Al_2O_3-MgO-SiO_2-AlN$ melts. Primarily, they were interested in noting the extent and effect of nitrogen on the properties of the resulting glasses.

Rapid quenching was achieved by taking the hot melt at 1700° C in an induction furnace and immediately immersing the melt crucible in liquid nitrogen. Using this quench technique, the solubility limit of nitrogen is the glasses was about 3.1 atomic %.

Experimental observations also showed that the glass transition temperature, density, and microhardness values increased with nitrogen additions.

Shelby, et al.,[72] investigated calcium fluoroaluminate glasses in which CaF_2 was used to replace CaO. Their investigations show that the transformation range viscosity, refractive index, and glass transformation temperature decreased as CaF_2 was substituted for CaO in the glasses. The thermal expansion and electrical conductivity increased with CaF_2 substitution. No detectable change in the infrared cutoff wavelength was noted during the CaF_2 substitution. Through the use of magic angle spinning nuclear magnetic resonance, they confirmed that the aluminum ions in these glasses were in tetrahedral coordination. This confirmed the work previously outlined by others.

Shelby, et al.,[72] noted that the hydroxyl content of the base glass for the calcium aluminates decreases upon the addition of CaF_2. The hydroxyl content decreased roughly by a factor of two with the addition of 5 mole % CaF_2. Only a small change in hydroxyl content was seen with further additions of CaF_2. This showed that only a small amount of fluorine was needed to remove whatever hydroxyl content could be removed by this process. These results are shown in Table II.4.

Mol % CaF_2	Cutoff wavelength (μm)	Relative hydroxyl concentration (Abs/mm)
0	6.10	0.204
5	6.12	0.086
10	6.11	0.078
15	6.11	0.074

Table II.4 – Infrared properties of calcium fluoroaluminate
glasses (after Shelby, et al., reference # 72)

J. E. Shelby and C. E. Lord[73] continued the work on the ternary system CaO-Al_2O_3-CaF_2. They showed that calcium fluoroaluminate glasses could be formed in 10-gram quantities with compositions ranging between 30 and 40 mole percent Al_2O_3 and with 18 to 20 mole percent CaF_2. They suggested that the structure of these glasses is analogous to those of similar silicate glasses. In the structure, aluminum ions replace silicon ions and fluorine acts as a non-bridging anion.

J. E. Shelby and R. M. Slilaty[74] investigated calcium gallioaluminate glasses. They were interested in determining if the substitution of gallium, a heavier and lower field strength ion than alumina, would shift the infrared cut-off wavelength to larger values than for calcium aluminate glasses.

Glasses were prepared containing 63 or 67 mole percent CaO with varying ratios of Ga_2O_3 and Al_2O_3. Their results showed that the replacement of alumina by gallia strongly reduces the glass forming ability of the melts. As the gallia concentration increased, smaller batches and quenching methods were necessary in order to form glasses. They did, however, prove that the replacement of alumina by gallia improves the infrared transmission of glasses. The infrared cut-off wavelength increased from 5.95 to 6.5 μm as Ga_2O_3 replaced Al_2O_3.

W.A. King and J.E. Shelby[75] investigated strontium containing calcium aluminate glasses. As with other J.E. Shelby investigations, a novel additive was identified for addition to calcium aluminate glasses to improve glass formation without reducing the infrared transmission. In this particular study, strontium was used as replacement for calcium. Using conventional melting techniques, glasses were produced containing 0 to 17 mole percent SrO, 45 to 70 mole percent CaO, and 30 to 40 mole percent Al_2O_3.

The results of their investigation showed that the glass formation limit was shifted slightly towards higher alumina content as strontium oxide was added. Glasses containing no crystals were produced in 5-gram quantities in compositions with less than 17 mole percent SrO. A sudden onset of crystallization was seen for larger SrO additions.

In compositions containing constant alumina content, the glass transformation temperature decreased slightly with increasing SrO concentration. This behavior is consistent with the current structural model for calcium aluminate glasses. In this model, calcium ions reside in interstices in the glass network and provide charge compensation. As the larger Sr ion substitutes for Ca ions, the modifier field strength is lowered and the overall structure is not as tightly bonded. This causes the glass transformation temperature to be lowered.

The infrared spectra studies indicated that the replacement of calcium by strontium had very little influence on the infrared cut-off frequency. This result was surprising. It was expected that the larger mass of the strontium ions and the decrease in field strength would cause a slight upward shift in this cut-off wavelength. Overall, King and Shelby were able to show that the partial substitution of SrO for CaO improved the glass-forming ability of calcium aluminate glasses without degrading or significantly improving the infrared properties.

II.7. Sol-Gel Calcium Aluminates

M. Uberoi and S. H. Risbud[76] investigated using the sol-gel technology to produce amorphous powders in the $CaO-Al_2O_3$ system. They recognized that calcium

aluminate glasses required high processing temperatures during conventional melt-quench techniques. The strong tendency of these glasses to crystallize during the cooling of the melt poses many problems for glass formation by melt quenching processes. They sought to use the sol-gel techniques to synthesize pure and homogeneous $CaO-Al_2O_3$ powders at temperatures lower than those used in melt processing.

Synthesis of calcium aluminate gels was accomplished by using aluminum chelate and calcium nitrate as starting materials. These materials were added to isopropanol and stirred for several hours. After stirring in water and HCl, the solution was poured into covered petri dishes and allowed to dry slowly for 14 to 18 days. The gels were then heated to $900^{o}C$ at a heating rate of $5^{o}C$ per minute. The gels were kept at $900^{o}C$ for 16 hours. By this method, they were able to produce highly reactive, x-ray amorphous calcium aluminate powders containing 63 mol% CaO.

A.A. Goktas and M.C. Weinberg[77] investigated the synthesis, characterization, and crystallization behavior of several calcium aluminate compositions by the sol-gel method. Three calcium aluminate gels of the following compositions (in wt%) were produced: $30CaO^.70Al_2O_3$, $50CaO^.50Al_2O_3$, and $70CaO^.30Al_2O_3$.

The three calcium aluminate gels were prepared by using aluminum sec-butylate $(Al(OC_4H_9)_3)$ as the source of alumina, and $Ca(NO_3)_2^.4H_2O$ as the CaO source. An H_2O-HCl solution, precise mixing times and methods, and ethanol were required to produce amorphous bulk gels. The amorphous nature of these bulk gels was confirmed using x-ray diffraction analysis.

Crystallization behavior of the gels was studied by using long-time heat treatments. All bulk samples showed relatively low crystallization temperatures in the range of 500 to 900°C. No glasses were reported to the obtained from these bulk gels.

II.8. IR Transparent Glass-Ceramic

Calcium aluminate glasses have also been investigated for use as glass ceramic materials. J.A. Topping[78] studied the system $CaO-Al_2O_3-SiO_2$ for this purpose. Using 18 wt% TiO_2 as a nucleating agent, Topping sought to determine the extent of the range of compositions from which useful glass ceramics could be made.

The optimum nucleation range was found to be near the annealing point of the glasses. Therefore, a ceramic heat treatment of 5 hours at 750°C followed by 1 hour at 950 °C produced fine-grained, bulk-nucleated glass ceramics. The thermal expansion coefficients are in the range of 69 to 82 X 10^{-7} °C^{-1} for these materials. Topping suggested that a potential commercial use for these calcium aluminate glass ceramics would be for specialty glass/ceramic/metal seals.

A.K. Nandi, et al.,[79] prepared glass ceramic materials from calcium aluminate glass containing no silica. Calcium aluminate glass, of the composition $Ca_{12}Al_{14}O_{33}$, was prepared by melting $CaCO_3$ and Al_2O_3 in a platinum crucible at 1500°C. Crystallization of the glass was achieved by taking the air quenched glass melt and heating it at 1150 °C for one hour. X-ray diffraction techniques confirmed the glass ceramic to be a single phase calcium aluminate, $Ca_{12}Al_{14}O_{33}$, with some glassy phase.

Nandi, et al.,[79] showed that there was a large infrared window for these calcium aluminate glass ceramics between the hydroxyl absorption band at 2.895 μm and the

infrared cutoff at approximately 11.11 μm. The transparency spectrum is comparable to currently used infrared materials such as sapphire, ALON, spinel, yttria, ZnS and $CaLa_2S_4$. This optical characteristic makes the calcium aluminate glass ceramic suitable for missile dome materials. In addition, the high refractive index (1.605) makes it suitable for use as antireflective materials.

II.9. Ultraviolet Sensitivity

The development of photosensitive materials has recently been driven by an increasing requirement for information storage devices accessible by light. The photosensitivity reported for most oxide glasses is provided by doping optically active components. As an example, Stookey invented a photosensitive soda lime silica glass by doping it with Ce^{3+} and Au^+.[80]

In 1985, Hosono, et al.,[81] discovered that dopant free calcium aluminate glasses displayed a photosensitivity affect. They found that dopant free glasses in the binary system, $CaO-Al_2O_3$, exhibit a high sensitivity to ultraviolet radiation.

Glasses were prepared in the compositional range of 63 to 65 mol % CaO using conventional melt quenching techniques. The resulting 1.5-mm thick glass plates were illuminated with a 500-watt deep UV lamp supplying energy of approximately 530 J/cm^2. Using a spectrophotometer, Hosono, et al., showed that there was the distinct change in the transmission spectrum upon illumination with UV radiation. These induced absorptions were preserved after the interruption of the illumination at ambient temperature. The change in the transmission spectrum is noted in Figure II.14.
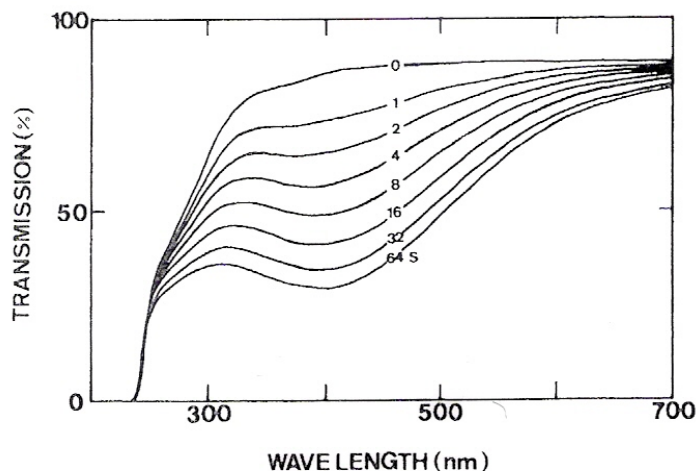
Figure II.14 – Change in the transmission spectrum of $60CaO-40Al_2O_3$ (mol%) glass (1.5 mm thick) on illumination with ultraviolet radiation (numbers on curves represent illumination time) (after Hosono, reference #81)

Hosono, et al., attributed the photosensitivity of these glasses to the appearance of new absorption bands around 400 nm. These induced bands could be bleached out completely by heating the sample up to about 250 °C. The coloring-bleaching process was shown to be completely reversible by repeated cycling of illumination and heating. Using electron spin resonance (ESR) equipment, a clear correlation was found between the intensities of the UV-induced optical absorption and an aluminum-oxygen hole center defect concentration in the glass.

During the course of continued investigations, Hosono, et al., showed a number of photosensitive characteristics of calcium aluminate glasses.[82] The coloring-bleaching was observed in binary $CaO-Al_2O_3$ compositions ranging from 46 to 75 mol % CaO. In addition, they showed that the UV sensitivity was markedly reduced by the addition of silica or germania to calcium aluminate glasses. This is compatible with the fact that conventional aluminosilicate glasses are insensitive to UV rays.

The UV sensitivity of calcium aluminate glasses depends strongly on the wavelength of illumination. As the illuminating wavelength decreases below 270 nm, the induced absorption bands appear, rapidly increase to a maximum, and then decreased. The decreasing in the absorption bands at lower ultraviolet illumination wavelengths is attributed to a rapid increase in the absorption coefficient for wavelengths below the transmission edge of the glass.

The UV induced optical bands and ESR signals indicated the presence of two types of paramagnetic color centers responsible for the UV induced coloring. Hosono, et al., concluded that these color centers are an aluminum-oxygen hole center (Al-OHC) and an ozonide (O_3^-). They proposed the following mechanism to explain the high UV sensitivity of dopant free calcium aluminate glasses:[83,84] Upon exposure to ultraviolet radiation, a peroxy linkage that connects two tetrahedrally coordinated Al^{3+} atoms, homolytically dissociates. This dissociation results in a pair of Al-OHC's by absorbing UV quanta. One of the resulting Al-OHC's combines with a nearby oxygen molecule to form an ozonide. The rapid coloring by the radiation is attributed to high quantum efficiency for homolytic cleavage of peroxy linkages. The ozonide formation prevents the re-combination of the Al-OHC pair by separating the distance between the unpaired electrons. This causes the stabilization of UV induced coloring. The thermal bleaching would correspond to this reaction in reverse, starting with the decomposition of the ozonide.

Hosono and Abe examined the effects of melting atmosphere and heat treatment on the photosensitivity of dopant free calcium aluminate glasses.[85] Batches were melted under atmospheres of oxygen, air, nitrogen, and carbon monoxide. Their results showed

that the photosensitivity of calcium aluminate glasses is significantly suppressed as the partial pressure of oxygen is reduced in melt atmosphere. They speculated that a reduction partial pressure of oxygen in melting atmosphere might bring about a decrease in the concentration of the peroxy linkage as well as the dissolved oxygen molecule.

Hosono, et al.,[86,87] continued to investigate calcium aluminate glasses by exploring the photosensitivity in strongly reduced samples. They found that strongly reduced calcium aluminate glasses show photochromic responses. Graphite crucibles with graphite plate covers were utilized to obtain the strongly reduced condition in calcium aluminate melts. Upon illuminating the reduced calcium aluminate glasses with UV radiation, absorption bands centered around 600 nm appeared rapidly. When the illumination was interrupted, the induced absorptions decayed to the original level at ambient temperature, but remained stable at 77 $^{\circ}$K. Using information obtained by ESR, they speculated that the absorption was occurring from an electron-trapped center. This center is an electron trapped at the site of certain oxygen vacancies surrounded by Ca^{2+}.

II.10. Infrared Glass Material Overview

The ability for a glass to transmit in the infrared region is determined by the frequency of vibration of the cation-anion bonds. The highest wavelength in the infrared that the glass will transmit is called the absorption edge cutoff wavelength. The calculation of this vibrational frequency is difficult in glasses because of their inherent disordered structure.

An estimation of vibrational frequency can be made from the following equation:

$$v = \frac{1}{2}\pi\sqrt{k/\mu}$$, where for given masses m_1 and m_2;

μ = the reduced mass, $m_1m_2/(m_1 + m_2)$

k = the force constant, indicative of bond strength

The calculation of the fundamental absorption frequency for a linear polar diatomic molecule can made from this equation. However, when this diatomic molecule is situated in a glass structure, the calculated frequency is changed by the influence of all the other components in the structure. For example, bond strengths and bond lengths vary in a glass structure.

The influence of network forming components on the infrared absorption edge of a glass can be approximated from the field strength, Z/r^2, where Z is the ionic charge and r is the crystal ionic radius. Generally speaking, glasses that transmit in the infrared are composed of larger anion and cations with lower field strengths. However, lower field strengths and the resulting weaker chemical bonding will limit the available compositions that form glasses. Weaker bonding causes a degradation of physical and chemical properties. [88] Table II.5 shows the mass and field strength of glass forming ions.

	Charge (z)	Mass (m)	Radius (r)	Field strength (z/r^2)
B	+3	11	0.23	57
P	+5	31	0.35	41
Si	+4	28	0.42	23
Be	+2	9	0.35	16
Ge	+4	73	0.53	14
Al	+3	27	0.51	12
As	+3	75	0.58	8.9
Ga	+3	70	0.62	7.8
Hf	+4	179	0.78	6.6
Zr	+4	91	0.79	6.4
Sb	+3	122	0.76	5.2
Te	+4	128	1.02	3.8
Th	+4	232	1.02	3.8
Bi	+3	209	0.96	3.3
Pb	+2	207	1.20	1.3
O	−2	16	1.32	1.15
S	−2	32	1.84	0.59
F	−1	19	1.33	0.57
Se	−2	79	1.91	0.55
Te	−2	128	2.11	0.45
Cl	−1	35	1.81	0.30
Br	−1	80	1.96	0.26
I	−1	127	2.20	0.21

Table II.5 – Mass and field strength of glass-forming ions (atomic mass and crystal ionic radii in angstroms (after Dumbaugh, reference #88)

After the proper composition for making a stable glass with good infrared transmission is determined, the presence of contaminants that cause infrared absorption must be eliminated. The two most common are ferrous iron and water. Ferrous iron absorbs in the near infrared with a broad absorption band at 1050 nm in silicate glasses. Water is incorporated into a glass structure as a hydroxyl group. The fundamental O-H stretching vibration is at about 2.75 μm in vitreous silica.[89] This is an extremely strong absorber of infrared energy. If the hydroxyl concentration is very high, an overtone at 1.38 μm can also be seen. When the field strength of the network former decreases, the fundamental O-H stretching vibration wavelength shifts to 3.0 μm.[88]

The three major glass compositions for infrared transmission are those based on oxide glasses, fluoride glasses, and chalcogenide glasses. All three will be discussed in more detail following sections.

Oxide Glasses

In oxide based glass systems, the silicate glasses have the largest stable compositional area. Silicates formed glasses that have excellent physical and chemical properties. However, their infrared transmission is limited by the first overtone of the fundamental Si-O-Si stretching vibration at 9.1 μm. This overtone limits their transmission edge in the infrared region to only 4 to 5 μm.

Calcium aluminate glasses can be used to transmit into the infrared about one μm further than pure vitreous silica. Although they have better infrared transmission, problems such as their extreme tendency to crystallize, especially when fabricating large pieces, absorption by O-H in the glass network, it reduced resistance to weathering.

Germanate glasses, based on germanium oxide as the network former, offer extended infrared transmission without the disadvantages of glasses such as calcium aluminates. Germanium oxide forms a very good glass in that its outer electron structure is the same as that of silicon. The larger size of the germanium atom, as compared to the silicon atom, will give better infrared transmission due to the weaker bonding. However, a smaller range of stable glasses is available than for silicates.

Other novel oxide glasses based on tungsten, molybdenum, arsenic, and antimony, have shown transmission out to 6 to 7 μm. Poor stability and chemical and physical properties have limited the use of these glasses.

Tellurite glasses, based on TeO_2 as the network former, have been shown to transmit to just beyond 6 μm. They can be formed into large, colorless pieces.

Oxide glasses were based on lead and bismuth show great potential as infrared transmitting oxide glasses because they are the heaviest non-radioactive oxides.

However, they are difficult to form without accelerated quenching techniques. The additions of cadmium oxide, gallium oxide, and ferric oxide to these glasses have enhanced their glass forming ability without decreasing the infrared transmission. A lead-bismuth-gallate glass has been shown to transmit to 7 μm.[90]

Table II.6 shows a comparison of the properties of oxide glasses. Figure II.15 shows a comparison of the infrared transmittance of these oxide glasses.

		A	B	C	D
	SiO_2	100	--	29.1	--
Cation %	GeO_2	--	100	--	29.1
	Al_2O_3	--	--	42.3	42.3
	CaO	--	--	28.6	28.6
Expansion coefficient $(25-300°C)\times 10^7/°C$		5.5	76.3	59.5	63.6
Annealing point, °C		1180	541	832	758
Density, g/cm^3		2.2	3.65	2.80	3.35
Knoop hardness (100 g)		515	--	595	512
Young's modulus $\times 10^{-3}$ kg/mm^2		7.44	4.42[b]	10.05	9.56
Refractive index (589.3 nm)		1.458	1.607[c]	1.605	1.660
Abbe number		67.8	41.6[c]	55.0	46.4

Table II.6 – Properties of Infrared Transmitting Oxide Glasses (after Dumbaugh, reference #88)
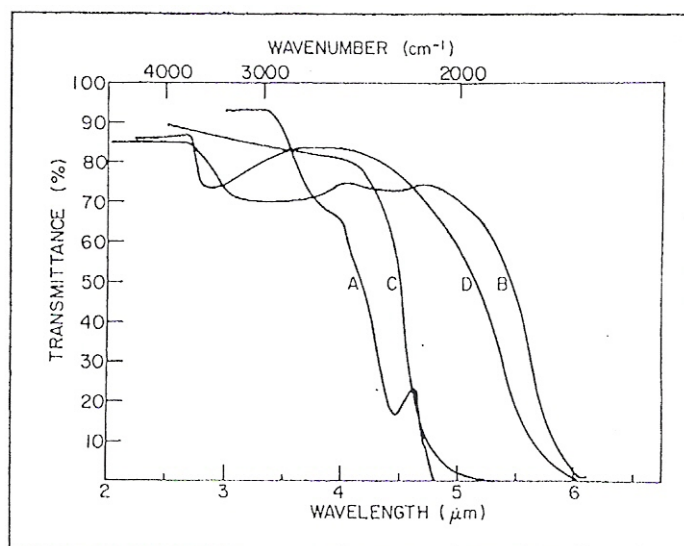
Figure II.15 – Comparison of Infrared Transmission of Glasses in
Table II.6 (after Dumbaugh, reference #88)

Halide Glasses

Halide glasses are mainly composed of multi-component fluoride, chloride, and bromide compositions.[91] Single component halide glasses based on BeF_2 and ZnF_2 have been fabricated, but both have problems which limited their uses. BeF_2 based glasses extend the infrared transmission range only slightly beyond that of silica. ZnF_2 based glasses have good infrared transmission, however they are extremely hygroscopic and susceptible to devitrification. Glasses based on multi-component chlorides and bromides have very low glass transition temperatures and are extremely hygroscopic, making them extremely soft and weak.

Multi-component fluoride glasses show the best results for infrared transmission in the halide system. The network formers of fluoride glasses are ZrF_4, HfF_4, and ThF_4. A network stabilizer is LnF_3, and a network modifier would be BaF_2. Multi-component fluoride glasses generally contain about 60 to 70 % mole ZrF_4 as the main constituent and

about 30 mole % BaF_2 as the network modifier.[92] A transmission spectrum for a bulk

sample of a ZrF_4- BaF_2-$GdF3_2$ glass is shown in Figure 16. ZrF_4 based glasses are low

melting temperature materials. The temperatures of crystallization, fusion, and glass

transition are in the ranges of 370 to 450 ^{o}C, 550 to 600 ^{o}C, and about 330 ^{o}C,

respectively.
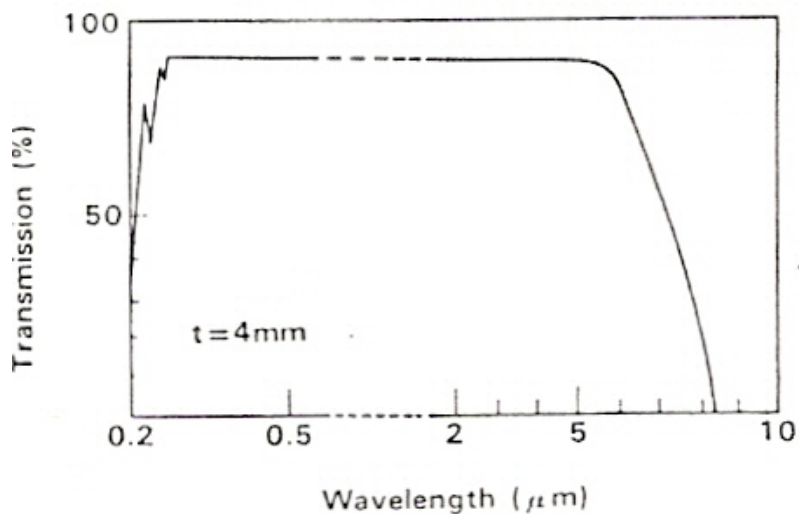
Figure II.16 – Optical transmission in the ZrF_4-BaF_2-GdF_3 glass.
(after Miyashita, et al., reference #92)

Chalcogenide Glasses

Chalcogenide glasses are one of the few materials that transmit in the infrared

region from 3 to 11 μm. This glass system is composed of metals such as arsenic,

germanium, and antimony combined with the heavier elements in the oxygen family such

as sulfur, selenium, and tellurium. High-quality chalcogenide glasses are prepared by

mixing, melting, homogenizing, and solidifying and the high purity components in silica

glass ampoules which are under vacuum.[93]

Chalcogenide glasses are typically very weak. Tensile strengths of fibers made from these compositions are in the range of 100 to 170 MPa (about 15 to 25 kpsi) depending upon the fiber diameter. It is usually undesirable to expose these glasses to temperatures exceeding 150 ^{o}C for extended periods of time.[93]

II.11. Improved Infrared Transmittance Using Calcium Aluminates

In 1948, the National Bureau of Standards began studying glasses capable of extending the transmission of infrared energy. At that time, silica was the best of the ordinary glass formers as far as the transmittance of infrared energy was concerned. However, silicate glasses, of 2 mm thicknesses, do not transmit much energy of wavelengths beyond about 4.5 μm because of the absorption by Si - O bonds at 4.45 μm.

Florence, et al.,[2] conducted a study to determine the infrared transmitting glasses that could be produced in blanks of appreciable size, and could be melted in platinum. These included glasses made from $CaO + Al_2O_3$, GeO_2, or BeF_2.

The glasses made from BeF_2 were readily attacked by water, and were given no further consideration. These samples made from GeO_2 showed interesting properties, but the high cost and availability of germanium limited the amount of samples made.

The base glass for the calcium aluminate work was the low silica eutectic composition from the $CaO-Al_2O_3-SiO_2$ phase diagram. This glass, named C-1458, is the ternary eutectic composition. This composition contained 41.2 weight percent Al_2O_3, 52.0 weight percent CaO, and 6.8 weight percent SiO_2. This glass showed transmittance out to 6 μm in 2 mm thick samples.

Florence, et al.,[2] stated that the major difficulty in preparing this family of glasses is their high melting temperature and their tendency toward devitrification when poured into thick slabs. The temperature required to melt these glasses was 1550 $^{\circ}$C. They also noted that the glasses had distinct color ranging from amber to brown. This color did not seem to affect the glasses' infrared transmitting properties. They attributed this color to platinum dissolved from the crucibles in which they were melted.

The substitution of other oxides for silica was also investigated, leaving only the CaO-Al_2O_3 as the glass former. The glass in which BeO was substituted for silica produced a crystal free glass. This glass showed improved transmittance between 2.8 and 3.8 μm, but decreased transmittance from 3.8 to greater than 5 μm in comparison with the CaO-Al_2O_3-SiO_2 glasses.

They were able to obtain glasses in a wide range of compositions in the CaO-Al_2O_3-BaO system. These ranges were: Al_2O_3 - 39 to 47 percent; CaO - 38 to 42 percent; BaO - 10 to 22 percent.

It became apparent during this study that the usefulness of calcium aluminate glasses for transmission of infrared energy is limited because of the high water absorption. This was indicated by the absorption bands noted at 2.9 and 4.7 μm. They could somewhat overcome this difficulty by using a dry air treatment. The treatment entailed introducing dry air into the bottom of the melts by means of a platinum tube for two hours during the fining process.

Florence, et al.,[2] noted that these calcium aluminate glasses had very high Young's modulus. One in particular had a modulus over 15.2 million psi. They noted that this glass could find special applications because of this characteristic.

Hafner, et al.[3], performed a study of infrared transmitting materials for use at wavelengths to at least 6 μm. They focused this study on materials that had a softening range above 500°C, thermal shock and strength properties similar to conventional silicate glasses, and the capacity to be formed into relatively large and intricate shapes and at reasonable cost. It became apparent early in the work that glass systems would most reasonably meet the requirements.

The glass systems under consideration included:

1) Oxide Glasses; Silicates (SiO_2 as the glass former), Borates (B_2O_3 as the glass former), Phosphates (P_2O_5 as the glass former), Germanates (GeO_2 as the glass former), Antimonates (Sb_2O_5 as the glass former), Calcium aluminates ($CaO:Al_2O_3$ as the glass former), and Tellurates (TeO_2 as the glass former).

2) Elemental Glasses; Tellurides and Selenides.

3) Sulfide Glasses; Arsenic Trisulfide variations and Germanium Sulfides.

The second and third groups were eliminated because of their inherent low melting temperatures, low strength properties, and/or high cost. An oxide glass system therefore became focal area of the work.

Upon further examination of the oxide group, several systems were eliminated for the following reasons;

- Borates and Phosphates due to lack of infrared transmission,

- Silicates due to an infrared cut off at about 5 μm for a reasonable glass thickness,

- Germanates due to the high cost of germanium compounds,

- Antimonates due to problems with refractory container and melting problems,

- Tellurates due to the low melting temperature and reactions with platinum containers.

This elimination process caused the Calcium Aluminate system to be selected for further development.

Their work established that additions of SiO_2 would increase the glass forming region of the calcium aluminate system, but would move the infrared cutoff edge towards the visible region with increasing the SiO_2 percentages. The following mole percentages were found to be the most useful SiO_2 containing and non-SiO_2 containing compositions:

SiO_2 Containing;

$NaO_{0.5}$	$KO_{0.5}$	CaO	$AlO_{1.5}$	MgO	BaO	$LaO_{1.5}$	$FeO_{1.5}$	SiO_2
7.5	2.5	32.5	57.5	2.0	2.0	2.0	2.0	2.5

Non-SiO_2 Containing;

$NaO_{0.5}$	$KO_{0.5}$	CaO	$AlO_{1.5}$	MgO	BaO	TiO_2	$FeO_{1.5}$	ZrO_2
7.5	2.5	32.5	57.5	2.0	2.0	1.0	2.0	1.0

It should be noted that the compositions took into account the volatilization of components during melting.

This work established a number of iron-containing calcium aluminate compositions for producing glass in quantities up to 10 pounds when cast in one inch slabs. The silica containing composition actually produced melts up to 30 pounds without devitrification.

In general, this research showed that additions of 2.5 to 5.0 mole percent SiO_2 to a calcium aluminate glass containing 2 mole percent at $FeO_{1.5}$ improved the glass forming properties of the composition substantially. The use of concentrations of SiO_2 above and below this range produced glasses of inferior quality.

Hafner, et al.[3], noted several major problems when working with these glasses. These were; the calcium aluminate glasses devitrified when reheat to the softening temperature, the water band between 2.5 and 3.0 μm was not eliminated, and the glasses were not resistant to moisture attack. They did show that the glass surface could be completely protected by vacuum coating with either MgF_2 or at SiO_2.

Uhlmann, et al.,[7] studied the likelihood of improving the glass forming ability of calcium aluminate glasses. This was done through the additions of non-network formers, including alkali and alkali earth oxides, to the base glass composition. No silica was added to the compositions in order to maximize the infrared transmission.

Four calcium aluminate compositions were evaluated in this study. These included: $64CaO\cdot36Al_2O_3$ (CA), $6Na_2O\cdot58CaO\cdot36Al_2O_3$ (CAN), $6BaO\cdot6Na_2O\cdot52CaO\cdot36Al_2O_3$ (CANB), and $6SrO\cdot6Na_2O\cdot52CaO\cdot36Al_2O_3$. All compositions were melted at 1580 ^{o}C for 2.75 hours, and then held at 1440 ^{o}C for 15 minutes. Sample melts were allowed to cool to room temperature in air on a metal plate. Optical microscopy and x-ray diffraction were used to check the samples for crystallization. Differential thermal analysis (DTA) was used to check the thermal properties. Infrared spectra were obtained using an FTIR.

Uhlmann, et al.,[7] realized that assessing the glass forming ability and glass stability could be a difficult task. For example, the measurement of cooling rates is difficult without disturbing the samples. For larger samples, cooling rates will not be uniform throughout the sample. Also, critical cooling rate information is only useful for compositions that devitrify homogeneously. If bulk heterogeneities are the source of crystallization, then measured critical cooling rates can fluctuate greatly from one

experiment to another. In addition, if surface crystallization is predominating, this will be greatly affected by the sample size, shape, and surface polish.

In all samples where crystallization was in evidence, Uhlmann, et al.,[7] found it initiated at the surface. For the aforementioned reasons, the preparation procedures were varied to better quantify the glass forming ability of each composition.

As expected, the binary system (CA) showed the worst glass forming ability. Only the small 7 gram batch formed a glass. The addition of Na, Sr, and Ba clearly improved the glass forming ability of the calcium aluminates. Using melt size and cooling rates as the criteria, the CANB composition was the best glass former. It is interesting to note that pouring the samples after melting produced crystallization in all cases. It might be expected that the increased cooling rate from pouring would reduce crystallization. Uhlmann, et al.,[7] speculated that the introduction of heterogeneities during pouring induced the crystallization.

X-ray diffraction results indicated the existence of $C_{12}A_7$ and C_3A primary crystal phases in the binary composition, CA, and the CAN and CANS compositions. The crystals found in the CANB compositions were predominately $C_{12}A_7$, with the addition of minor amounts of C_3A and barium aluminate.

III. EXPERIMENTAL METHODS

III.1 Sample Selection

The best commercially available calcium aluminate glasses were obtained for this study. Two companies were identified that could provide high quality calcium aluminate glasses. They included;

Sassoon Advanced Materials Limited
Vale of Leven Industrial Estate
Dumbarton
Scotland G82 3PP

Schott North America
400 York Avenue
Duryea, PA 18642
USA

Sassoon Advanced Materials Limited, one of the largest manufacturers of CAG, utilizes advanced vacuum glass melting technology and high purity starting materials to obtain large glass blanks of CAG. Schott North America would not disclose their glass melting techniques.

Three different compositions were obtained from these manufacturers. These included a barium-doped glass from Schott Glass (IRG-11), a silica-doped glass from Sassoon Advanced Materials Ltd., and a second barium-doped glass from Sassoon. Table III.1 shows the compositions of the CAG samples, where available.

Sassoon Ltd. – Silica doped Calcium Aluminate Glass (WB37A)
Alumina – 40.8%, Calcia – 49%, Magnesia – 4.1%, Silica – 6.1% (Wt%)
Silica used to increase stability

Sassoon Ltd. – Barium doped Calcium Aluminate Glass (BS39B)
Alumina – 45%, Calcia – 36.9%, Magnesia – 4.7%, Baria – 13.4% (Wt%)
Baria used to increase IR edge to 5.5 μm

Sassoon compositions virtually water free.

Schott Glass — Barium doped Calcium Aluminate Glass (IRG 11)
Commercially confidential composition. Similar to BS39B.
Contains 1000 ppm water.

Table III.1 - Calcium Aluminate Bulk Glass Compositions in Study

III.2 Physical Properties of Bulk Glasses in Study

    A list of the important published physical properties of the CAG samples under

study is seen in Table III.2.

Young's Modulus
Sassoon Ltd., WB37A – 107 GPa
Sassoon Ltd., BS39B – 104 GPa
Schott Glass, IRG 11 – 107.5 GPa

Hardness (Knoop)
Sassoon Ltd., WB37A – 726
Sassoon Ltd., BS39B – 726
Schott Glass, IRG 11 – 610

Thermal Expansion Coefficient –
Sassoon Ltd., WB37A – 9.5 x 10^{-6}/$^{\circ}$C from 20 to 500°C
Sassoon Ltd., BS39B – 9.7 x 10^{-6}/$^{\circ}$C from 20 to 400°C
Schott Glass, IRG 11 – 8.2 x 10^{-6}/$^{\circ}$C from 20 to 300°C

Table III.2 - Physical Properties of CAG Samples

III.3 Optical Properties of Bulk Glasses in Study

The refractive indexes of the CAG samples in study obtained from the manufacturers product brochures are listed in Table III.3.

Sassoon Ltd., WB37A – 1.6647 at 0.6563 μm
Sassoon Ltd., BS39B – 1.6720 at 0.6563 μm
Schott Glass, IRG 11 – 1.6763 at 0.6563 μm

Table III.3 - Refractive Indices of CAG Samples under Study

The optical transmission curves obtained from the manufacturers product brochures for the three glasses under study, WB37A, BS39B, and IRG11, are shown in the next three figures.

The WB37A is the higher purity version of an earlier Sassoon standard purity CAG BS37A. Both transmission curves are seen in Figure III.1. A large transmission window from approximately 0.3 to 5 μm is clearly visible.
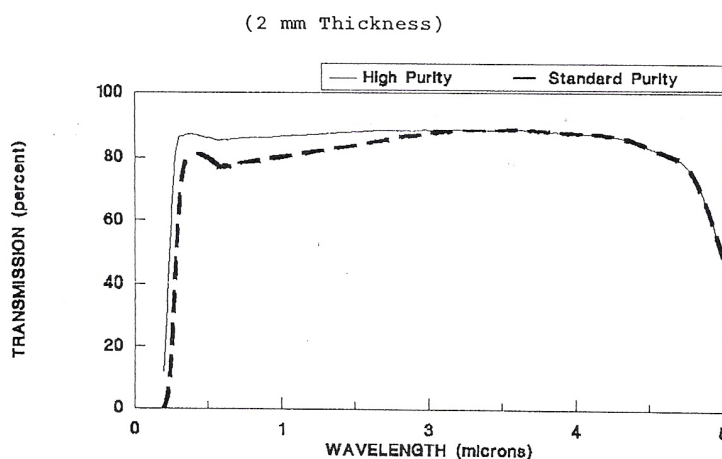
Figure III.1 - Sassoon WB37A (High Purity) and Sassoon BS37A (Standard Purity)

Figure III.2 shows the optical transmission window for the Sassoon BS39B. The extended infrared transmission of the BS39B versus the WB37A is due to the absence of silica in the BS39B composition.
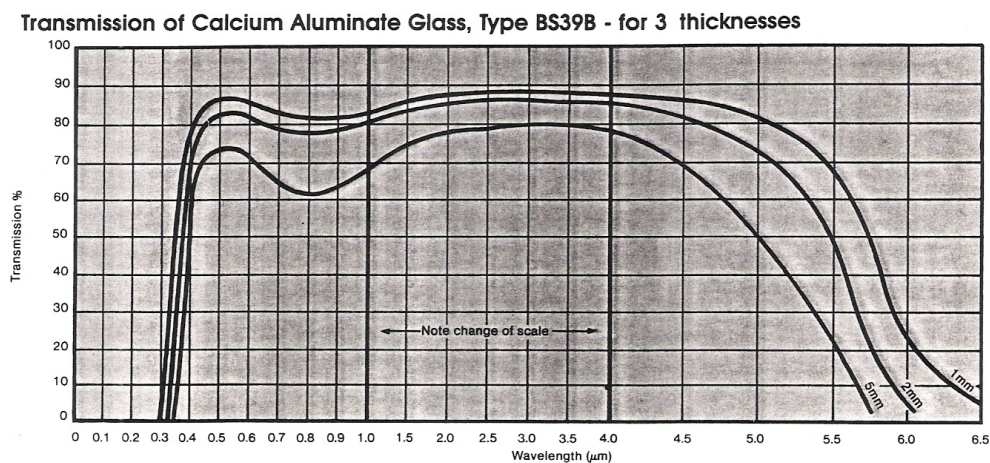
Figure III.2 - Sassoon BS39B Optical Transmission

The optical transmission window for the IRG11 is shown in Figure III.3. The absorption due to the presence of 1000 ppm water in this composition is evident at approximately 2.9 μm on the curve. IRG11 has a similar transmission curve to BS39B, except for this absorption from the high water content.
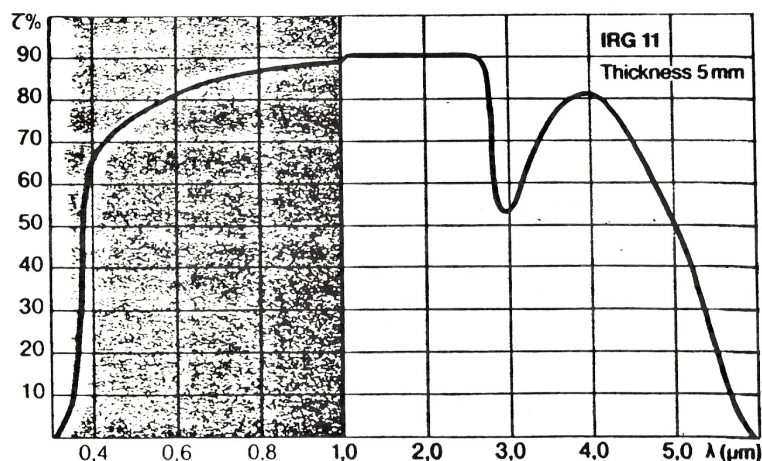
Figure III.3 - Schott IRG11 Optical Transmission

III.4 Spectroscopy Measurements

The spectroscopic measurements of the CAG bulk and fiber samples were done using a Perkin Elmer Fourier Transform Infrared Unit. This instrument was modified to allow for external beam operation. The external beam operation was necessary for obtaining the fiber loss measurements.

The ends of sample rods and fibers were polished to obtain good spectroscopy data. The ends were polished on the two end surfaces in order to obtain a mirror finish. The polishing is done in stages of decreasing surface roughness. Typically, a polish with 15 μm diamond slurry was the starting point to polishing. This progressed down to 6 μm then 1 μm lapping films, then down to 0.3 μm diamond slurry. An optical microscope with a fiber illuminator was used for viewing the ends during the polishing process.

III.4.1   Bulk Glass Sample Preparation

Five mm thick samples of the Sassoon silica doped composition (WB37A) and the Schott Barium doped composition (IRG11) were prepared for comparison. The 5 mm thick samples were polished on the two surfaces down to 0.3 μm grit size in order to obtain a mirror finish. Scans were run from 1 μm out to 7 μm. Visible and near IR transmission was done on the Sassoon silica doped composition (WB37A) in order to confirm the visible side of the transmission window.

III.4.2   Attenuation Measurements

Attenuation measurements were made by comparing the transmitted intensity of a long length of fiber sample to that of a short length of fiber sample. The launch conditions, end surface preparation, and detector configuration was kept constant as much as possible. In most cases, a 1 to 1.5 meter long fiber section was used as the long length. This was then cut back to 200 to 300 mm section for the short length. Care was taken to insure the outside of the glass fibers were not touch with bare hands so as to contaminate the surface, increasing the scattering at the surface.
Loss spectra were calculated using the equation

$$\text{Loss (OD)} = \log \frac{I_0}{I}$$

where I_0 is the transmitted intensity through the short sample and I is the transmitted intensity through the longer sample. The loss per unit length in the fiber sample is calculated by dividing the loss measured by the length difference between the two

samples. In this dissertation, losses are reported in dB/m. The optical density units (OD) can be calculated by using the conversion

$$1 \text{ OD} = 10 \text{ dB}$$

The Perkin Elmer FTIR was outfitted with an external detector for the infrared loss measurements. The infrared emission from the spectrometer source was focused into the input end of the fiber sample. The detector was aligned to capture the emission exiting the other end of the fiber sample. Maximum throughput was obtained by carefully aligning the fiber. An absorption scan was then acquired. Then, the longer fiber was cut back to a shorter length, keeping the input end the same. A spectrum was then collected on the shorter fiber length. The loss was calculated using both sets of spectra.

III.5   Scattering Measurements

The measurement of the wavelength dependence of scattering losses in glass samples can be helpful in understanding the mechanisms that cause them. Scattering losses were measured using integrating spheres. Figure III.4 shows the basic set up for the scattering measurement for bulk and drawn fiber samples.

Schematic Diagram of integrated scatter measurement
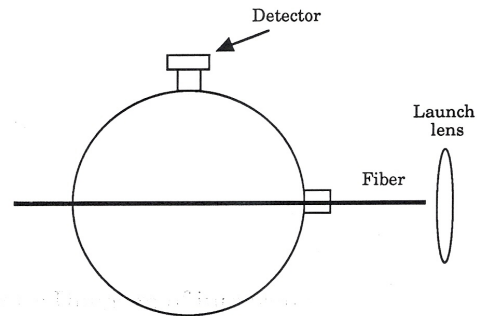
Fiber in position to measure scattered intensity.
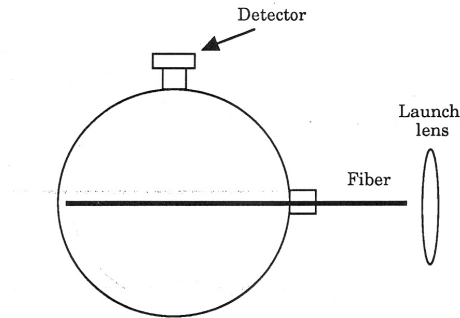
Fiber in position to measure transmitted intensity.

Figure III.4 – Scattering Measurement Set Up for Bulk and Fiber Samples

The visible scattering measurements were accomplished using a barium coated 1 inch sphere and silicon detectors. The scattered intensity was measured by positioning the sample end out a small exit hole in the sphere. Transmitted light was measured by moving the exit sample end back into the sphere. The scattering loss, α_{sc}, can be calculated in units of dB/m by using the formula

$$\alpha_{sc} = \frac{434 \, I_{sc}}{(I_{tr})(l)}$$

where l is the length of the integrating sphere in cm.

III.6 Draw Sample Preparation

Glass rods and tubes were required for the optical fiber draw studies. The CAG samples were provided by the manufacturers in glass blanks, typically 150 mm x 150 mm x 12.5 mm. To form glass rods, the blanks would have to be cut to 100 mm long rectangular bars. These bars would then need to be machined to form 100 mm long by 8 to 10 mm diameter rods.

III.6.1 Rods

A Kent dicing saw was used to cut the rectangular glass bars from the supplied glass blanks. The glass blanks were secured onto a ceramic plate using wax before placing on the Kent dicing saw table. A hot plate was used to heat the plate and wax, firmly securing the glass sample. The glass sample/ceramic plate sandwich was then placed onto the movable table of the saw. Slices were then cut into the glass blanks using a diamond saw blade with cooling water flowing on it. Care was taken to insure that the slices yielded a symmetric square cross section geometry of 12 mm by 12 mm with a length of approximately 100 mm. This would insure that the blanks could be polished to as perfectly round rods as possible.

After dicing, the glass blanks were removed from the ceramic plate by heating on a hot plate. Any residual wax was removed using a solvent rinse.

A polishing wheel was utilized to grind off the edges of the rectangular bars to get them close to a rod shape. Coarse 60 grit polishing paper was used for initial material removal, followed by progressively fine grit polishing paper to smooth the outside surface.

A small Sherline machining lathe was modified to enable the surface of the glass rods to be polished to a round cross section profile and to obtain a mirror surface finish. It is well known that obtaining a smooth surface finish will improve the resulting fiber strength. Scratches and pits on the surface act as effective stress concentrators when the fiber is under strain. The samples were chucked into the Sherline lathe so that each end was held by the headstock and tailstock. The samples were spun in the lathe. The polishing paste was applied against the spinning sample surface. Coarse grinding paste was used for the initial surface removal, followed by progressively fine grit polishing paste to smooth the outside surface down to a 0.3 μm grit finish. The rod surface was rinsed thoroughly before proceeding to the next finer grit polishing paste to avoid contamination of coarser particles into the finer polishing.

After polishing was complete, the samples were rinsed thoroughly with ethanol, dried, and then placed into a nitrogen glove box for storage until drawing.

III.6.2   Hollow Waveguide Fabrication

Tubes of the CAG were required for attempting the fabrication of hollow CAG waveguides for high power propagation studies. Hollow waveguides have been used to deliver CO_2 laser radiation for industrial and surgical laser applications.[94] In particular, hollow waveguides made from certain oxide glasses[95] and crystalline[96] materials have the unusual property that their refractive index n is less than 1 at CO_2 laser wavelengths. That is, the region of anomalous dispersion in some oxide materials fortuitously occurs in the 9 to 10 μm region and, therefore, hollow guides can be made from n < 1 materials that have core indices (air, n = 1) greater than clad indices (n < 1). This yields hollow

structures that are fiber-like in operation. In general, we may think of the n < 1 fiber as an attenuated total reflectance waveguide in that most of the energy is reflected from the inner-wall material, in contrast to the hollow metallic waveguides, which are leaky waveguide structures.

Hollow n < 1 lead-based glass fibers were first made by Hidaka and his coworkers in 1981.[97] Subsequently Worrel and Skarda,[98] Falciai et al.,[99] Scheggi et al.,[100] and Nagano et al.[101,102] made hollow fibers from lead- and germanium-based oxide glass, and Wilson[103] studied the bulk optical constants of these glasses as well as those of aluminate glasses. All these glasses had the property that n was less than 1 over some portion of the output spectrum of the CO_2 laser. Harrington and Gregory[96] observed a similar behavior in crystalline material, notably Al_2O_3. The theory behind the losses in hollow waveguides was studied many years ago by Marcatili and Schmeltzer (MS).[104] They used a wave optic formalism to express the losses expected for a hollow structure in terms of the optical constants n and k, the wavelength, and the inner radius α of the guide. Their research was followed by further calculations by Miyagi and Karasawa[105] on bending losses in these structures. The results of this research give, in simplest terms, two important relationships for the attenuation coefficient α that govern the losses in hollow guides. That is,

$$\alpha \propto \frac{1}{\alpha^3}, \qquad \alpha \propto \frac{1}{R}.$$

Simply put, the loss of hollow guide increases dramatically as the core diameter is decreased, and there is an additional loss that is due to bending that increases with the

reciprocal of the bend radius, R. This is a special property of hollow waveguides that distinguishes them from solid-core fibers.

Calcium aluminate glass is a particularly attractive candidate for a n < 1 hollow fiber because n is less than 1 at 10.6 μm. Saggese and Harrington[106] have studied the optical parameters n and k for this glass system. They found that calcium aluminate glass containing little or no silica had the lowest loss at 10.6 μm. For these glasses they calculated a theoretical loss from MS theory to be less than 0.5 dB/m for a 1000 μm bore fiber. The problem with this glass, however, is that it is difficult to draw into fiber without devitrification. In particular it is especially difficult to draw the low-silica-content glass into fiber, yet this is the glass composition most desirable from the viewpoint of low 10.6 μm loss.

The base calcium aluminate glass system is 40 wt. % Al_2O_3 and 60 wt. % CaO.[3] This binary system has a high glass-transition temperature, and SiO_2 and other modifiers are often added to improve its glass-forming ability. Schott IRG-11 calcium glass was chosen for this part of the study because it contains no silica, and thus it has the lowest loss at 10.6 μm. The IRG-11 CAG was obtained in the form of a solid rod, and this rod was core drilled and highly polished to form the preform tube. The preform was heated to approximately $920^{\circ}C$ and drawn in an argon atmosphere into hollow fibers with inner diameters ranging from 370 to 500 μm.

The optical parameters n and k for the bulk calcium aluminate glass were obtained from reflectivity measurements made on a polished plate of IRG-11 glass. The reflectivity was measured on a Perkin-Elmer1725X Fourier transform infrared spectrophotometer in near-normal incidence. Parameters n and k were then calculated

with a Fast Fourier transform- based Kramers-Kronig analysis.[107] Finally the power

attenuation coefficient 2α for a straight waveguide was calculated with the MS equation,

$$(2\alpha) = \left(\frac{U_{nm}}{2\pi}\right)^2 \frac{\lambda^2}{a^3} \left[\frac{\frac{1}{2}(\nu^2 + 1)}{(\nu^2 - 1)^{1/2}}\right],$$

$$(1)$$

where U_{nm} is the mode-dependent parameter, α is the bore radius, and υ is the complex

refractive index, $\upsilon = n - ik$.

III.7 Draw Tower Equipment

A commercial grade Heathway draw tower was used for the fiber drawing

experiments. Figure III.5 shows a drawing of the tower with the important features

noted. The sample rod is fed into the top of the draw tower furnace at a steady controlled

rate by the tower's downfeed. The draw furnace heats the sample rod up to the drawing

temperature. At the draw temperature, the sample rod will soften and begin stretching

out under the force of gravity, forming a "drop". As the drop exits the bottom of the

draw furnace, the operator grabs the resulting fiber and cuts off the drop. The fiber is

feed down through the tower equipment to the capstan, or draw tower tractor unit. Below

the furnace on the draw tower, the fiber goes through a laser diameter monitor. The laser

diameter monitor reads the fiber diameter across the fiber draw line and measures the

fiber in two axes. This information is fed to the tower control cabinet. The control

cabinet regulates the capstan rotation speed to achieve the desired fiber diameter. If the

fiber diameter drops below the target fiber diameter, the capstan will slow down. If the

fiber diameter increases above the target fiber diameter, the capstan will speed up.
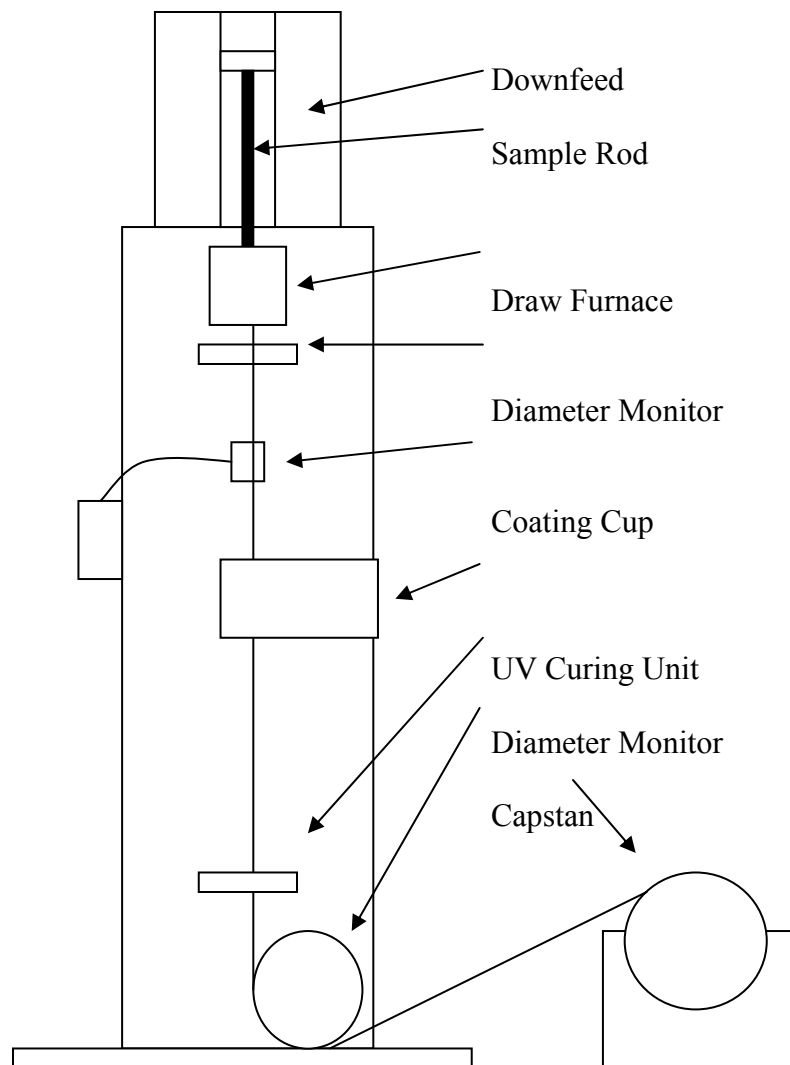
Figure III.5 – Draw Tower Overview.

The coating cup is used to apply a polymer coating to the outside of the fiber.

Coating is pumped from a reservoir to the coating cup by a delivery line. The coating is

applied to the outside of the fiber inside the coating cup. The coating cup consists of a

top entrance die and a bottom exit die. These dies are separated by a spacer area, into

which the coating is applied. The coating dies have a conical shaped funnel area running

horizontally in the die center. The funnel shape in the top die aids in the fiber feeding

through the die. The funnel shape in the bottom die assists in attaining concentric coating application.

The coating is fluid when it is applied to the fiber. It is cured onto the fiber by UV curing or thermally curing the coating to a solid. These curing units are located under the coating cup unit.

After the coating is cured in the UV curing unit, the fiber proceeds downward through a second diameter monitor. This unit provides the overall fiber diameter after coating. The fiber is pulled by the capstan and onto the fiber collection drum, or drumwinder. A dancer arm unit is used to provide a constant tension in the fiber line between the capstan and drumwinder enabling a controlled precision wind onto the collection drum.

III.8 Draw Furnace Development

The proper design of the optical fiber draw furnace is critical for successfully drawing any optical material. The furnace must provide for the even heating of the draw sample without contaminating the sample surface in any way. This is especially true with a glass composition that has a relatively narrow drawing temperature window, such as CAG.

Initial CAG draw trials were conducted on the draw tower using the standard carbon resistance draw furnace manufactured by Centorr/Vacuum Industries. This furnace has a heat zone vertical length of approximately 30 mm. 100 mm long by 10 mm diameter CAG sample rods were hung in the furnace and heated up to 920 $^{\circ}$C, the estimated drawing range. It was hoped the sample rod would elongate under the force of

gravity forming a drop, as in normal fiber draws. Draw samples were heated up in the furnace at a rate of 10^oC/minute. However, all CAG sample rods devitrified in the furnace before forming a drop using this draw furnace. It became apparent that a smaller heat zone and active pulling of the rod out into a drop was going to be required if fiber drawing was possible from CAG samples.

A custom draw furnace was fabricated specifically for the drawing of CAG rod samples. This work included modifying a Heathway, Inc. soft glass induction furnace that was capable of reaching temperatures of 1200^oC. Figure III.6 shows a schematic of this renovated furnace. The furnace has a silica liner tube which defines the draw atmosphere inside it. The silica liner tube has a step in it to support the carbon susceptor ring in the heat zone center.
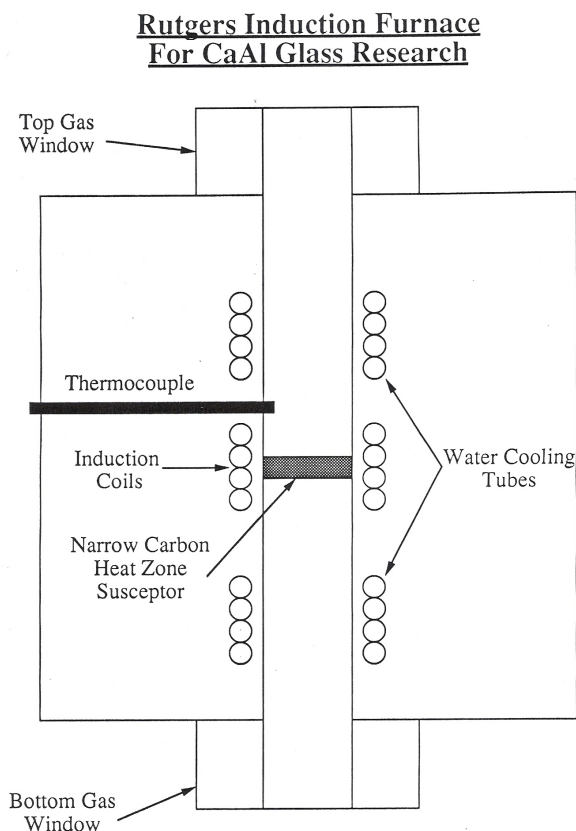

Figure III.6 – Custom Draw Furnace

The furnace modifications included adding top and bottom gas inputs to the top and bottom of the furnace. These inert gas input areas are specially designed to flow the inert gas 360 degrees around the furnace centerline. This would insure the even distribution of the inert gas into the furnace. Gas flow meters were added to allow the flow of inert gas from 0 to 5 lpm at the furnace top and bottom.

A Centorr/Vacuum Industries gettering unit was also added to the input gas flow stream before the gas reached the furnace. By using the gettering unit, the flow of argon, the inert gas of choice, could have the oxygen level in the gas purified down to levels of 10^{-7} ppm or better. A low oxygen level in the argon gas would protect the carbon susceptor from oxidizing at high temperature. Any oxidized carbon in the heat zone can cause soot which will coat the resulting glass fiber. These soot particles can act as stress concentrators on the fiber and cause the fiber to be weak, breaking at these stress concentrators. In the gettering unit, the argon gas is flowed over titanium metal flakes which are at 800°C. At this temperature, any oxygen which may be in the flow stream is removed through the oxidation of the metal flakes. As sensor system is part of this gettering unit, indicating the final oxygen levels in the argon flow to the furnace. Water cooling coils were added above and below the heat zone to provide the ability to narrow the heat zone vertical length. Flow meters were installed providing 0 to 2 gallons/minute water flow at each location. In this way, the water flow could be adjusted to tune the heat zone profile to the desired condition.

The induction furnace heat zone susceptor supplied with the furnace was a ring shape of 20 mm in height by 25 mm outside diameter with 8 mm wall thickness. In order to narrow the furnace heat zone area even further, new carbon susceptors were

manufactured to dimensions 8 mm in height by 4 mm in wall thickness by 25 mm in outside diameter.

III.9   Sample Coupling Arrangement

Initial drawing trials with the standard Centorr draw furnace and the modified small susceptor draw furnace did not yield any good fiber samples because the glass rod samples would devitrify in the furnace before a drop would form. It became apparent that an active pulling arrangement must be designed to aggressively begin the fiber draw process before the glass rod had a chance to fully devitrify. A sample coupling arrangement was designed. This coupling arrangement is shown in Figure III.7.

Alumina tubes with inside diameters of 8 to 10 mm were attached to the top and bottom of the CAG rod samples using zirconia based high temperature cement. The cement was allowed to dry overnight before attempting any sample drawing.

Sample Coupling Arrangement for Drawing
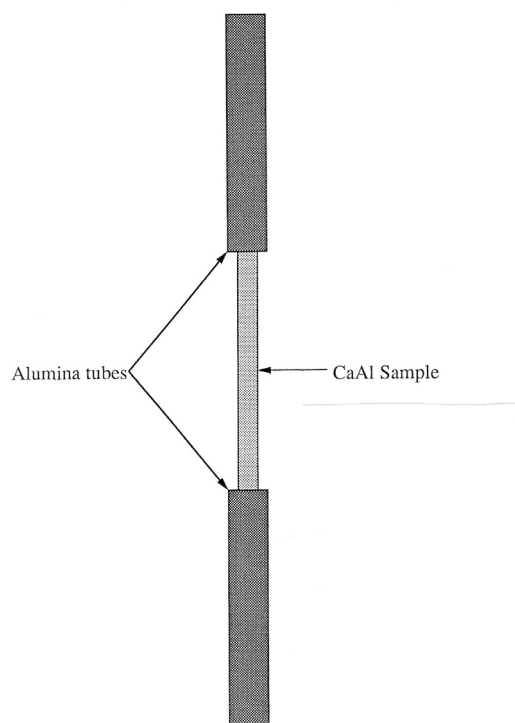
Figure III.7 – Sample Coupling Arrangement

The sample coupling arrangement was set up in the furnace as follows. The top alumina tube was chucked onto the preform feed chuck on the draw tower. The sample was then lowered into the furnace so that the lower part of the exposed sample was at the level and in the middle of the small carbon susceptor ring. The bottom alumina tube extended from the sample and out of the bottom of the custom modified induction furnace. The sample was then heated up to the draw temperature range, approximately $920^{o}C$. As the temperature reached $900^{o}C$, the bottom alumina tube was put under tension so as to actively begin the fiber drawing before the glass rod could devitrify.

III.10 Teflon Clad Fiber Production

The CAG fibers produced did not contain a core and clad. As such, a way of applying an optical coating to the outside of the fibers was investigated. This method involved the application of perfluoronated-ethylene-propylene (Teflon FEP 100) onto the outside of the drawn fiber. This same process was used to clad the outside surface of silica fibers. The wire and cable industry employs the extrusion of polymer coatings quite extensively.

Teflon extrusion involves the melting of the polymer and forcing it through a die at high pressure. The fiber is run through the die at a set speed and the polymer is extruded around it. As the fiber exits the die, the polymer is cooled and coats the fiber completely. The overall finished diameter of the fiber after coating is determined by the die temperature, extrusion pressure, and the speed the fiber is feed through the die. The polymer extruder used in this work was constructed by Heraeus LaserSonics and was donated to Rutgers University.

III.11 CaAl Core/Silica Clad Fiber Production

Following the work of Snitzer and Tumminelli,[108] optical fiber with a CAG core and a silica cladding was attempted to be produced. If successful, the resulting CAG fiber core could be used for the increased infrared transmission capability, with the silica cladding providing the high strength protection. Silica fiber drawing is well established in industry and research, with resulting high fiber strength levels of 5 Gpa.
Fiber optic grade silica tubing was obtained from Heraeus Tenevo. The dimensions of the tubing were approximately 30 mm OD by 6 mm ID by 1 meter long. The bottom

section of the silica tubing was closed off in the draw furnace so the silica tubing could support the core glass rod placed inside.

A blank of CAG glass of the silica doped glass sample from Sassoon was used for this part of the project. A sample rod was fabricated in the same way as the draw samples. The CAG rod sample was polished to achieve a 6 mm OD. The resulting rod was 50 mm long.

The 6 mm OD CAG rod was then placed into the silica tube. The resulting preform was hung in the draw tower downfeed with the CAG core rod section at the bottom. The preform was lowered into the draw furnace and centered in the heat zone. The furnace temperature was then ramped at 20°C/min. up to the final silica draw temperature of 2000°C. After approximately 5 minutes, a drop formed from the preform and lowered out of the bottom of the furnace. This drop was clipped off and the resulting fiber strung through the rest of the tower equipment. Once the fiber was drawn out to the target OD of 250 μm, the fiber was cut and fed through the coating cup to apply a UV curable coating to it. The resulting fiber was spooled up onto a collection drum.

III.12 DTA – Differential Thermal Analysis

A measure of the stability of glasses is the difference between the crystallization temperature (Tx) and the glass transition temperature (Tg). The viscosity decreases rapidly in the region of crystallization and thus (Tx-Tg) provides a measure of the steepness of the viscosity slope and hence an indication of the width of the stable region[7]. Therefore, for fiber drawing, it is desirable to have a "stability window" as large as possible.

The thermal analysis of three calcium aluminate glass compositions was conducted in dry, moist, and dehydrating environments in an effort to maximize their stability and thus to optimize the processing conditions for fiber drawing. Glass chips were obtained from samples by means of a Leco VC—50 glass saw. The chips were then ground to a fine powder via a mortar and pestle in a nitrogen atmosphere glove box. This was believed necessary due to the sensitivity of these glasses to moisture. The chips were ground to ensure maximum thermal contact with the thermocouple during the analysis. All three compositions were stored in the glove box for the duration of the investigation and every effort was made to minimize their exposure to moisture when removed for analysis.

A Perkin Elmer DTA 1700 with System 7/4 Thermal Analysis Controller was used for this study with a temperature precision of +/- 2°C. An alumina liner was filled with pure Al_2O_3 powder before being placed into the platinum reference cup. Twenty milligrams of sample was placed into an identical liner and then covered with Al_2O_3 powder for the sample cup. Great care was taken to ensure that the sample and the reference cup weights were equal and that each sample was the same weight (20 mg).

The analyses were conducted from 300 to 1200°C with a heating rate of 20°C/min. Four different atmospheres were studied: air, dry nitrogen, moist nitrogen, and a chlorine/nitrogen mixture (3.5% high purity Cl_2). The flow rates were kept at 40cc/min. for the duration of the experiments and a reproducible baseline was obtained before each analysis. Moist nitrogen was obtained by passing nitrogen through a water bubbler prior to entering the apparatus. For the chlorine runs, a scrubber arrangement

was set-up in which the exhaust gas from the apparatus passed through a potassium hydroxide solution before proceeding.

Three gold temperature calibration runs were conducted at various times during the investigation yielding an average analyzer temperature lag of 2.5°C. To ensure reproducibility, five runs were conducted of each sample for each atmosphere, except for the chlorine atmosphere where only three replications were conducted. The Tg and Tx onset temperatures were determined by use of the analyzer computer system.

III.13 Fiber Mechanical Strength Measurement

The mechanical testing of the fiber strength involved determining the strain to failure of the CAG fibers. 4-point bending apparatus was used for these measurements.[109] A schematic of the testing jig, along with the equation for determining the strain to failure is seen in Figure III.8.

4 Point Bend Apparatus

4a

Fixed

2a

Fiber to be
tested
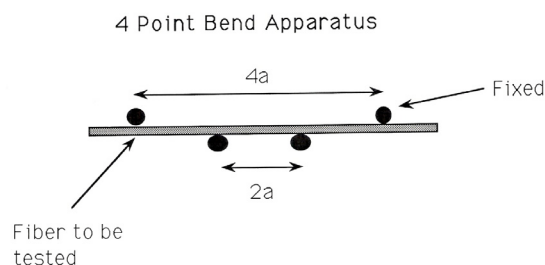
$$E_f = \frac{3\,D\,d}{8a^2}\,\gamma$$

E_f – Strain at Failure
D – Distance to Break
d – Diameter of Fiber
a – Dimension of Bender
γ – Correction Factor
    (Nelson & Matthewson)
    ACS Conv. 1991

Figure III.8 – 4 Point Bend Apparatus (after Nelson, et al., reference #109)

The distance to break is determined by traversing the two points separated by 2a through the two points separated by 4a, causing a bend in the fiber and eventually breakage. The dimension "a" of the 4 point bender is 7.937 mm.

The minimum bend radius, R, can be calculated from the strain to failure by using equation

$$R = d/2E_f$$

III.14 Crystallization Products Assessment

The products of the surface crystallization were assessed with the following techniques.

1. Energy Dispersive Analysis (EDA)

2. Scanning Electron Microscopy (SEM)

3. Hot Stage X-Ray diffraction

4. Guinier Camera X-ray diffraction

III.14.1 Energy Dispersive X-Ray Spectroscopy (EDS)

Energy dispersive X-ray spectroscopy is a technique used for the elemental analysis of a sample. EDS analysis of a sample involves the interactions between electromagnetic radiation and matter, and analyzing the x-rays emitted by the matter in response to being hit with the electromagnetic radiation. Characterization of matter by EDS works by the fundamental principle that each element has a unique atomic structure. This allows x-rays that are characteristic of an element's atomic structure to be identified uniquely from each other.

In order to stimulate the emission of characteristic X-rays from a specimen, a high energy beam of charged particles such as electrons or protons, or a beam of X-rays, is focused into the sample being studied. An atom at rest within the sample contains ground state (or unexcited) electrons in discrete energy levels or electron shells. These electrons are bound to the nucleus. The incident beam may excite an electron in an inner shell, ejecting it from the shell while creating an electron hole where the electron was. An electron from an outer, higher-energy shell then fills the hole. The difference in energy between the higher-energy shell and the lower energy shell may be released in the form of an X-ray. An energy dispersive spectrometer is used to measure the number and energy of the X-rays emitted from a sample. The elemental composition of the specimen is measured from the characteristic energy of the X-rays, the difference in energy

between the two shells, and of the atomic structure of the element from which they were emitted.

EDS was used in this dissertation to look at the glass compositions in the bulk where they were not crystallized, and the neckdown region of the drawn samples where surface crystallization had occurred.

III.14.2 Scanning Electron Microscope (SEM)

Scanning Electron Microscope (SEM) was used to take high magnification photomicrographs of the sample fibers and areas of crystallization on the fibers and draw rod neckdown regions. This high magnification view was helpfully in understanding the crystallization that was occurring.

III.14.3 X-Ray diffraction

III.14.3.1 Hot Stage Analysis

The major obstacle to successful fiber fabrication of CAG is the formation of crystals on the fiber surface during drawing. In order to better understand the crystal formation that occurred during drawing, a high temperature x-ray diffractometer was utilized. The analysis was performed on a Siemens D500 diffractometer using Ni-filtered CuKα radiation. The divergent slit was set at of 1 degree and the receiving slit at 0.05 degree. The operating voltage was 40 KV and the current was 30 mA. The detector was a scintillation counter. The data was collected by a DACO microprocessor using a stepwidth of 0.04 degree two theta and a measuring time of 2 seconds. The high

temperature furnace used was an Edmund Buhler HDK 2.3 electrical resistance furnace powered by a Power Unit LET 2400 and equipped with a water cooling system. The temperature was controlled by means of a Micristar Model 828D controller. The furnace was fitted with a Leybold-Heraeus vacuum system consisting of a vane pump Model D8A and a turbomolecular pump.

Crystalline phases were identified by matching with standard patterns of the JCPDS (Joint Committee of Powder Diffraction Standards) file. A schematic of the Siemens high temperature x-ray diffractometer is shown in Figure III.9. This unit allows for the heating of a sample on a platinum or iridium heating strip while the unit can run x-ray scans at varying temperatures. Normally the unit is designed to achieve a high vacuum to allow for a clean environment and to avoid oxidation of the costly components. To better assimilate the fiber drawing process, a high purity argon source was attached to the unit. This gave a better model of what is happening when the fiber process is active. The argon was first flowed through a Centorr Oxygen Gettering unit to bring oxygen levels down to around 10^{-7} ppm. This low oxygen level provided protection to all the critical furnace parts at high temperature in the absence of the normal vacuum. A flow of 1 lpm of argon was used through the high temperature x-ray during the scans.

Figure III.9

High Temperature X-Ray Set Up
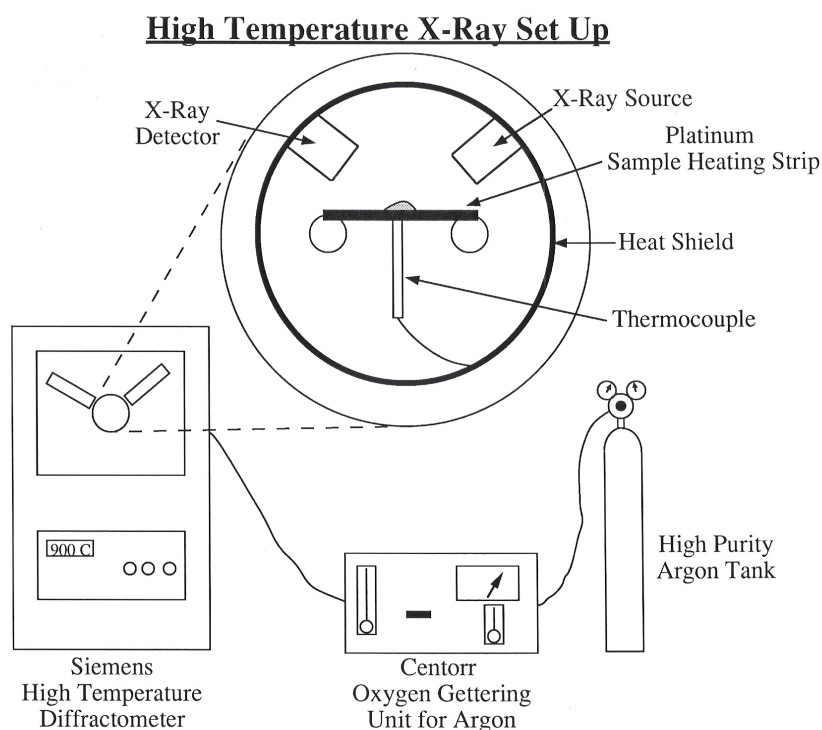
Powder samples of the three compositions were used in order to allow for greater

surface area and increased homogeneity. The powder was placed on the center of the

heating strip and the temperature was monitored by a platinum rhodium thermocouple.

The heat-up was restricted to 20 degrees per minute to again model the true fiber draw

parameters. At 900 ^{o}C and 1000 ^{o}C the x-ray patterns were achieved with the radiation

source and detector.

III.14.3.2 Guinier Camera Analysis of Drawn Fibers

In order to further the understanding of the crystallization process occurring

during drawing, drawn fibers of each bulk composition were crushed in an agate mortar

and pestle and analyzed for the presence of crystals by scanning with a transmission

Guinier-deWolff camera. The camera uses monochromatized CUKα radiation, an operating voltage of 40 KV, current of 30 mA and an exposure time of 12 hours.

III.15 Power Propagation Assessment in Solid Fibers

A Focused Er Yag laser beam was used to study the power propagation capabilities in solid fiber made from Sassoon WB37A glass fiber. The Er YAG laser emits a 2.9 μm beam. The beam was focused down to a spot size of 0.041 mm^2. The fiber investigated was a 550 μm Teflon Clad Fiber and was 1 meter in length. Both ends of the fiber were polished down to 0.3 μm polishing grit size.

IV. EXPERIMENTAL RESULTS AND DISCUSSION

IV.1 Bulk Transmission Measurements

The visible and near IR transmission scan is shown in Figure IV.1 for the Sassoon

silica doped sample. It is clear that the glass is quite transparent throughout this region.

Figure IV.1

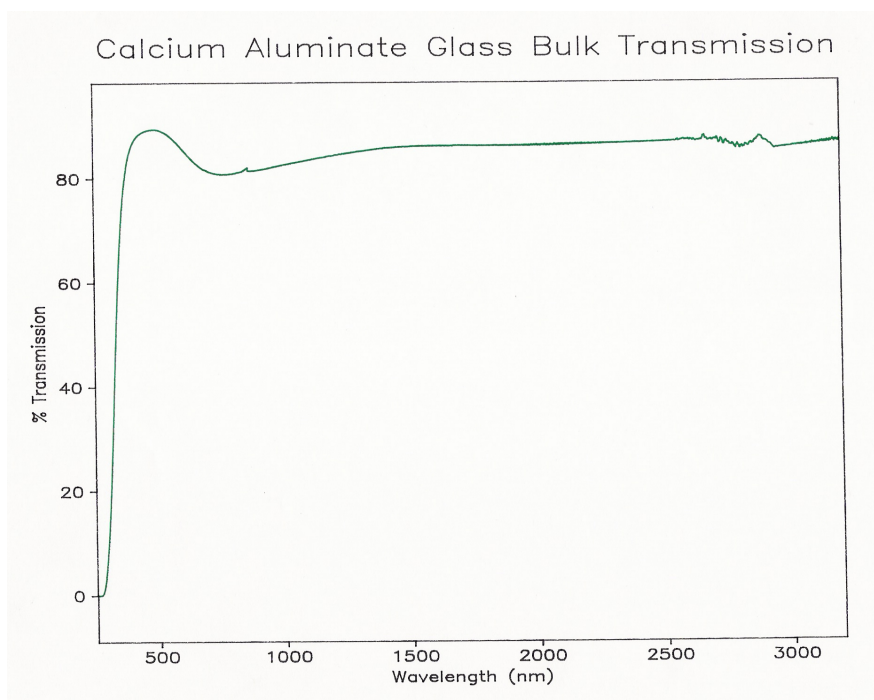Visible and Near IR transmission of Sassoon Silica doped Sample, t = 5mm

The bulk glasses transmission scan results from the Fourier Transform Infrared

Spectrometer is shown in Figure IV.2 for the Sassoon silica doped sample and the Schott

Barium doped sample. The results clearly show that both glasses transmit very well out

to about 5 μm. As expected, the high water content of the Schott barium doped

composition causes a large drop in the transmission centered at 2.9 μm. As we move further out into the infrared region, the transmission of this sample increases to be almost comparable to the Sassoon silica doped sample. The Schott barium doped composition transmits slightly longer into the infrared than the Sassoon silica doped composition. This is due to the additions of silica into the Sassoon composition reducing the infrared transmission in that glass.
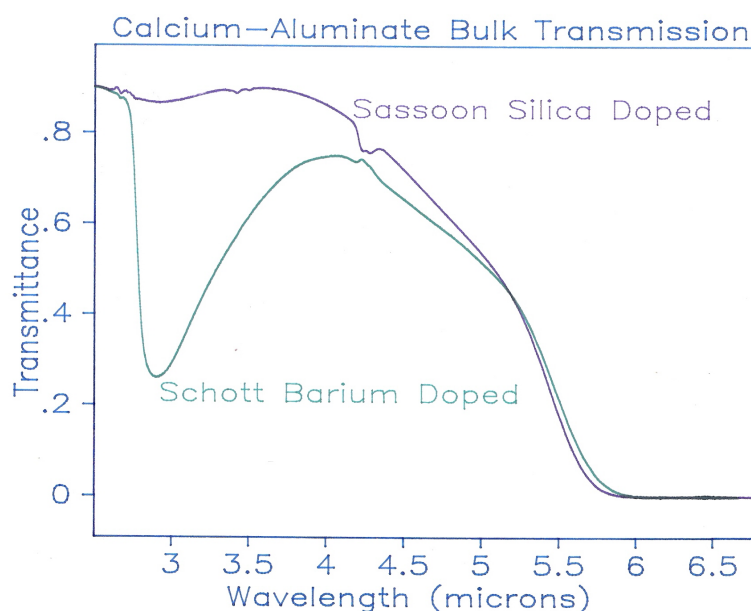

Figure IV.2

FTIR Bulk Glass Transmission of Sassoon WB37A vs. Schott IRG11, t = 5 mm

IV.2 Bulk Glass Scattering Measurements

The bulk glass scattering of the Sassoon WB37A (silica doped) sample is shown in Figure IV.3. The bulk scattering of the Schott IRG11 is shown in Figure IV.4. The scattered intensity is plotted versus the wavelength of the four lasers used in the

measurement. The laser wavelengths used were 540 nm, 594.1 nm, 632.8 nm, and 1150.0 nm. A curve fit to the data shows a $1/\lambda^4$ relationship for both glasses. This $1/\lambda^4$ relationship shows that the scattering is Rayleigh in nature. Rayleigh scattering is elastic related to structural defects and density fluctuations. An indication of the scattering in an optical material being Rayleigh shows that it is of acceptable optical quality.

Scattering of Bulk Glass

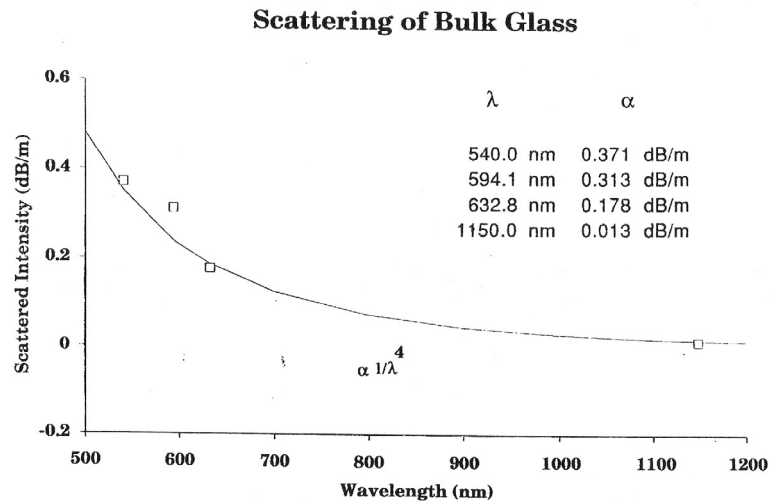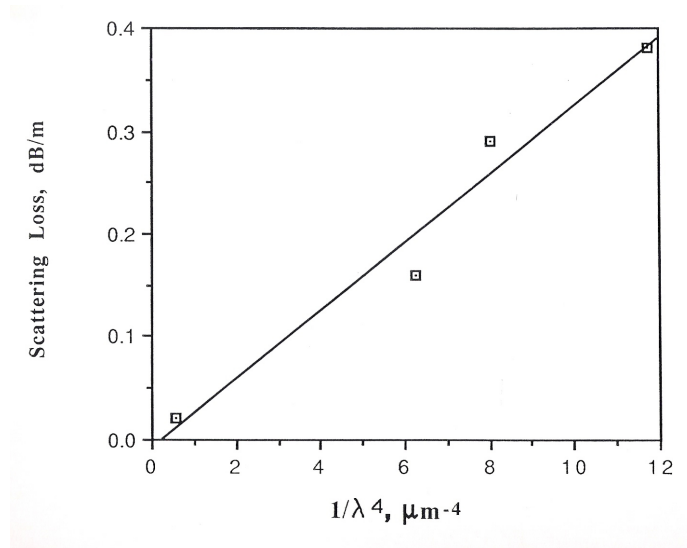| λ		α	
540.0	nm	0.371	dB/m
594.1	nm	0.313	dB/m
632.8	nm	0.178	dB/m
1150.0	nm	0.013	dB/m

Figure IV.3 - Sassoon WB37A

Figure IV.4 - Schott IRG11 Bulk Scattering

IV.3 DTA Analysis Results

Table IV.1 lists the average glass transition temperatures (Tg), crystallization

temperatures (Tx), and the resulting (Tx-Tg) for the runs conducted. For the silica-doped

Sassoon sample, WB37A, it was found that (Tx-Tg) was a maximum in dry nitrogen at

162.0°C. However, at the 95% confidence interval, using the Student t-test distribution,

the 159.5°C value obtained for the glass in air was not significantly different from the dry

nitrogen value. Clearly the moist nitrogen environment greatly affected the glass stability

range, as was demonstrated by the forty degree drop in Tx-Tg to 119.8°C. Contrary to

expectations, chlorine did not have the effect of maximizing the stability of this glass. In

fact, the average Tx-Tg of 131.1°C was distinctly lower than the dry air and nitrogen

values. Although the average values listed in Table I imply that the stability was

somewhat greater in chlorine than in the moist nitrogen environment, at the 95%

confidence interval the difference in the two values was statistically insignificant.

	Sassoon WB37A			Sassoon BS39B			Schott IRG11		
	Silica doped			Baria doped			Baria doped		
ATM.	Tg	Tx	Tx-Tg	Tg	Tx	Tx-Tg	Tg	TX	Tx-Tg
AIR	811.2	970.7	159.5	808.6	929.4	120.8	844.9	975.6	130.7
DRY N2	813.3	975.3	162.0	810.7	937.7	127.0	844.6	973.8	129.1
MOIST N2	808.9	928.7	119.8	800.1	907.4	107.3	840.1	967.2	127.1
C12/ N2	811.5	942.6	131.1	813.7	906.9	93.2	849.0	974.0	125.0

Table IV.1 – DTA Results, in ^{o}C

Figure IV.5 is a graphical representation of typical curves generated in the silica-doped Sassoon WB37A samples for each of the four atmospheres. It should be noted that the glass transition region, which appears as an endothermic peak, was fairly constant in position, while the crystallization region shifted for the moist nitrogen and chlorine runs. A striking feature of the chlorine curve was the distinct exothermic peak immediately following the glass transition peak. It is believed that this exotherm may be due to the reaction of chlorine with surface moisture on the glass to form HCl. Also the fairly broad crystallization peak with a shoulder implied that two phases undergo crystallization in this range. X-ray diffractometry (XRD) confirmed the presence of mayenite ($Ca_{12}Al_{14}O_{33}$) and a very small quantity of an unidentifiable phase. XRD also confirmed

that the extent of crystallization was much less in the chlorine atmosphere compared to the run in dry nitrogen.
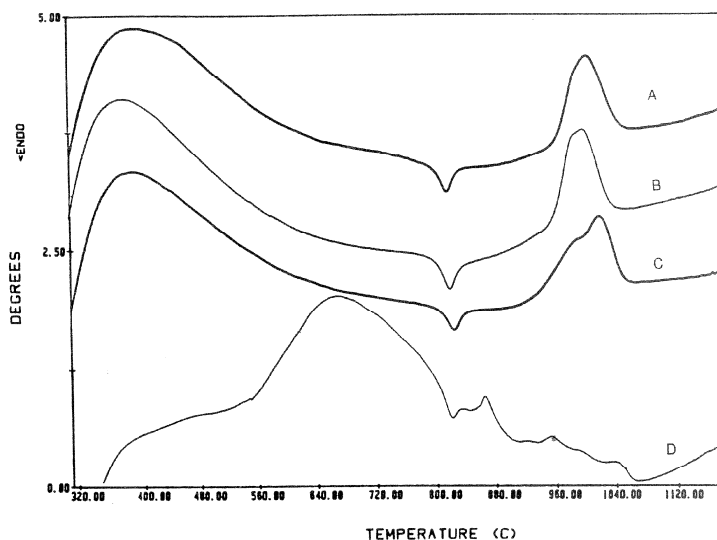

Figure IV.5 – DTA Curves for the WB37A Samples in Atmospheres;
A. Dry Nitrogen, B. Air, C. Moist Nitrogen, D. Chlorine

The average values of Tx-Tg for the barium-doped Schott IRG11 glass are shown in Table IV.1. It is important to note that at the 95% confidence interval none of these values are statistically different. Therefore, neither the moist nitrogen nor the chlorine environment made a substantial impact upon the stability of this glass. It was found, however, that both the glass transition and the crystallization temperatures were shifted to lower temperatures in the moist nitrogen atmosphere. This can be seen, along with the typical curves for the other environments in Figure IV.6. The small exotherm between the glass transition and the crystallization temperatures is again thought to be due to HC1 formation, as in the Sassoon WB37A glass. Although the DTA crystallization exotherm is indicative of only one phase forming, XRD indicated the formation of barium aluminate along with mayenite. The decrease in the extent of crystallization caused by

the presence of chlorine in the Sassoon WB37A glass did not occur in this barium-doped glass.
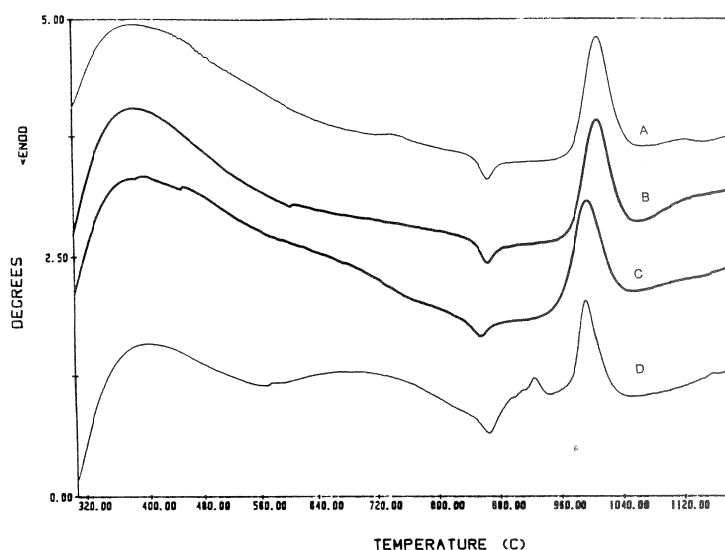
Figure IV.6 – DTA Curves for the IRG11 Samples in Atmospheres;
A. Dry Nitrogen, B. Air, C. Moist Nitrogen, D. Chlorine

The barium-doped Sassoon BS39B glass was the only sample in which the "stability window" was statistically different. As is shown in Table IV.1, the stability of this glass was a maximum in dry nitrogen ($Tx-Tg = 127.0^{o}C$). The stability then decreased successively in air, moist nitrogen, and chlorine. These reductions were all statistically significant at the 95% confidence level. The twenty degree drop in Tx-Tg in moist nitrogen clearly showed that this glass was affected by a humid environment. As for the silica-doped glasses, the differences in Tx-Tg were mainly due to crystallization shifts as opposed to glass transition movement. One exception did occur, however, in that the glass transition temperature seemed to move to a slightly lower temperature in moist nitrogen, a phenomenon also seen in the barium-doped Schott IRG11 glass. Yet

again, the chlorine environment diminished the stability of this glass by reducing the Tx-Tg value to 93.2°C. Figure IV.7 shows a typical curve obtained for this glass in each of the four environments. XRD of this glass indicated the presence of mayenite in samples crystallized in both nitrogen and chlorine environments, with less crystallization occurring in the chlorine environment. The presence of barium aluminate was, however, confirmed in only the nitrogen environment. A small quantity of an additional phase that did not quite match that of barium aluminate was found in the sample run in the chlorine environment.

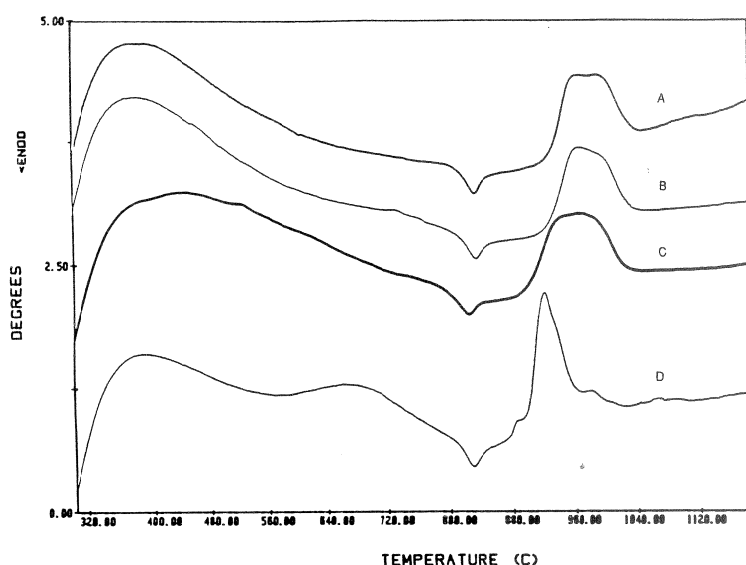Figure IV.7 – DTA Curves for the BS39B Samples in Atmospheres;
A. Dry Nitrogen, B. Air, C. Moist Nitrogen, D. Chlorine

IV.4 DTA Analysis Discussion

The fact that sample Sassoon WB37A had the overall largest stable region was not surprising. Higby, et al.,[34] have shown that the addition of silica to calcium aluminates stabilizes the glasses towards devitrification. It is important to note, however,

that silica additions also degrade the infrared optical properties of the material. Sassoon WB37A also suffered the largest loss of stability in moist nitrogen. Two factors are thought to be responsible for this. First, this sample was thought to contain the least amount of water. It thus follows that it would be the most sensitive to moisture, as compared to samples with sizable water content. Second, it has been shown that when the molar ratio of CaO/Al_2O_3 is greater than one in these glasses, the further addition of CaO acts as a network modifier and thus creates a more open structure.[34] The relevant ratio for Sassoon WB37A was found to be 2.19, which is greater than that of Sassoon BS39B (1.82). Thus moisture would find a more susceptible glass in sample Sassoon WB37A and would affect it with greater intensity.

The effect of chlorine on this glass, however, is not clearly understood. It was thought that the chlorine was reacting with adsorbed surface moisture of the glass and, therefore, greatly reducing the extent of crystallization. Again the greater openness of the structure of this glass may be a consideration, by allowing chlorine to penetrate further into the sample than in the other compositions. This may explain why the extent of crystallization may have been affected much more dramatically in Sassoon WB37A than in the other samples that had either a denser structure or larger water content.

The seemingly inert behavior of glass Schott IRG11 to the different atmospheres can be explained with similar logic. Because of its higher water content, this glass did not have as strong an affinity for moisture. Thus the moist nitrogen did not noticeably degrade its stability. Since it had a large bulk water content, the chlorine may not be able to effectively dehydrate the glass, as it can affect only the surface. Since the exact composition of this glass was unknown, the structural effects cannot be speculated upon.

The stability of glass Sassoon BS39B was affected by moisture, but not as severely as the silica-doped sample. This difference is believed to be due to the differences in the openness of their structures. The barium-doped glass being less open would be less susceptible to variations caused by moisture.

IV.5 CaAl Core/Silica Clad Work

The silica doped Sassoon CAG core fiber was produced with a silica cladding. Several draw trials were necessary before successful fiber drawing was produced. A variety of draw temperatures were tried from 1950°C to 2050°C. The best fiber was produced with a fiber drawing temperature of 1950°C. This was due to the CAG core rod being in a low viscosity liquid state at the normal silica fiber draw temperature of 2000°C. Drawing at 1950°C allowed the silica cladding tube to be at a higher viscosity state, thus resisting deformation of the circular geometry from the low viscosity core liquid. The most stable draws were those done at 1950°C. The coated fiber had an overall diameter of 320 μm.

Scanning electron micrographs are shown in Figures IV.8 and IV.9. Figure IV.8 shows the fiber endface with an outside diameter of 250 μm and a core diameter of 50 μm. The polymer coating was removed from the fiber before placing into the scanning electron microscope. A flat cleave was difficult to produce in this fiber. This is due to the difference in thermal expansion coefficient between the CAG core and the silica cladding. The silica doped Sassoon CAG has a thermal expansion of $9.5 \times 10^{-6}/^{\circ}$C and the silica tubing has a thermal expansion of $0.55 \times 10^{-6}/^{\circ}$C.
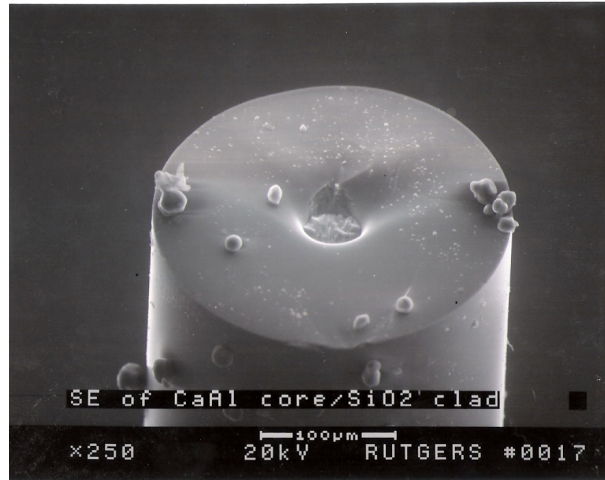
Figure IV.8 - SEM Photomicrograph of CAG core/Silica Clad Fiber

Figure IV.9 is a close up of the core region of the resulting fiber. The core region is clearly visible with uneven cracking throughout. The silica cladding cleave face curves smoothly down towards the core region. Approximately 50 cleaves were attempted to achieve an ideal cleave. Figure IV.9 is the best result obtained.

Figure IV.9 - SEM Photomicrograph of CAG Core/Silica Clad Fiber
Core Region - Close up

The difficulties getting good cleaves across the fiber endface prohibited any good optical transmission measurements on the 50 μm/250 μm CAG core/silica cladding fiber. The production of the fiber did prove that this design could be made.

In order to obtain CAG core/silica cladding fiber with better cleave endfaces, a smaller diameter CAG core was produced. This fiber endface is shown in Figure IV.10. To produce this fiber, a single 200 μm OD fiber sample of drawn silica doped Sassoon CAG was used. This fiber was placed into a starting silica glass tube of the dimensions 25 mm OD by 3 mm ID by 1 meter long and drawn out into 250 μm fiber.

Figure IV.10 - SEM Photomicrograph of 8 μm/250 μm CAG/Silica Fiber

A flat cleave was obtained throughout the fiber endface. A close up of the core region of this fiber is seen in Figure IV.11. The core region took on a rectangular shape. This was not expected since the starting cladding tube inside diameter was round, and the starting core fiber was round. Closer investigation of the neck down region of the preform after the draw revealed that the CAG core fiber had stuck to the side of the inside

of the silica cladding tube as it was collapsed into CAG fiber. This caused an asymmetric consolidation of the core region, resulting in the non-circular shape. The core had approximate dimensions of 4 μm by 10 μm.

Figure IV.11 - SEM Photomicrograph of 8 μm /250 μm CAG/Silica Fiber
Core Region Close up

Numerical aperture measurements (NA) were performed on the fiber. A 0.633 μm wavelength helium neon laser was used for this experiment. The NA was calculated as 0.69. Obviously diffusion of silica from the cladding plays a role since the calculated NA would be 0.815 at 0.6563 μm.

The V value was calculated for this fiber configuration. Optical fibers are characterized by their structure and by their properties of transmission. Basically, optical fibers are classified into two types. The first type is single mode fibers. The second type is multimode fibers. As each name implies, optical fibers are classified by the number of modes that propagate along the fiber. The structure of the fiber can permit or restrict modes from propagating in a fiber. The basic structural difference is the core size.

Single mode fibers are manufactured with the same materials as multimode fibers. Single mode fibers are also manufactured by following the same fabrication process as multimode fibers.

The core size of single mode fibers is small. The core size (diameter) is typically around 8 to 10 μm in a silica optical fiber. A fiber core of this size allows only the fundamental or lowest order mode to propagate around a 1300 nanometer (nm) wavelength. Single mode fibers propagate only one mode, because the core size approaches the operational wavelength. The value of the normalized frequency parameter (V) relates core size with mode propagation.

In single mode fibers, V is less than or equal to 2.405. When V equals 2.405, single mode fibers propagate the fundamental mode down the fiber core, while high-order modes are lost in the cladding. For low V values (ie; 1.0), most of the power is propagated in the cladding material. Power transmitted by the cladding is easily lost at fiber bends. The value of V should remain near the 2.405 level in silica fibers. Single mode fibers have a lower signal loss and a higher information capacity (bandwidth) than multimode fibers. Single mode fibers are capable of transferring higher amounts of data due to low fiber dispersion. Basically, dispersion is the spreading of light as light propagates along a fiber. Signal loss depends on the operational wavelength. In single mode fibers, the wavelength can increase or decrease the losses caused by fiber bending. Single mode fibers operating at wavelengths larger than the cutoff wavelength lose more power at fiber bends. They lose power because light radiates into the cladding, which is lost at fiber bends. In general, single mode fibers are considered to be low-loss fibers, which increase system bandwidth and length.

As their name implies, multimode fibers propagate more than one mode. Multimode fibers can propagate over 100 modes. The number of modes propagated depends on the core size and numerical aperture (NA). As the core size and NA increase, the number of modes increases. Typical values of silica fiber core size and NA are 50 to 100 μm and 0.20 to 0.29, respectively.

A large core size and a higher NA have several advantages. Light is launched into a multimode fiber with more ease. The higher NA and the larger core size make it easier to make fiber connections. During fiber splicing, core-to-core alignment becomes less critical. Another advantage is that multimode fibers permit the use of light-emitting diodes (LEDs). Single mode fibers typically must use laser diodes. LEDs are cheaper, less complex, and last longer. LEDs are preferred for most applications.

Multimode fibers also have some disadvantages. As the number of modes increases, the effect of modal dispersion increases. Modal dispersion (intermodal dispersion) means that modes arrive at the fiber end at slightly different times. This time difference causes the light pulse to spread. Modal dispersion affects system bandwidth. Fiber manufacturers adjust the core diameter, NA, and index profile properties of multimode fibers to maximize system bandwidth.

The V value calculated for this fiber configuration was 13.67 using a 0.633 μm wavelength helium neon laser.

Strength testing on these SiO_2-clad fibers was performed on the 50 μm/250 μm fiber and the 10 μm /250 μm fiber. Two point bend testing was the technique used for this investigation. The 50 μm/250 μm fiber was very brittle and all samples broke while loading into the testing jig. No breaking measurements were possible with this fiber.

This was due to the high level of thermal expansion mismatch between the CAG core glass and the silica cladding. This high residual stress in this fiber is evident in the fiber endface SEM photomicrographs shown in Figures IV.8 and IV.9.

The 8 μm/250 μm fiber also appeared to be under high residual stress. Of the 50 fibers that were tested in the two point bending jig, 30 broke during loading. Of the 20 remaining samples, there was a wide range of stain calculated. These measurements ranged from 1.549 to 11.431 %.

IV.6 CAG Fiber Drawing

Initial CAG draw trials were conducted on the draw tower using the standard carbon resistance draw furnace manufactured by Centorr/Vacuum Industries. This furnace has a heat zone vertical length of approximately 30 mm. 100 mm long by 10 mm diameter CAG sample rods were hung in the furnace and heated up to 920°C, the estimated drawing range. It was hoped the sample rod would elongate under the force of gravity forming a drop, as in normal fiber draws. Draw samples were heated up in the furnace at a rate of 10°C/minute. However, all CAG sample rods devitrified in the furnace before forming a drop using this draw furnace. It became apparent that a smaller heat zone and active pulling of the rod out into a drop was going to be required if fiber drawing was possible from CAG samples.

A custom draw furnace was fabricated specifically for the drawing of CAG rod samples. This work included modifying a Heathway, Inc. soft glass induction furnace that was capable of reaching temperatures of 1200°C. The furnace has a silica liner tube

which defines the draw atmosphere inside it. The silica liner tube has a step in it to support the carbon susceptor ring in the heat zone center.

Successful drawing of the CAG glass fibers was accomplished through the use of the custom renovated drawing furnace and the sample coupling arrangement. In order for the fiber drawing to start successfully, tension needed to be applied to the bottom alumina tube of the sample holding arrangement as the draw temperature was reached. If no tension was applied to the CAG glass rod sample to start the draw, the sample would devitrify completely and no fiber would be obtained.

IV.7 Propane/Argon Atmosphere Draw

Following the work of Wallenberger[55-64, 66-69], propane was added to the furnace gas flow stream to try and inhibit the formation of surface crystallization. The normal argon gas flow settings for the custom renovated were 2 lpm at the top furnace gas input and 2 lpm at the bottom furnace gas input. To these normal argon gas flows, 1 lpm of commercial grade propane was added. All gases were run through 0.3 µm gas filters before entering the furnace. This filtering would insure that no particle contamination would enter the furnace heat zone, degrade, coat the fiber, and cause fiber weakness.

Different propane flows were tried to optimize the flow and fiber production. The propane flow ranged from 0.25 to 5 lpm. At flows above 1 lpm propane, no successful fiber drawing was accomplished. At these higher propane flow levels, large amounts of carbon soot coated the neckdown region of the rod. When this happened, the initial fiber drawing came down in clumps, stopping further drawing.

Lower propane flow rate 0.25 to 0.75 lpm did not seem to help the fiber drawing. No carbon coating was apparent on the fiber. 1 lpm gave the best results. A slight gray film was apparent on the fiber at this flow level. Diameter control of the fiber during the drawing at 1 lpm propane flow was difficult to maintain. Fiber diameters deviated in excess of +/- 50 μm during the draw, which is far worse than the normal +/- 10 microns seen on other draws.

The attenuation curve for the silica doped Sassoon CAG is shown in Figure IV.12. The fiber was 500 μm in diameter. It is apparent in these results that the water peak around 2.9 μm is suppressed. This showed that the propane addition to the furnace gas flow stream did indeed suppress surface moisture in the resulting fiber. The lowest loss of this fiber is seen at approximately 3.2 μm. At this wavelength, the loss level was approximately 10 dB/meter.
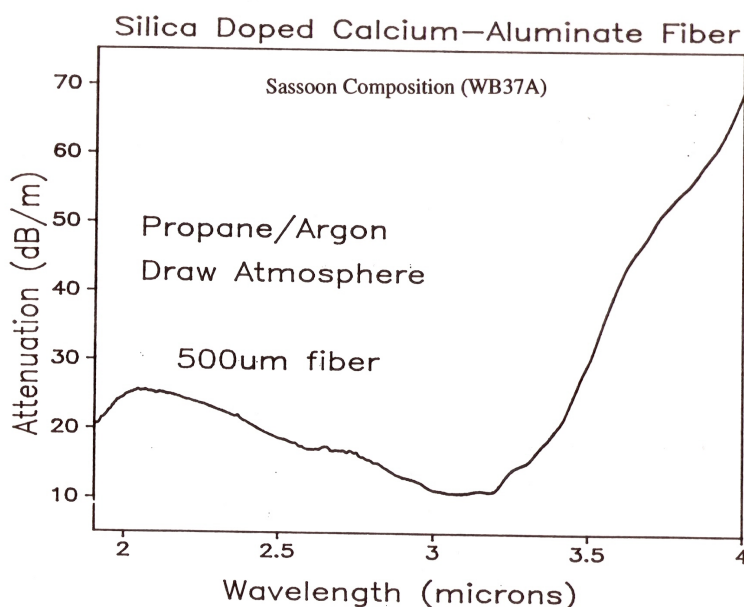

Figure IV.12 – WB37A Fiber Attenuation Drawn with Propane Atmosphere

IV.8 NF$_3$ Reactive Atmosphere Drawing

Reactive atmosphere drawing of the CAG glass fibers was tried to attempt the suppression of surface crystallization during drawing. A schematic of the equipment set up is shown in Figure IV.13.

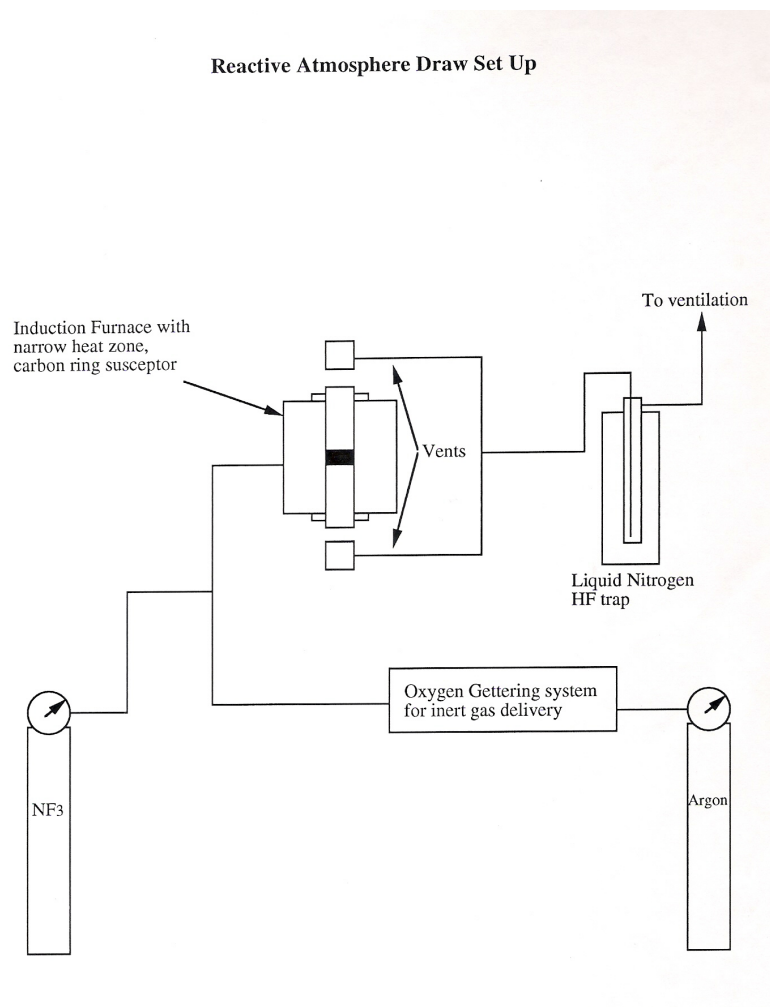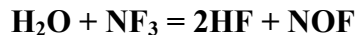**Reactive Atmosphere Draw Set Up**

Figure IV.13 – Reactive Atmosphere Draw Set Up

NF$_3$ added to furnace gas flow stream in an attempt to remove water from furnace atmosphere and water on glass surface. It was hoped that this water removal would prevent surface crystallization.

The reaction of NF_3 with water is as follows;

$$H_2O + NF_3 = 2HF + NOF$$

Similar to normal drawing conditions, argon gas was flowed through a gettering unit, to remove oxygen. The NF_3 is then added to the argon flow stream into the furnace at the top and bottom gas flow inlets. The gases were pulled away from the furnace through the use of venting.

Due to the known formation of HF in the reaction of NF_3 with water, a gas scrubbing unit was fabricated. Venting caps were placed at the top and bottom of the furnace to collect any furnace gases. The liquid nitrogen trap caused any HF that was formed to precipitate in the scrubbing vessel before releasing to atmosphere. The temperature of draw (920^oC) caused rapid fluorination of sample surface. Calcium and aluminum fluoride formation on glass surface prevented any drawing from being accomplished.

IV.9 Hollow CAG Waveguide

Using the lessons learned during the drawing trials of solid CAG fiber, hollow CAG waveguides were obtained. This hollow tube fiber was reasonably brittle as a result of some devitrification, but 50 to 100 cm long pieces were obtained for the measurements.

In Figure IV.14, the optical parameters obtained for IRG-11 glass are shown. It can clearly be seen that n is less than 1 over the longer-wavelength CO_2 laser bands, i.e., from 10.2 to 12.1 μm. If silica is present in the calcium aluminate glass, then the n < 1 range is shifted to shorter wavelengths.
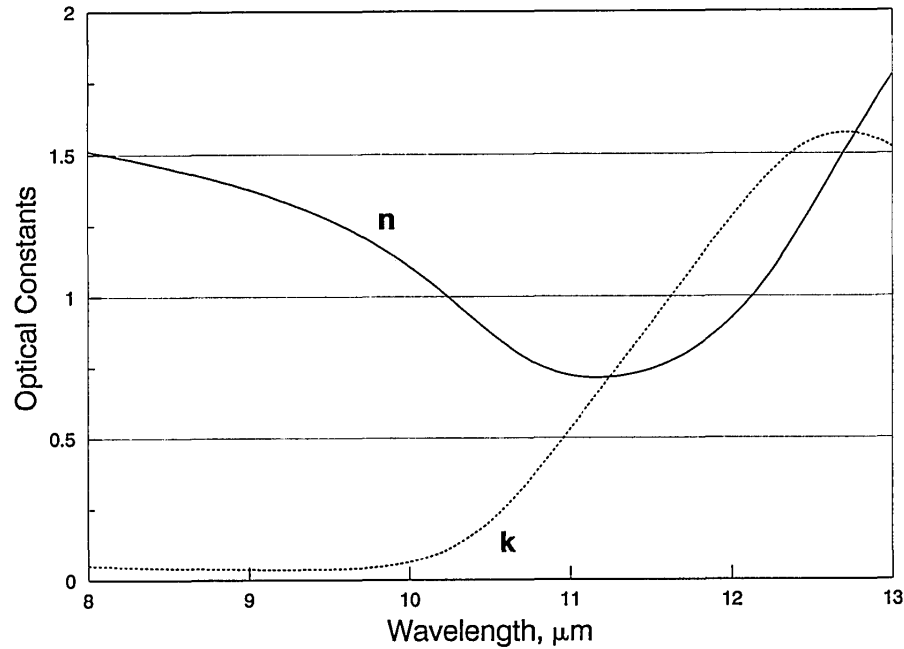
Figure IV.14 – Optical Constants n and k for IRG11 Calcium Aluminate

The loss for a 500 μm bore IRG-11 waveguide, calculated with Eq. (1) from

section III.6.2 and the n and k values given in Figure IV.14, is shown along with the

experimental data in Figure IV.15. The data points from 9.22 to 10.78 μm were taken

with a tunable CO_2 laser. The calculated loss for the 500 μm diameter tube at 10.6 μm,

with $\upsilon = 0.83 — i0.26$, is 6.4 dB/m. This is the loss for the lowest-order HE_{11} mode.

From Equation (1) it can be seen that the contribution to the attenuation coefficient from

higher-order modes increases with U_{nm}^2 and thus adding only a contribution from the

HE_{12} mode to the HE_{11} mode, for example, can appreciably increase the waveguide loss.

The spatial profile of the output beam of the guides was measured and found to be nearly

Gaussian, and thus there is the belief that there is only a small contribution from higher-

order modes to the total loss. A similar situation was observed by Gregory and

Harrington[96] for the n < 1 lead-based Corning 0120 glass. In fact they found that the loss

measured in this hollow 0120 glass fiber agreed with the theoretical MS loss for the HE_{11}

mode. For the calcium aluminate fiber in this paper, however, the experimental loss is

8.6 dB/m at 10.6 μm. To account for the additional 2.4 dB/m loss, mechanisms are
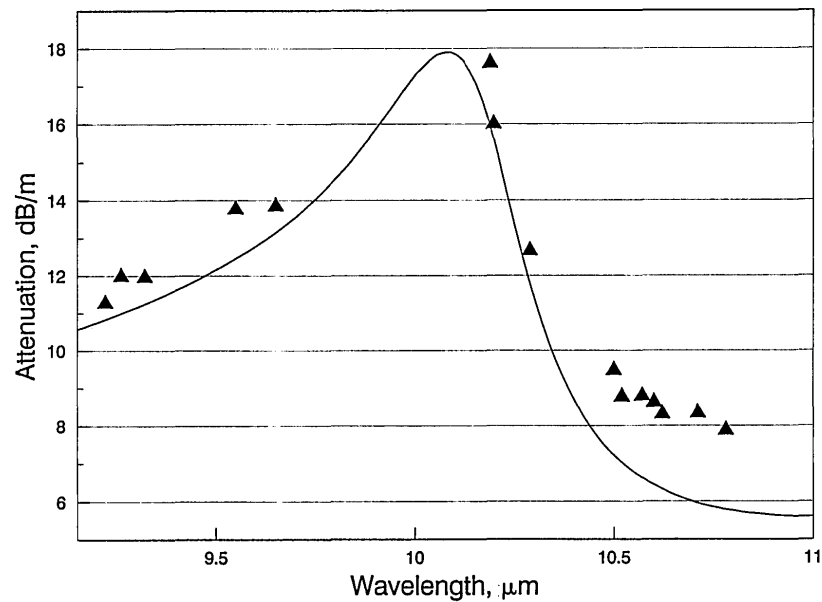
investigated in addition to higher-order modes.

Figure IV.15 – Theoretical (Solid Curve) and Experimental (Data Points)
Attenuation over the Tunable CO_2 Laser Wavelength Region

The most likely source of this additional loss is inner-surface roughness. This is

seen in fibers, and there is a belief that the surface roughness in part is due to small

crystals on the inner surface, which occur as a result of devitrification during the drawing

of the fibers. The roughness of the fiber, however, is not due to the surface of the

preform, because the preform has a highly polished inner surface. From profilometer

scans of the inner surface of the fiber significant roughness was found. On closer

examination, small crystals were discovered that were on the average 150 μm in length

and 10 μm in height, randomly distributed on the surface. Danilov, et al.,[110] have included the effects of surface roughness on total hollow waveguide loss for a periodic roughness variation. In this paper the surface does not have a uniform roughness, but it is believed, based on the size of the scatterer, that the additional loss can be easily attributed to the small crystallites on the inner surface of the fiber. A similar effect was observed by Gregory and Harrington[96] for hollow sapphire fibers. For sapphire, however, the roughness was uniform, and Danilov's theory accurately predicted the additional roughness loss.

The attenuation for hollow calcium aluminate fibers with different bore radii is shown in Figure IV.16. Again the lower MS loss predicted for the glass compared with the experimental results can be seen in these data. As discussed above, it is believed that this primarily is due to surface roughness and some mode mixing. The higher loss at smaller bore radii reflects the increase in attenuation with decreasing bore radius, as predicted by Equation (1). In general, it can be seen from the data that both theoretical and experimental losses are quite high for these bore radii. These losses are too high for most practical applications, and thus one would want to use a larger bore tube, for example, a 1000 μm bore tube for a lower loss.
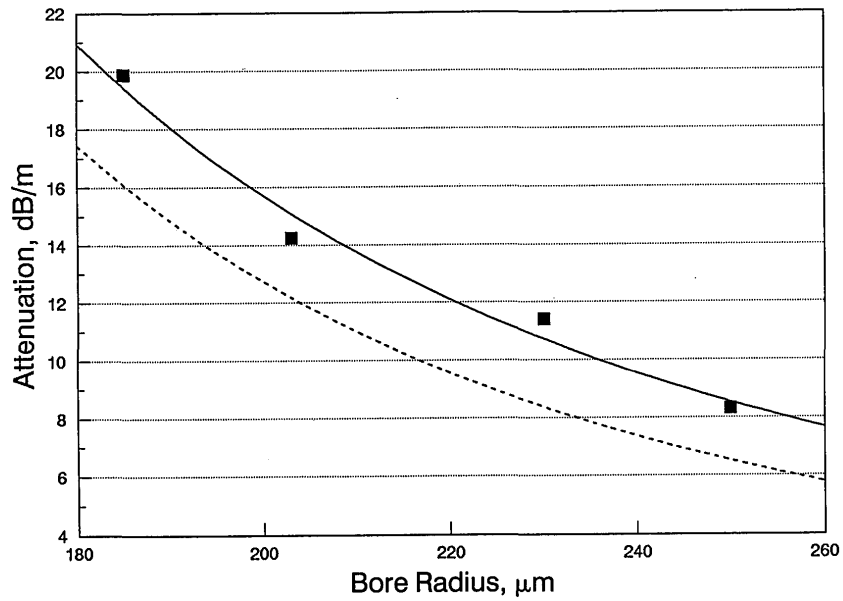
Figure IV.16 – Losses for different bore radii (data points) compared
with MS theory (dashed curve) for the lowest-order HE_{11} mode.
The solid curve is a fit to the experimental data.

The bending loss for the 50 cm long 460 μm bore hollow glass waveguide is

shown in Figure IV.17. The loss is seen to increase with increasing curvature, as

predicted by Miyagi and Karasawa.[105] Their theory yields a 1/R dependence for the

attenuation coefficient, and this is confirmed in the data shown in Figure IV.17.

Unfortunately, this hollow glass fiber tube was not able to be bent into radii smaller than

50 cm because the glass was uncoated. A polymer coating could improve this situation.

In spatial profile measurements, the profile of the bent guide was virtually identical to the

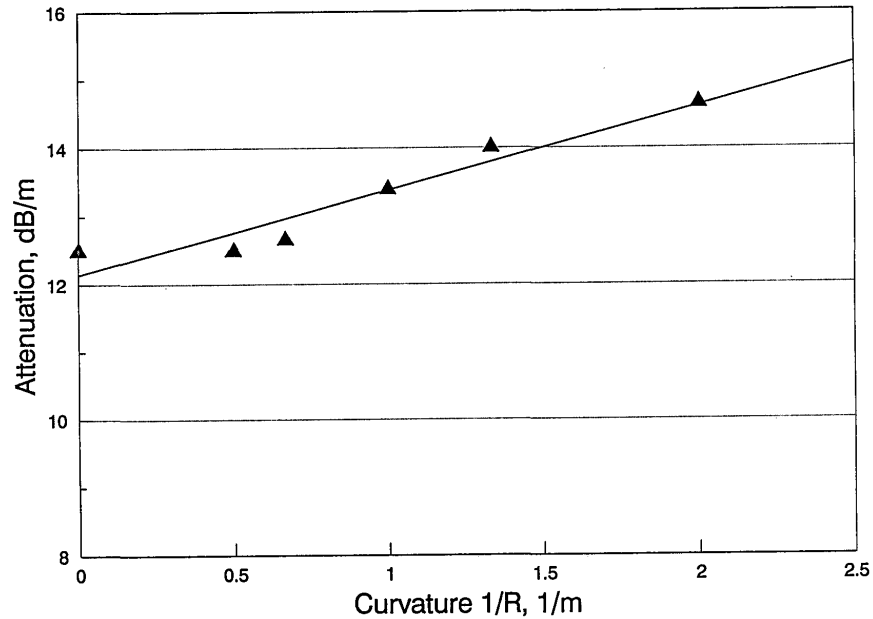Gaussian profile measured when the guide was straight.

Figure IV.17 – Bending losses for the 500 μm hollow glass fiber

Calcium aluminate glass has many ideal properties for hollow fiber optics. It has a glass-transition temperature near that of silica and it is nontoxic, which is important for surgical laser applications. It is also a relatively inexpensive glass that can be fabricated into long lengths of hollow fibers with fiber-drawing technology. In contrast, hollow sapphire is grown at slower rates, and it is stiffer than most types of glass. The disadvantage is that calcium aluminate is difficult to fabricate without some effects of devitrification. Nevertheless, there are not too many types of glass that have n < 1 at 10.6 μm and that can be drawn into fibers, so calcium aluminate remains a good candidate for CO_2 laser-power- delivery applications. In tests 24 watts of CO_2 laser power was launch in before the hollow fiber failed. By reducing the losses in these fibers to their theoretical values, as has been done for the lead-based oxide glass,[95] a fiber capable of delivering even greater laser power should be obtained and thus a good fiber for CO_2 lasers.

IV.10 Solid Fiber Power Delivery – Laser Damage

Fibers made from the Schott IRG11 sample composition were fabricated for investigating the Erbium YAG laser power propagation through the solid fiber. One meter lengths of Teflon coated 550 μm glass diameter fiber were used. The fiber endfaces were polished down to 0.3 μm grit size to achieve mirror finishes. An Erbium YAG laser beam was focused onto the input fiber end. The spot size of the beam was 0.041 mm^2. The results of the of the power propagation experiments through solid fiber are shown in Table IV.2. The average power output recorded was 7.22 J/mm^2. At higher powers than those recorded, the ends of the fibers would show laser damage.

Table IV.2

Laser Damage Measurements

Output to ref. Detector *	Multiplication Factor =	Energy	Energy density E/Area
2.645 mJ	157	415.265 mJ	10.13 J/sq. mm
2.059 mJ	157	323.263 mJ	7.88 J/sq. mm
2.360 mJ	157	370.520 mJ	9.04 J/sq. mm
1.860 mJ	157	292.020 mJ	7.12 J/sq. mm
0.975 mJ	157	153.075 mJ	3.73 J/sq. mm
1.420 mJ	157	222.940 mJ	5.44 J/sq. mm

Spot size 0.041 mm^2

Figures IV.18 and IV.19 are SEM photomicrographs of the fiber endfaces after the laser damage. It clearly shows that at the higher powers, the fiber endface cracks out in a scallop type shape.
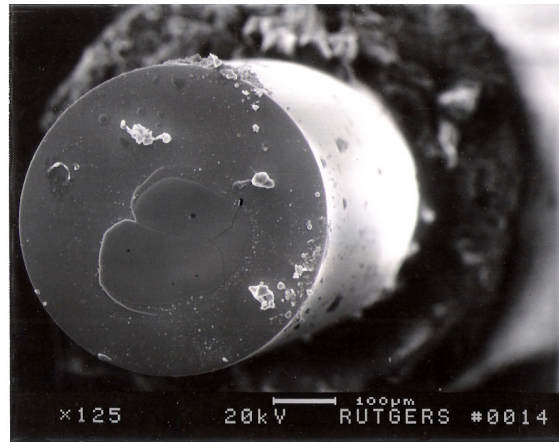
Figure IV.18 - SEM Photomicrograph of Laser Damage to Fiber Endface
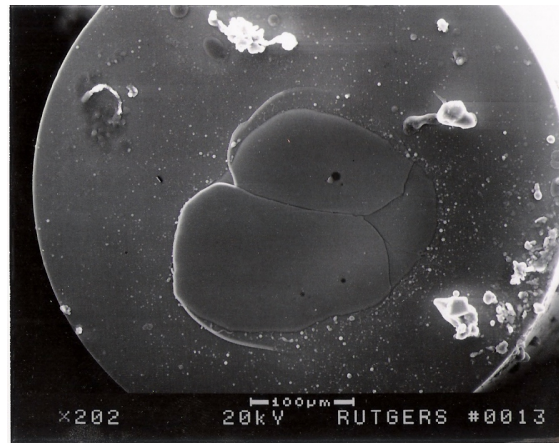
Figure IV.19 - Close up of SEM Photomicrograph of Laser Damage to Fiber Endface

IV.11 Fiber Strength Data

The four point bend testing results are shown in Table IV.3. As the data show, the fiber strength of the Schott IRG11 fibers was the best. Since this composition had a high degree of water in it, this was surprising. It is believed that the strength data are more related to the amount of surface crystallization that occurred during the drawing of fibers. It was difficult to start and maintain the fiber drawing in the same way during each sample draw. If the start of the draw was slower than the average, more surface

crystals would form. As noted, these fiber strengths were much less than the typical silica fiber strength levels obtained.

Strength Tests
(4-point bending, 500 μm diameter, in ambient conditions)
MPa

Silica doped Sassoon	Barium doped Sassoon	Barium doped Schott
450 - 720	670 - 940	820 - 1290

Silica fibers of 125 μm diameter have a typical strength of 5 GPa in ambient conditions.

Table IV.3 – Four Point Strength Measurement Data

Table IV.20 show the Weibull distribution for the strength data for the 500 μm IRG11 fiber samples done in air and in liquid nitrogen. The data reveal much higher strain levels obtained in liquid nitrogen than in air. This shows that the surface water initiates the fatigue in these fibers.
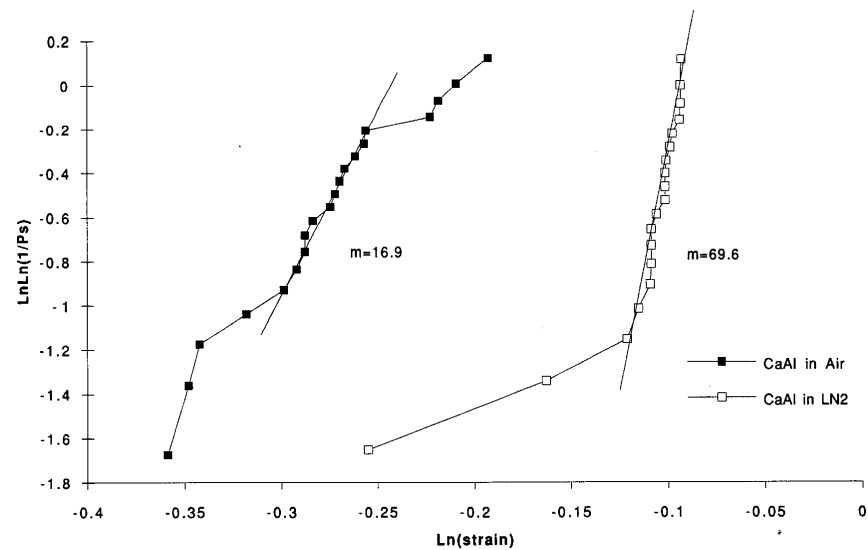

Figure IV.20 – Weibull Distribution for 500 μm IRG11 Fiber Strength

IV.12 Crystallization Product Assessment

The products of the surface crystallization were assessed with the following techniques.

5. Scanning Electron Microscopy (SEM)

6. Energy Dispersive Analysis (EDA)

7. Hot Stage X-Ray diffraction

8. Guinier Camera X-ray diffraction

IV.12.1 Surface Crystallization on Drawn Fibers - SEM

In order to get a better idea of the surface crystallization that was occurring during drawing, the fiber neckdown region was investigated through the use of the scanning electron microscopy (SEM). These images are seen in Figures IV.21 and IV.22. Figure IV.21 is at 600X, and Figure IV.22 is the same image at 1000X. It is clear from these photomicrographs that the crystallization forms at the neckdown region and is broken off into chips and pulled down with the drawn fibers. These chips act as stress concentrators, causing the fiber weaknesses.
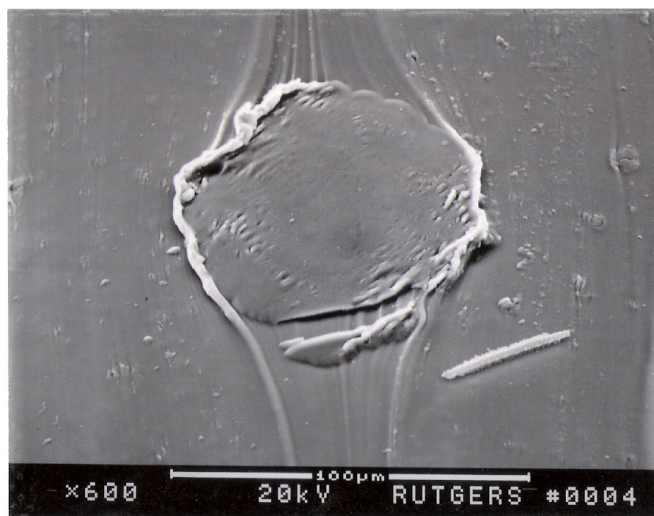
Figure IV.21 - SEM Photomicrographs of Fiber Surface Crystallization, 600X
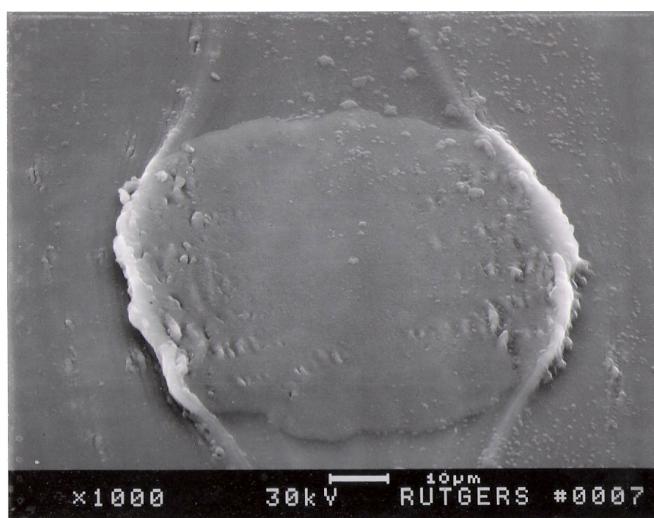
Figure IV.22 - SEM Photomicrographs of Fiber Surface Crystallization, 1000X

Surface crystallization on all three CAG neckdown regions is shown in Figure IV.23. The surface crystallization is clearly aggressive during the heating of the CAG rods for fiber drawing. The Sassoon samples in particular show distinct crystal faceting on the neckdown surface. The crystallization of the Schott sample neckdown appears to be more irregular in nature.

Sassoon Ba doped CaAl Neckdown ↑

Sassoon Si doped CaAl neckdown ↑

Schott Ba doped CaAl neckdown →
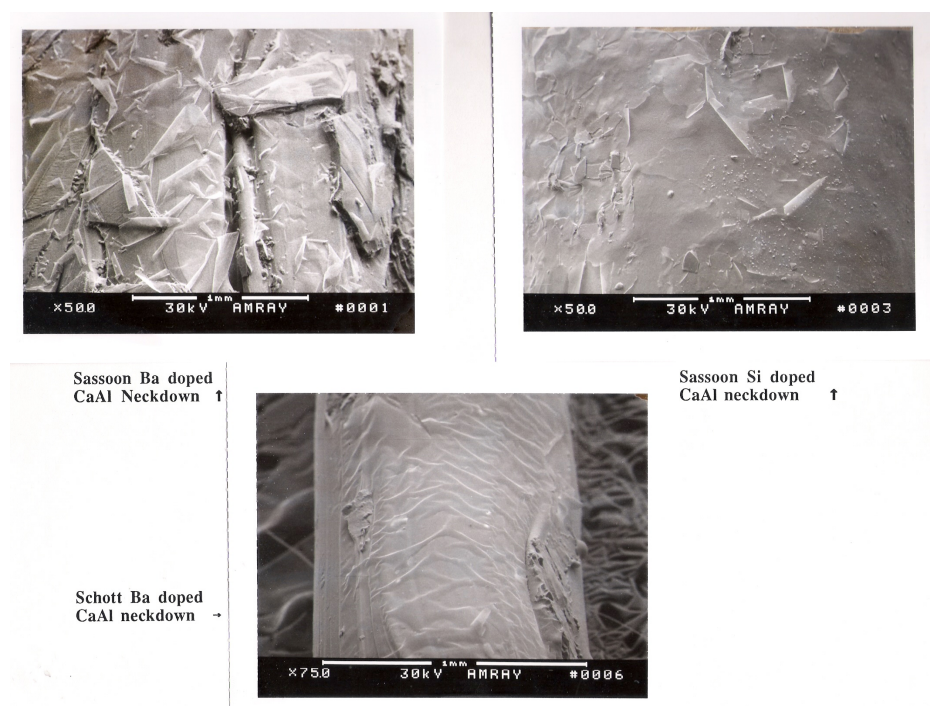
Figure IV.23 - SEM Photomicrographs of Neckdown Region Surface Crystallization

IV.12.2 Energy Dispersive Analysis (EDA)

Energy dispersive analysis on the SEM was used to understand the compositional changes that are occurring at the crystallized surface of the draw sample neckdown region. Base glass compositional analysis is overlayed on the scan taken at the crystallized neckdown region of the sample rods.

Figure IV.24 shows the scans of the silica doped Sassoon sample. The "basesicaal1" is the scan of the non-crystallized base glass. The "sicaalnk" is the scan of the crystallized neckdown region. It is clear from these scans that the crystallization products have an increase in the content of calcium and a decrease in the content of aluminum relative to the base glass composition.

Silica doped Sassoon CaAl base glass vs Neck-down region
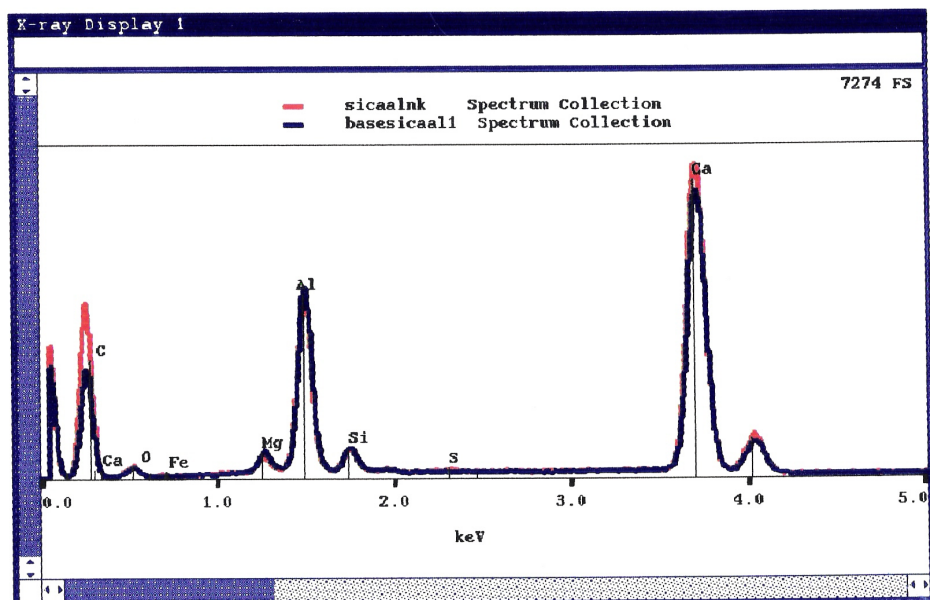
Figure IV.24 - EDS Scan of WB37A

Figure IV.25 shows the scans of the barium doped Sassoon sample. The "bassassbacaal1" is the scan of the non-crystallized base glass. The "bacaalnk" is the scan of the crystallized neckdown region. It is clear from these scans that the crystallization products also have an increase in the content of calcium and a decrease in the content of aluminum relative to the base glass composition.

Barium doped Sassoon CaAl base glass vs Neck-down region

Figure IV.25 - EDS Scan of BS39B
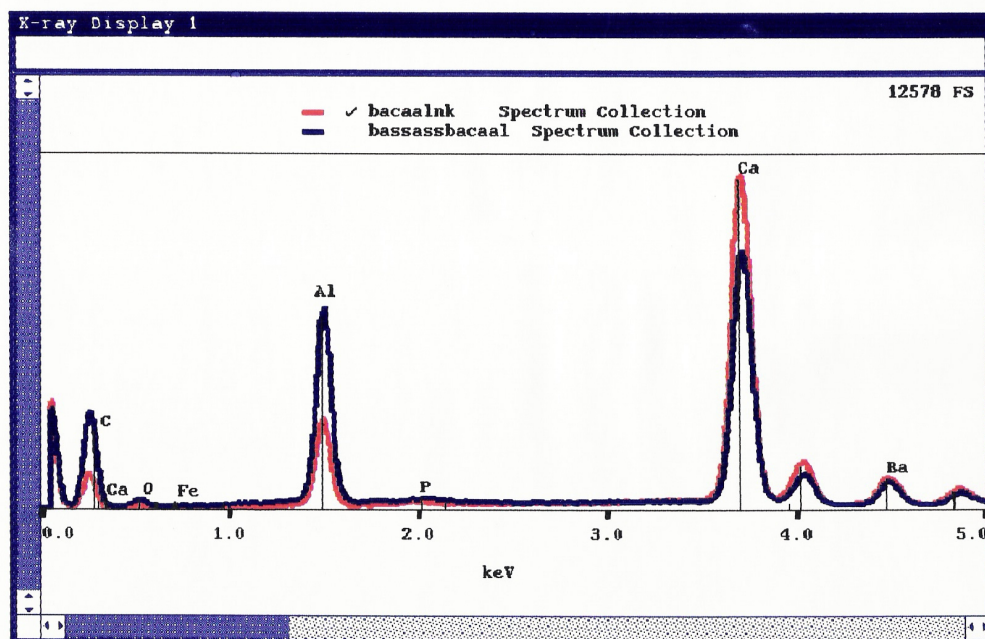
Figure IV.26 shows the scans of the barium doped Schott sample. The "basebacaal1" is the scan of the non-crystallized base glass. The "schbacaaltb" is the scan of the crystallized neckdown region. It is clear from these scans that in the crystallization products the content of calcium remains the same and there is a large increase in the aluminum content relative to the base glass composition.

Barium doped Schott CaAl base glass vs drawn tube surface
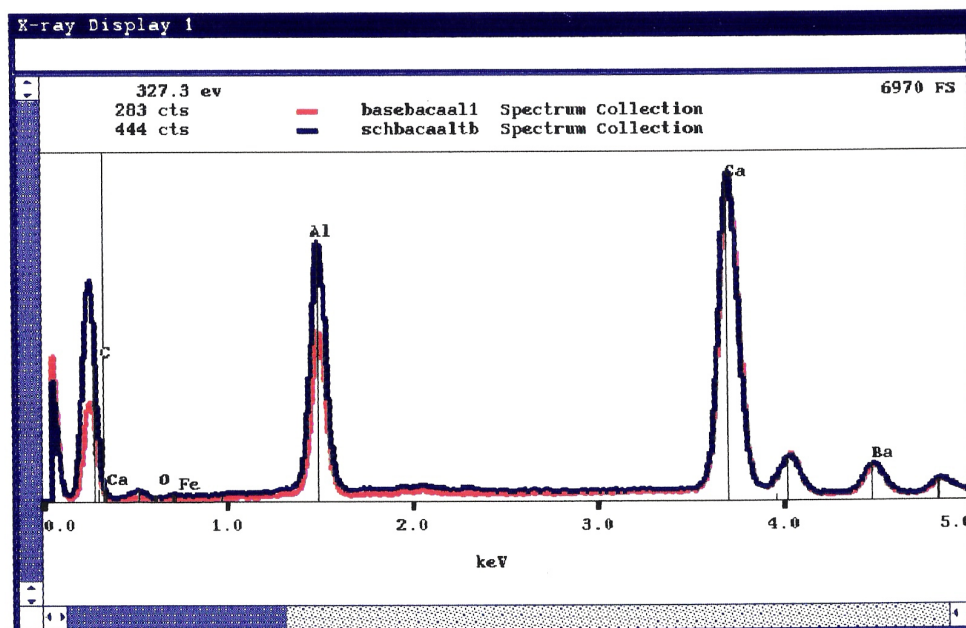
Figure IV.26 - EDS Scan of IRG11

IV.12.3 X-ray Diffraction Studies

IV.12.3.1 Hot Stage XRD of Glass Powder Samples

The results of the high temperature X-Ray diffraction scans on the three glass powders are shown in the next three figures. Figure IV.27 is of the Si-doped Sassoon glass WB37A, Figure IV.28 is of the Ba-doped Sassoon glass BS39A, and Figure IV.29 is of the BA-doped Schott glass IRG11. The large peak shown on the right of all three scans results from the Iridium heating strip and is not a function of the glass powders. All three scans were run with a in a high purity argon atmosphere with a flow of 1 lpm of argon into and out of the system. This models the fiber draw process.

Figure IV.27 - Hot Stage X-Ray Scan of WB37A (Sassoon Silica Doped) Powders

The Si-doped Sassoon glass powder sample scans did not show crystallization peaks at 900° C. This would be consistent with the amorphous nature of the glass. However, at 1000° C, a tricalcium aluminate crystal peak is clearly noted.
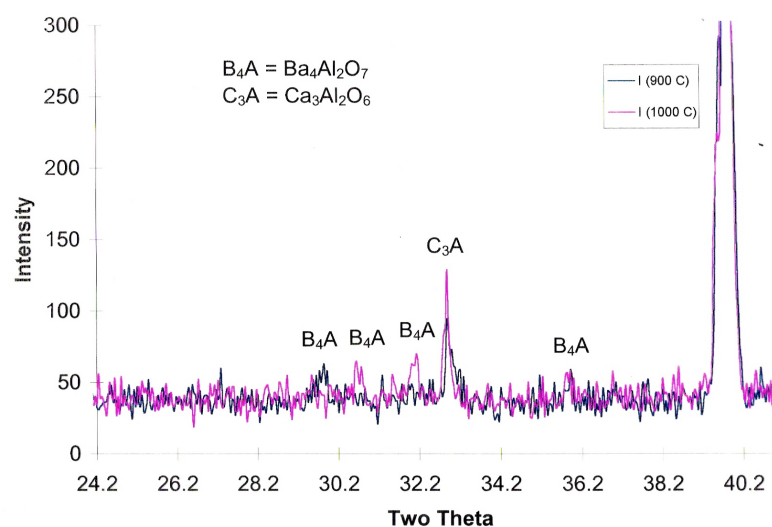
Figure IV.28 - Hot Stage X-Ray Scan of BS39B (Sassoon Baria Doped) Powders

The Ba-doped Sassoon glass powder sample scans showed the formation of the tricalcium aluminate crystal at $900^{\circ}C$, along with a barium aluminate crystalline phase. Both these crystal species grew as the temperature was increased to $1000^{\circ}C$.
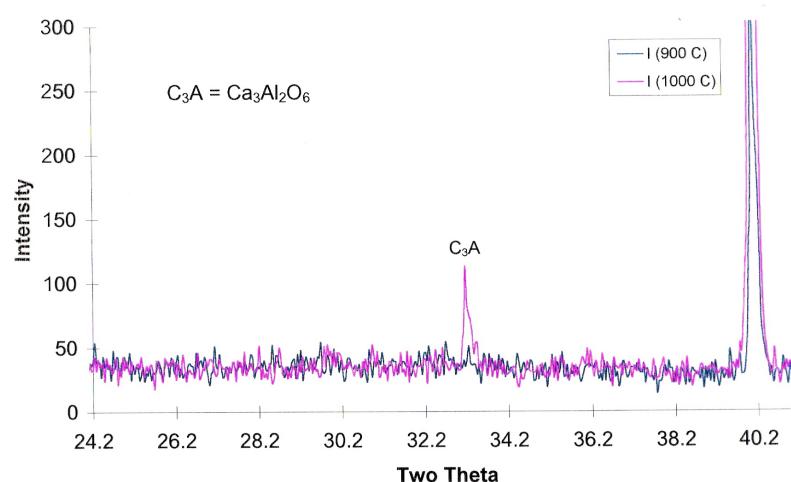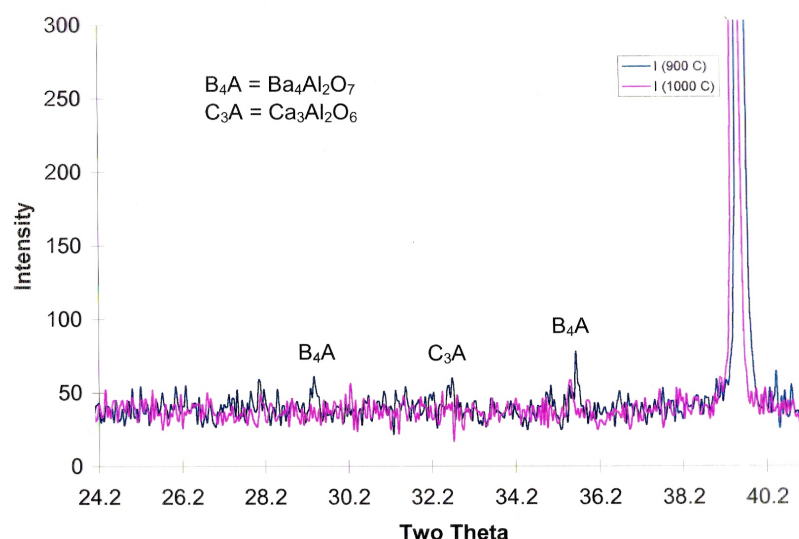

Figure IV.29 - Hot Stage X-Ray Scan of IRG11 (Schott Baria Doped) Powders

The Ba-doped Schott glass powder sample scans showed both tricalcium aluminate and barium aluminate phases at $900^{\circ}C$. Although it was expected that these phases would increase at $1000^{\circ}C$, no crystals formed there. Upon inspection of this sample after cooling, the powder had agglomerated and formed a dark glassy bead. It appeared that the powders had remelted to form a glass. This was most likely the result of the increased moisture content causing a decrease in the glass melting range.

IV.12.3.2 X-Ray Diffraction of Crystallized Samples with Guinea Camera

The Guinier X-Ray camera was run on the crushed fiber samples for 12 hours in order to achieve higher sensitivity due to the lower concentration of crystals on the glass

fiber surfaces. The crystal species present in the Si-doped Sassoon fiber scan were

$Ca_3Al_2O_6$. The crystal species present in the Ba-doped Sassoon fiber scan were $Ca_3Al_2O_6$

and $Ba_4Al_2O_7$. The crystal species present in the Ba-doped Schott fiber scan was also

$Ca_3Al_2O_6$ and $Ba_4Al_2O_7$. These results are consistent with the high temperature x-ray

scan results.

IV.13. Fiber Attenuation Measurements

The fiber attenuation scans for the three glass compositions are shown in the next

three figures. Figure IV.30 shows the attenuation scan for WB37A. The lowest loss

obtained was about 32 dB/m at 2.7 μm for the 500 μm bare fiber. This figure also shows

the attenuation scan of the same size glass fiber diameter with a Teflon cladding on it. It

is clear that the Teflon cladding only adds a slight amount of extra loss to the fiber

attenuation, but provides a protective layer to the bare fiber.
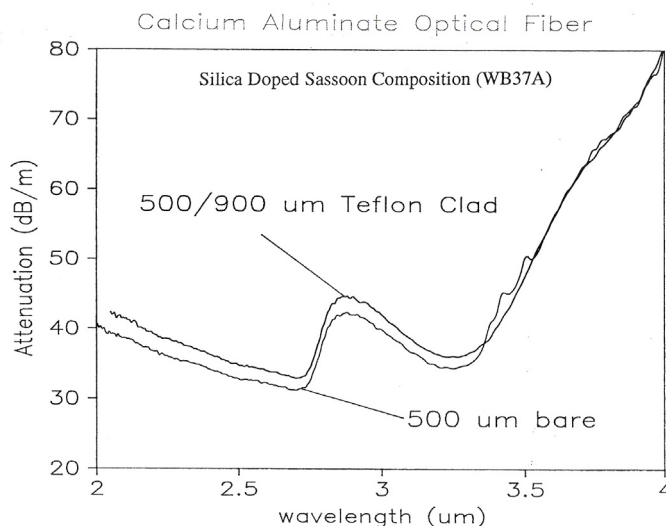
Figure IV.30 – Attenuation Scan of 500 μm WB37A fiber with
and without Teflon Cladding

Figure IV.31 shows the attenuation scan for the 500 μm diameter BS39B. The lowest loss is 7dB/m at approximately 2.7 μm. This represents the lowest loss obtained for any CAG fiber draws done in this study. This also represents the lowest loss reported for fiber drawing of the CAG glass system.
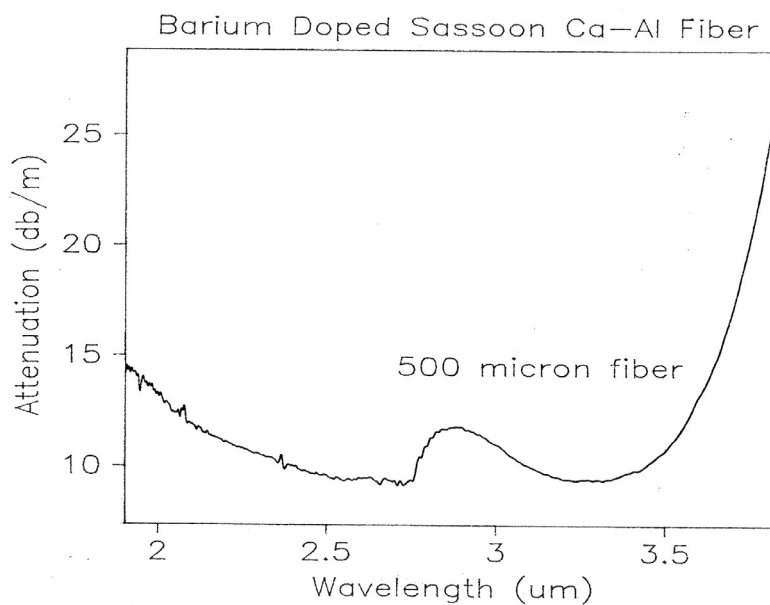

Figure IV.31 – Attenuation Scan of BS39B

Figure IV.32 shows the attenuation scan for the 470 μm diameter IRG11 fiber. The lowest loss is 18 dB/m at approximately 2.15 μm. Clearly the high water content of the IRG11 glass. The loss increases rapidly above 2.6 μm, which is the water absorption peak in these glasses.
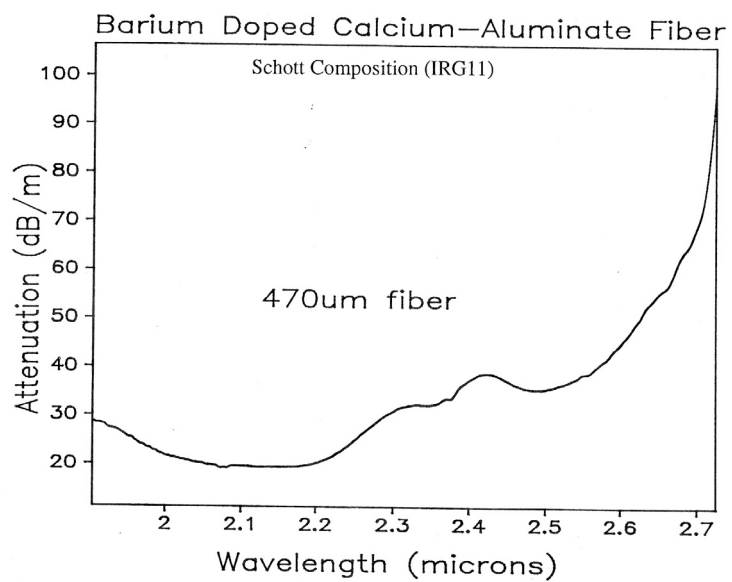
Figure IV.32 – Attenuation Scan for the 470 μm Diameter IRG11 Fiber

V. CONCLUSIONS

The fabrication of glass optical fibers from CAG was investigated in this study. High quality bulk glasses were obtained from the best industrial sources available. These glasses included silica and baria doped CAG compositions from Sassoon Ltd., and a baria doped CAG composition from Schott Glass Inc.

A preform fabrication method was developed to obtain drawing samples from the glass blanks provided from industry. This included the fabrication of rods for drawing into solid fibers and the fabrication of tubes for drawing into hollow waveguides. The polishing of the samples down to 0.3 μm surface finish was critical for obtaining fiber from the preform samples. A surface rougher finish than 0.3 μm would result in extensive devitrification of the fiber surface, eliminating the ability to obtain any fiber.

The custom modification of an optical fiber draw furnace was required to achieve fiber drawing from the CAG sample compositions. This included renovating an induction furnace to minimize the heat zone susceptor and adding water cooling to further narrow the heat zone temperature profile. Any attempts to draw the CAG compositions using standard draw furnaces resulted in complete devitrification of the draw samples.

Solid fiber was drawn from all three CAG compositions through the use of a novel sample holder arrangement and draw method. The best draw results came from using the Schott IRG11 glass, a surprise considering the water content of this glass. It was originally expected that the water in this composition would cause extensive crystallization during drawing.

Hollow fiber waveguides were drawn from the Schott IRG11 CAG composition. This composition as picked for the hollow waveguides due to the better ability to draw and its lack of silica in the composition. Silica was shown to increase the absorption in the infrared spectrum. The hollow fibers obtained were shown to be useful as waveguides for CO_2 power propagation. 24 Watts of CO_2 power were successfully launched down a 44 cm length of 460 μm bore hollow waveguide.

Solid CAG fiber was fabricated and investigated for the delivery of Er:YAG laser power. The Schott IRG11 sample composition was made into one meter lengths of Teflon coated 550 μm glass diameter fibers. The fiber endfaces were polished down to 0.3 μm grit size to achieve mirror finishes for the best results. An Erbium YAG laser beam was focused onto the input fiber end. The average power output recorded was 7.22 J/mm^2. At higher powers than those recorded, the ends of the fibers would show laser damage.

Several methods to improve the drawing calcium aluminate glass fiber fabrication were investigated. These included adding propane or NF_3 to the drawing furnace atmosphere in an attempt to remove surface water. Neither method was successful in improving the fiber drawing of the CAG compositions.

The solid and hollow CAG waveguides, and CAG core/silica clad waveguides obtained represents the first successful fiber drawing of this glass system. Teflon coating for optical cladding and strength protection was also investigated. The Teflon coating provided an optical cladding and a protective buffer for the fibers.

Infrared Spectroscopy was used to assess the attenuation in the drawn fibers. The Sassoon silica doped CAG composition WB37A showed a loss of 32 dB/m at 2.7 μm for

the 500 μm bare fiber. The Schott baria doped IRG11 CAG composition showed a loss of 18 dB/m at 2.15 μm. The high water content of the IRG11 clearly inhibited the propagation in the infrared spectrum.

The Sassoon baria doped CAG composition BS39B showed a loss of 7 dB/m at 2.7 μm. This represents the lowest loss documented for drawn fibers from CAG.

Fiber strength testing was performed on the CAG fibers through the use of four point bend testing. The best strength obtained was 1290 MPa for baria doped Schott IRG11 CAG 500 μm fiber. The best strength obtained for baria doped Sassoon BS39B CAG 500 μm fiber was 940 MPa. The best strength obtained for baria doped Sassoon WB37A CAG composition was 720 MPa.

Glass stability of the CAG compositions was assessed using Differential Thermal Analysis (DTA). Moisture was concluded to degrade the stability of calcium aluminate glasses depending upon the water content of the glass and the openness of the glass structure. The largest effect was found in the glass with the lowest water content and the most open structure, while virtually no effect was observed in a glass with large water content. Also it was concluded that no substantial gain in stability resulted by using dry nitrogen over air as the atmosphere.

The presence of chlorine in the furnace atmosphere seemed to reduce the stability and may diminish the extent of crystallization at the surface for at least the glasses containing no water.

Fiber surface crystallization products were characterized using Energy Dispersive Analysis, Scanning Electron Microscopy, a specially modified Hot Stage X-Ray, and Guinier Camera X-Ray Analysis. The surface crystallization analysis revealed the

formation of $Ca_3Al_2O_6$ in the silica doped CAG fibers and $Ca_3Al_2O_6$ and $Ba_4Al_2O_7$ in the baria doped CAG fibers.

CAG fibers have been shown to be useful as waveguides for the propagation in the visible and infrared spectrum. The delivery of CO_2 and Er:YAG laser power has also been successfully demonstrated.

VI. FUTURE WORK

The fabrication and characterization of calcium aluminate glass fibers has demonstrated that these compositions can be drawn into useful waveguides. Suggestions of future work in this area include;

1. Fabrication of drawing equipment to standardize the draw process. This would enable all compositions to be drawn at the start up speed. Different drawing sample results could then be better compared. This would include a pulling tractor for initial start up.

2. Development of a vacuum melting facility similar to the Sassoon production facility. This would enable the development and optimization of CAG compositions for draw.

3. Development of rod-in-tube drawing techniques. This would enable the obtained fibers to have an optical glass cladding, instead of an air or Teflon cladding. Attenuation results should then be improved significantly.

4. Development of a hermetic coating technique for the fiber draw furnace to protect against surface water attack. This should improve the resulting strength of the fiber. The hermetic coating could be applied right at the exit of the furnace.

5. Investigation of the effect of water on the drawability of CAG compositions.

VII. REFERENCES

1. Sun, K.H., (1949), "Aluminate Glasses", Glass Industry, vol. 30, 4, pp. 199-200, 232.

2. Florence, J.M., Glaze, F.W., and Black, M.H., (1955), "Infrared Transmittance of Some Calcium Aluminate and Germanate Glasses," Journal of Research National Bureau of Standards, vol. 55, 4, pp. 231-237.

3. Hafner H.C., Kreidl, N.J., Weidel R.A., (1958), "Optical and Physical Properties of Some Calcium Aluminate Glasses", Journal of the American Ceramic Society, vol. 41, 8, pp. 315-323.

4. Sassoon Advanced Materials Limited Product Brochure (1992).

5. Lines, M.E., (1988), "A Possible Non-halide Route to Ultralow Loss Glasses", Journal of Non-Crystalline Solids, vol.103, pp. 279-288.

6. Lines, M.E., MacChesney, J.B., Lyons, K.B., Bruce, A.J., Miller, A.E., and Nassau, K., (1989), "Calcium Aluminate Glasses as Potential Ultralow Loss Optical Materials at 1.5 -1.9 um", Journal of Non-Crystalline Solids, vol. 107, pp. 251-260.

7. Uhlmann, E.V., Weinberg, M.C., Kreidl, N.J., Goktas, A.A., (1993), "Glass Forming Ability in Calcium Aluminate-based System", Journal of the American Ceramic Society, vol.76, 2, pp. 449-453.

8. Shepherd, E.S., Rankin, G.A., and Wright, F.E., (1909), "The Binary Systems of Alumina with Silica, Lime, and Magnesia", American Journal of Science, Fourth Series, vol. 28, no. 166, pp. 293-333.

9. Rankin, G.A., and Wright, F.E., (1915), "The Ternary System $CaO-Al_2O_3-SiO_2$", American Journal of Science, vol. 39, pp. 1-79.

10. Rankin, G.A., and Merwin, H.E., (1916), " The Ternary System $CaO-Al_2O_3-MgO$", Journal of the American Ceramic Society, vol. 38, pp. 568-588.

11. McMurdie, H.F., and Insley, H.J., (1936), "Studies on the Quaternary System $CaO-MgO-2CaO^.SiO_2-5CaO^.3Al_2O_3$", Journal of Research National Bureau of Standards, vol. 16, pp. 467-474.

12. Dimbleby, V., English, S., Hobkins, F.W., and Turner, W.E.S., (1924), " Further Investigations of the Influence of Alumina on the Properties of Glass.", Journal of the Society of Glass Technology, vol. 8, pp. 173-181.

13. Weyl, W.A., (1943), "Coloured Glasses", Journal of the Society of Glass Technology, Transactions, vol. 27, no. 12, pp. 165.

14. Stevels, J.M., (1946), "The Physical Properties of Glass in Relation to Its Structure", Journal of the Society of Glass Technology, Transactions, vol. 30, part 3, pp. 30-53.

15. Zachariasen, (1932), "The Atomic Arrangement in Glass", Journal of the American Chemical Society, vol. 54, part 4, pp. 3841-3851.

16. Sun, K.H., (1946), "Glass Forming Substances", Glass Industry, vol. 27, no. 11, pp. 552-554, 580-581.

17. Safford, H.W., and Silverman, A., (1947), "Alumina-Silica Relationship in Glass", Journal of the American Ceramic Society, vol. 30, no. 7, pp. 203-211.

18. Stanworth, J. E., (1948), "On the Structure Of Glass", Journal of the Society of Glass Technology, vol. 32, pp. 154-172.

19. Bussem, W., and Eitel, W., (1936), Z. Krist., vol. 95, p. 175.

20. Rawson, H., (1967), "Inorganic Glass Forming Systems", Academic Press, pp. 26-29.

21. Kolesova, V.A., (1960), "A Study of the Structure of Alkali Aluminosilicate Glasses Based on Their Infrared Absorption Spectra", The Structure of Glass, vol. 2, Proceedings of the Third All-Union Conference on the Glassy State, Leningrad, pp. 177.

22. Chopra, S.K. and Taneja, C.A., (1965), "Co-ordination State of the Aluminium Ions in the $CaO-Al_2O_3-SiO_2$ Glasses", Journal of Applied Chemistry, vol. 15, pp. 157-161.

23. Yamane, M., and Okuyama, M., (1982), "Coordination Number of Aluminum Ions in Alkali-Free Alumino-Silicate Glasses", Journal of Non-Crystalline Solids, vol. 52, pp. 217-226.

24. Morikawa, H., Marumo, F., Koyama, T., Yamane, M., and Oyobe, A., (1983), "Structural Analysis of $12CaO.7Al_2O_3$ Glass", Journal of Non-Crystalline Solids, vol. 56, pp. 335-360.

25. Sargent, P.T. and Roy, R., (1969), "Reactivity of Solids", eds., Mitchell, J.W., DeVries, R.C., Roberto, R.W. and Cannon, P., Wiley, New York, p. 275.

26. McMillan, P., and Piriou, B., (1983), "Raman Spectroscopy of Calcium Aluminate Glasses and Crystals", Journal of Non-Crystalline Solids, vol. 55, no. 2, pp. 221-242.

27. McMillan, P.F., (1981), "A Stuctural Study of Aluminosilicate Glasses by Raman Spectroscopy", Ph.D. thesis, Arizona State University, Tempe, Arizona.

28. Engelhardt, G., Nofz, M., Forkel, K., Wihsmann, F.G., Magi, M., Samoson, A., and Lippmaa, E., (1985), "Structural Studies of Calcium Aluminosilicate Glasses by High Resolution Solid State ^{29}Si and ^{27}Al Magic Angle Spinning Nuclear Magnetic Resonance", Physics and Chemistry of Glasses, vol. 26, 5, pp. 157-165.

29. Shelby, J.E., (1985), "Formation and Properties of Calcium Aluminosilicate Glasses", Journal of the American Ceramic Society, vol. 68, number 3, pp. 155-158.

30. Topping, J.A., (1977), "Glass Ceramics from the System CaO-Al_2O_3-SiO_2", American Ceramic Society Bulletin, vol. 56, 6, pp. 574-577.

31. Balewick, L.A. and Shelby, J.E.,(1989), "Mixed Intermediate Effect in Calcium Alumino/Galliosilicate Glasses", Journal of the American Ceramic Society, vol. 72, 9, pp. 1751-1754.

32. Nishida, T., Ide, H., Takashima, Y., (1990), "A Linear Relationship between the Glass Transition Temperature and Local Distortion of Calcium Gallate, Barium Gallate, and Calcium Aluminate Glasses", Bulletin of the Chemical Society of Japan, vol. 63, 2, pp. 548-553.

33. Nishida, T., (1989), "A Review of Structural Studies of Superionic Conducting Borate and Semiconducting Vanadate Glasses by Mössbauer Spectroscopy and DTA", Journal of Non-Crystalline Solids, vol. 108, 1, pp. 87-98.

34. Higby, P.L., Ginther, R.J., Aggarwal, I.D., Friebele, E. J., (1990), "Glass Formation and Thermal Properties of Low-Silica Calcium Aluminosilicate Glasses", Journal of Non-Crystalline Solids, vol. 126, pp. 209-215.

35. Higby, P.L., Merzbacher, C.I., Aggarwal, I.D. and Friebele, E.J., (1990), "Effect of Small Silica Additions on the Properties and Structure of Calcium Aluminate Glasses", SPIE Properties and Characteristics of Optical Glass II, vol. 1327, pp. 198-202.

36. Higby, P.L., Busse, L.E., and Aggarwal, I.D., (1991), "Properties of Low-Silica Calcium Aluminosilicate Glasses", Materials Science Forum, vol. 67/68, pp. 155.

37. Huang, C. and Behrman, E.C., (1991), "Structure and Properties of Calcium Aluminosilicate Glasses", Journal of Non-Crystalline Solids, vol. 128, pp. 310-321.

38. Poe, B.T., McMillan, P.F., Massiot, D., Coutures, J.P., (1994), "Structure and Dynamics in Calcium Aluminate Liquids: High-Temperature ^{27}Al NMR and Raman Spectroscopy", Journal of the American Ceramic Society, v 77, 7, pp. 1832-1838.

39. Daniel, I., McMillan, P.F., Gillet, P. and Poe. B.T., (1996), "Raman Spectroscopic Study of Structural Changes in Calcium Aluminate ($CaAl_2O_4$) Glass at High Pressure and High Temperature", Chemical Geology, vol. 128, pp. 5-15.

40. Cormier, L., Neuville, D.R., and Calas, G., (2000), "Structure and Properties of Low-Silica Calcium Aluminosilicate Glasses", Journal of Non-Crystalline Solids, vol. 274, pp. 110-114.

41. Hannon, A.C., and Parker, J.M., (2000), "The Structure of Aluminate Glasses by Neutron Diffraction", Journal of Non-Crystalline Solids, vol. 274, pp. 102-109.

42. Benmore, C.J., Weber, J.K.R., Sampath, S., Siewenie, J., Urquidi, J., and Tangeman, J.A., (2003), "A Neutron and X-Ray Diffraction Study of Calcium Aluminate Glasses", Journal of Physics: Condensed Matter, vol. 15, pp. S2413-S2423.

43. Neuville, D.R., Cormier, L., Flank, A.M., Brios, V., and Massiot, D., (2004), "Al Speciation and Ca Environment in Calcium Aluminosilicate Glasses and Crystals by Al and Ca K-Edge X-Ray Absorption Spectroscopy", Chemical Geology, vol. 213, pp. 153-163.

44. Li, W and Mitchell, B.S., (1999), "Nucleation and Crystallization in Calcium Aluminate Glasses", Journal of Non-Crystalline Solids, vol. 255, pp. 199-207.

45. Machlan, G.R., (1955), "The Development of Fibrous Glass Having High Elastic Moduli", WADC Technical Report 55-290, Contract AF33, pp. 616-2422.

46. Capps, W. and Blackburn, D.H., (1957) "The Development of Glass Fibers Having High Young's Moduli of Elasticity", U.S. Department of Commerce, National Bureau of Standards, No. 5188.

47. Brown, S.D., and Onada, G.Y., Jr., (1966), "High Modulus Glasses Based on Ceramic Oxides", Technical Report R-6692, Contract NOW-65-0426-d, US Department of the Navy, Bureau of Naval Weapons, Washington DC.

48. Onada, G.Y., Jr. and Brown, S.D., (1968), "High Modulus Glasses Based on Ceramic Oxides", Technical Report R-7363, Contract N00019-67-C-301, US Department of the Navy, Naval Air Systems Command, Washington DC.

49. Onada, G.Y., Jr. and Brown, S.D., (1970), "Low Silica Glasses Based on Calcium Aluminates", Journal of the American Ceramic Society, vol. 53, 6, pp. 311-316.

50. Lowenstein, K.L., (1962), "Studies in the Composition and Structure of Glasses Possessing High Young's Moduli", Physics and Chemistry of Glasses, vol. 3, 2, pp. 59.

51. Schroeder, T.F. and Carniglia, S.C., (1969), "High Modulus Glasses Based on Ceramic Oxides", Technical Report R-7741, Contract N00019-68-c-0205, US Department of the Navy, Naval Air Systems Command, Washington DC.

52. Schroeder, T.F., Carpenter, H.W., and Carniglia, S.C., (1969), " High Modulus Glasses Based on Ceramic Oxides", Technical Report R-8079, Contract N00019-69-c-0150, US Department of the Navy, Naval Air Systems Command, Washington DC.

53. Cunningham, R.E., Rakestraw, L.F. and Dunn, S.A., (1978), "Inviscid Melt Spinning of Filaments", Spinning Wire from Molten Metal, ed., J. Mottern and W.J. Privott. AIChE Symposium Series, vol. 74, 180, pp. 20-32.

54. Wallenberger, F.T., (1990), "Melt Spinning of Amorphous Alumina Fibers", Ceramic Bulletin, vol. 69, 10, pp.1646-1648.

55. Wallenberger, F.T., Weston N.E., and Dunn S.A., (1990) "Inviscid Melt Spinning of Alumina Fibers: Jet Stabilization Dynamics", SAMPE Quarterly, vol. 22, 1, pp. 15-22.

56. Wallenberger, F.T., Weston, N.E., and Motzfeldt, K., (1991), "Inviscid Melt Spinning of Alumina Fibers: Jet Stabilization Mechanism", Ceramic Engineering and Scientific Proceedings, vol. 12, 7/8, pp. 1039-1047.

57. Wallenberger, F.T., Weston N.E., and Dunn S.A., (1990). "Inviscid Melt Spinning (IMS); as Spun Amorphous Alumina Fibers", Materials Letters, vol. 9, 4, pp. 121-127.

58. Wallenberger, F.T., Weston N.E., and Dunn S.A., (1991) "Inviscid Melt Spinning: Strength of Amorphous Alumina Fibers", Advanced Structural Inorganic Composites, ed. P. Vincencini. Elsevier, Amsterdam, pp. 47-55.

59. Wallenberger, F.T., Weston N.E., and Dunn S.A., (1990), "Inviscid Melt Spinning: Crystallization of Amorphous Alumina Fibers", SAMPE Quarterly, vol. 21, pp. 30-34.

60. Wallenberger, F.T., Weston N.E., and Dunn S.A., (1990), "Melt Spun Calcium Aluminate Fibers: Infrared Transmission", Journal of Non-Crystalline Solids, vol. 124, pp. 116-119.

61. Wallenberger, F.T., Koutsky, J. A., and Brown, S.D., (1991), "Melt Processing of Calcium Aluminate Fibers with Sapphirelike Infrared Transmission", Proceedings of SPIE - The International Society for Optical Engineering, vol. 1590, pp. 72-82.

62. Wallenberger, F.T., Weston, N.E., and Brown, S.D., (1991), "Melt-Processed Calcium Aluminate Fibers: Structural and Optical Properties", Proceedings of SPIE - The International Society for Optical Engineering, vol. 1484, pp. 116-124.

63. Wallenberger F.T., Weston, N.E, and Brown, S.D., (1991), "Calcium Aluminate Glass Fibers: Drawing from Supercooled Melts Versus Inviscid Melt Spinning", Materials Letters, vol. 1l, 8,9, pp. 229-235.

64. Davy, J.R., (1978), "Development of Calcium Aluminate Glasses for Use in the Infrared Spectrum to 5 um", Glass Technology, vol. 19, 2, pp. 32-36.

65. Wallenberger, F.T., Weston, N.E., Motzfeldt, K., Swartzfager, D.G., (1992), "Inviscid Melt Spinning of Alumina Fibers: Chemical Jet Stabilization", Journal of American Ceramic Society, vol. 75, 3, pp. 629-636.

66. Wallenberger, F.T. and Brown, S.D. (1994), "High-Modulus Glass Fibers for New Transportation and Infrastructure Composites and New Infrared Uses", Composites Science and Technology, vol. 51, pp. 243-63.

67. Wallenberger, F.T.; Brown, S.D.; and Koutsky, J. A, (1992), "Melt Processing of Optical Alumina Fibers. A Process Review and Product Outlook", SAMPE Quarterly, vol. 23, no. 2, pp. 17-28.

68. Wallenberger, F.T., Weston N.E., and Dunn S.A., (1990), "Melt Spun Calcium Aluminate Fibers: Product Value", International Conference on Electronic Materials, Materials Research Society Conference Proceedings, ed. R.P.H. Chang, T. Sugano, and V.T. Nguyen, Materials Research Society, Pittsburg, PA, pp. 295-300.

69. Sung, Y.M. and Sung, J. H., (1998), "Crystallization Behavior of Calcium Aluminate Glass Fibers, Part 1 – Differential Thermal Analysis Study", Journal of Material Science, vol. 33, pp. 4733-4737.

70. Mitchell, B.S., (2000), "Micro-Raman Analysis of Calcium Aluminate Fibers Formed by Inviscid Melt Spinning", Materials Letters, vol. 45, pp. 138-142.

71. Durham, J.A., Risbud, S.H., (1988), "Low Silica Calcium Aluminate Oxynitride Glasses", Materials letters, vol. 7, 5/6, pp. 208-210.

72. Shelby, J.E., Shaw, C.M., and Spess, M.S., (1989), "Calcium Fluoroaluminate Glasses", Journal of Applied Physics, vol. 66, 3, pp. 1149-1154.

73. Shelby, J.E., and C. E. Lord, (1990), "Formation and Properties of Calcia-Calcium Fluoride-Alumina Glasses", Journal of the American Ceramic Society, vol. 73, 3, pp. 750-752.

74. Shelby, J.E., and Slilaty, R.M., (1990), "Calcium Gallioaluminate Glasses", Journal of Applied Physics, vol. 68, 7, pp. 3207-3211.

75. King, W.A., and Shelby, J.E., (1996), "Strontium Calcium Aluminate Glasses", Physics and Chemistry of Glasses, vol. 37, 1, pp. 1-3.

76. Uberoi, M., and Risbud, S.H., (1990), "Processing of Amorphous Calcium Aluminate Powers at <900°C", Journal of the American Ceramic Society, vol. 73, 6, pp. 1768-1770.

77. Goktas, A.A., and Weinberg, M.C., "Preparation and Crystallization of Sol-Gel Calcia-Alumina Compositions", Journal of the American Ceramic Society, vol. 74, 5, pp. 1066-1070.

78. Topping, J.A., (1977), "Glass Ceramics from the System CaO-Al$_2$O$_3$-SiO$_2$", Ceramic Bulletin, vol. 56, 6, pp. 576-577.

79. Nandi, A.K., Chaudhuri, A.K., Thiagarajan, S. and Ghosh, S. (1993), "A New Approach to the Preparation of IR Transparent Ca$_{l2}$Al$_{14}$0$_{33}$ Material", British Ceramic Transactions, vol. 92, 2, pp. 81-82.

80. Stookey, S.D., (1949), " Photosensitive Glasses", Industrial Engineering Chemistry, vol. 41, 4, pp. 865-61.

81. Hosono, H., Yamazaki, K., and Abe, Y., (1985), "Dopant-Free Ultraviolet-Sensitive Calcium Aluminate Glasses", Journal of the American Ceramic Society, vol. 68, 11, pp. C304-C305.

82. Hosono, H., Yamazaki, K., and Abe, Y., (1987), "Photosensitive Characteristics of Dopant Free, Ultraviolet-Sensitive Calcium Aluminate Glasses", Journal of the American Ceramic Society, vol. 70, 12, pp. 867-870.

83. Hosono, H., Yamazaki, K., and Abe, Y., (1987), "Photosensitive Mechanism of Dopant Free, Ultraviolet-Sensitive Calcium Aluminate Glasses", Journal of the American Ceramic Society, vol. 70, 12, pp. 870-873.

84. Hosono, H., and Abe, Y., (1987), "Photosensitivity and Structural Defects in Dopant-Free Ultraviolet-Sensitive Calcium Aluminate Glasses", Journal of Non-Crystalline Solids, vol. 95-96, pp. 717-724.

85. Hosono, H., and Abe, Y., (1987), "Effects of Melting Atmosphere and Heat Treatment on the Photosensitivity of Dopant Free, Ultraviolet-Sensitive Calcium Aluminate Glasses", Diffusion and Defect Data, vol. 53-54, pp. 139-144.

86. Hosono, H., and Abe, Y., (1988), "Photochromism of Reduced Calcium Aluminate Glasses", Materials Research Bulletin, vol. 23, pp. 171-176.

87. Hosono, H., Asada, N., Abe, Y., (1990), "Properties and Mechanism of Photochromism in Reduced Calcium Aluminate Glasses", Journal of Applied Physics, vol. 67, 6, pp. 2840-2847.

88. Dumbaugh, W.H., (1985), "Infrared Transmitting Glasses", Optical Engineering, vol. 24, 2, pp. 257-262.

89. Florence, J.M., Allshouse, C.C., Glaze, F.W., and Hahner, C.H., (1950), "Absorption of Near-Infrared Energy by Certain Glasses," Journal of Research National Bureau of Standards, vol. 45, 2, pp. 121-2128.

90. Dumbaugh, W.D. and Lapp. J.C. (1992), "Heavy-Metal Oxide Glasses", Journal of the American Ceramic Society, vol. 75, 9, pp. 2315-2326.

91. Bendow, B., Rast, H. and El-Bayoumi, 0. (1985), "Infrared Fibers: an Overview of Prospective Materials, Fabrication Methods, and Applications", Optical Engineering, vol. 24, 6, pp. 1072-1080.

92. Miyashita, T. and Manabe, T., (1982), "Infrared Optical Fibers", IEEE: Transactions on Microwave Theory and Techniques, vol. MTT-30, 10, pp. 1420-1438.

93. Drexhage, M.G., (1991), "Glass Optical Fibers Enter the Infrared", Laser Focus World, June, pp. 149-153.

94. Harrington, J. A., ed., (1990), "Selected Papers on Infrared Fiber Optics", SPIE Milestone Series, Bellingham, Wash., vol. MS9.

95. Hidaka, T., Morikawa, T., and Shimada, J., (1981), "Hollow-Core Oxide-Glass Cladding Optical Fibers for Middle-Infrared Region", Journal of Applied Physics. vol. 52, pp. 4467-4471.

96. Harrington, J. A., and Gregory, C. G., (1990), "Hollow Sapphire Fibers for the Delivery of CO_2 Laser Energy", Optics Letters, vol. 15, pp. 541-543.

97. Hidaka, T., Kumada, K., Simada, J., and Morikawa, T., (1982), "GeO_2-ZnO-K_2O Glass as the Cladding Material of 940 cm^{-1} CO_2 Laser Light Transmitting Hollow-Core Waveguide", Journal of Applied Physics, vol. 53, pp. 5484-5489.

98. Worrel, C. A. and Skarda, V., (1989), "CO_2 Laser Waveguides from Germania Based Glasses", Journal of Physics D, vol. 22, pp. 535-541.

99. Falciai, R., Gironi, 0., and Scheggi, A. M., (1984), "Oxide Glass Hollow Fiber for CO_2 Laser Radiation Transmission," in "Novel Optical Fiber Techniques for Medical Applications", Katzir, A., ed., Proceedings of Society of Photo-Optic Instrumentation Engineering, vol. 494, pp. 84-87.

100. Scheggi, A. M., Falciai, R., and Gironi, G., (1985), "Characterization of Oxide Glasses for Hollow-Core Middle IR Fibers", Applied Optics, vol. 24, pp. 4392-4394.

101. Nagano, M. Saito, M. Miyagi, N. Baba, and N. Sawanobori, (1991), "Prediction of Optical Losses in SiO_2- and GeO_2-Based Glass Hollow Waveguides for the Infrared", Applied Physics Letters, vol. 58, pp. 1807-1809.

102. Nagano, N., Saito, M., Miyagi, M., Baba, N., and Sawanobori, N., (1992), "Refractive Indices of SiO_2- and GeO_2-Based Glasses Near the Infrared Absorption Peaks", Journal of Non-Crystalline Solids, vol. 135, pp. 114-121.

103. Wilson, S. J., (1987), "Hollow Core Glass Waveguides," in "New Materials for Optical Waveguides", Lucas, J., ed., Proceedings of the Society of Photo-Optic Instrumentation Engineering, vol. 799, pp. 54-61.

104. Marcatili, B. and Schmeltzer, R., (1964), "Hollow Metallic and Dielectric Waveguides for Long Distance Optical Transmission and Lasers", Bell Systems Technical Journal, vol. 43, pp. 1783-1809.

105. Miyagi, M. and Karasawa, S., (1990), "Waveguide Losses in Sharply Bent Circular Hollow Waveguides", Applied Optics, vol. 29, pp. 367-380.

106. Saggese, S. J. and Harrington, J. A., (1993), "Calcium-Aluminate Glass for Use as n < 1 Hollow Waveguides in the Delivery of CO_2 Laser Energy", Optical Materials, vol. 2, pp. 119-123.

107. Bortz, M. L., and French, R. H., (1989), "Quantitative, FFT based, Kramers-Kronig Analysis for Reflectance Data", Applied Spectroscopy, vol. 43, pp. 1498-1501.

108. Snitzer, E. and Tumminelli, R., (1989), "SiO_2-Clad Fibers with Selectively Volatilized Soft-Glass Cores", Optics Letters, vol. 14, 14, pp. 757-759.

109. Nelson, G., Matthewson, M.J., and Lin, B., (1996) "A Novel Four Point Bend Test for Strength Measurement of Optical Fibers and Thin Beams – Part I: Bending Analysis", Journal of Lightwave Technology, vol. 14, 4, pp. 555-563.

110. Daniov, 0. B., Zintchenko, M. I., Rubinov, Y. A., and Sosnov, E. N., (1990), "Transmission Losses and Mode-Selection Characteristics of a Curved Hollow Dielectric Waveguide with a Rough Surface", Journal of the Optical Society of America B, vol. 7, pp. 1785-1790.

VIII. VITA

Paul Robert Foy

1960	Born in East Orange, NJ on February 28, 1960
1982	Bachelor of Science, Ceramic Engineering - Rutgers University
1983-1985	Production Foreman, AFG industries, Cinnaminson, NJ
1986-1996	Draw Tower Laboratory Supervisor, Fiber Optic Materials Research Program, Rutgers University, New Brunswick, NJ
1990	Masters of Science, Ceramic Engineering - Rutgers University
1995	R&D 100 Award for improved optical fiber for laser surgery applications
1996-1998	Director, Fiber Optic Technologies, Royle Systems Group, Pompton Lakes, NJ
1998-2003	Engineering Manager, JDS Uniphase, VitroCom division, Mountain Lakes, NJ
2003-2005	Consultant, Paul R. Foy Fiber Optic and Glass Consulting, Berkeley Heights, NJ
2005	Director, Optical Fiber Laboratories, COMSET, Clemson University, Anderson, SC
2008	Ph.D. Materials Science and Engineering, Rutgers University, New Brunswick, NJ

Publications

Budy, S.M., Iacono, S.T., Hawkins, T.W., Foy, P.R., Ballato, J., and Smith, D.W., (2008), "Specialty High Performance Coatings for Optical Fiber Applications via Perfluorocyclobutyl (PFCB) Aryl Ether Polymers", Materials Research Society Symposium Proceedings Vol. 1030.

Siegman, A.E., Chen, Y., Sudesh, V., Richardson, M.C., Bass, M., Foy, P., Hawkins, T.W., and Ballato, J., (2006), "Confined Propagation and Near Single-Mode Laser Oscillation in a Gain-Guided, Index Antiguided Optical Fiber", Applied Physics Letters, vol. 89, 251101.

Vogel, E.M., Mann, J.D., Plitz, I.M., Bowmer, T.N., Frantz, R.A., Wieczorek, C.J., Keon B.J., and Foy, P.R., (1996), "The Effects Of Ink On The Performance Of Color Coded Fibers", Proceedings of the International Wire and Cable Symposium, pp.479-484.

Wojcik, A.B., Matthewson, M.J., Klein, L.C., Foy, P.R., Snitzer, E., and Wong, K.P., (1995). "Mechanical Behavior of Silica Optical Fibers Coated with Low Index, Low Surface Energy Perfluorinated Polymer", Proceedings of SPIE vol. 2611, pp.110 -116,

Wojcik, A.B., Klein, L.C., Rondinella, V.V., Matthewson, M.J., Foy, P.R., (1993), "Organically Modified Silicate Coatings For Optical Fibers", Proceedings of. SPIE vol. 2074, 135-141.

Rondinella, V.V., Matthewson, M.J., Foy, P.R., Schmid, S.R., Krongauz, V.V., (1993), "Enhanced Fatigue and Aging Resistance Using Reactive Powders in the Optical Fiber Buffer Coating", Proceedings of SPIE vol. 2074, 46-51.

Abel, T., Foy, P.R., Harrington, J., (1993), "Optical Properties of Hollow Calcium Aluminate Glass Waveguides, Applied Optics, vol. 33, 3919-3922.

Matthewson, M. J., Yuce, H.H., Rondinella, V.V., Foy, P.R., and Hamblin, J., (1993), "Effect of Silica Particles In The Polymer Coating On The Fatigue And Aging Behavior Of Fused Silica Optical Fiber", OFC/IOOC '93 Technical Digest Series vol. 4, PD21, pp. 87-90.

Wu, F., Puc, G., Foy, P.R., Snitzer, E., and Sigel, G. H., (1993), "Low-Loss Rare Earth Doped Single-Mode Fiber by Sol-Gel Method", Materials Research Bulletin, vol.28, pp. 637-644.

Snyder, J.R., Green, G.D., Swedo, R.J., Srivastava, C.M., Levy, A.C., Kovac, R.J., and Foy, P.R., (1993), "New Developments In Ultra-Violet Curable Optical Fiber Coatings Based On Vinyl Ether Technology", Proceeding of the Forty-Second International Wire and Cable Symposium, pp. 665-673.

Snyder, J.R., Green, G.D., Levy, A.C., Kovac, R.J., and Foy, P. R., (1992), "Vinyl Ethers, A New Material Technology For Ultra-Violet Curable Optical Fiber Coatings", Proceedings of the Forty-First International Wire and Cable Symposium, pp. 253-260.

Iqbal, T., Shahriari, M.R., Foy, P.R., Ulbrich, R., and Sigel, G.H., (1991), "A1F$_3$ Based Glass Fibres With Enhanced Optical Transmission", Electronic Letters, vol. 27, 110,.

Lucas, J., Zhang, X.H., Ma, H.L., Fonteneau, G., Heo, J., Foy, P.R., Saggese, S.J. and Sigel, G.H., (1990), "Loss Mechanism Analysis of Tellurium Halide Glass Optical Fibers", SPIE OE/Laser '90, p. 1228.

Shahriari, M.R., Iqbal, T., Foy, P.R., Saggese, S.J., and Sigel, G.H., (1989), "Fabrication of AlF$_3$ Based Glass Fibers", Materials Research Society, Symposium Proceedings, Optical Materials and Processing, vol. p. 172.